Graduate School Form 30
Updated 1/15/2015

PURDUE UNIVERSITY
GRADUATE SCHOOL
Thesis/Dissertation Acceptance

This is to certify that the thesis/dissertation prepared

By Yu-Hung Lin

Entitled

PROBING CELLULAR MECHANO-SENSITIVITY USING BIOMEMBRANE-MIMICKING CELL SUBSTRATES OF ADJUSTABLE STIFFNESS

For the degree of Doctor of Philosophy

Is approved by the final examining committee:

Christoph Naumann
Chair

Chittaranjan Das

David Thompson

Eric Long

To the best of my knowledge and as understood by the student in the Thesis/Dissertation Agreement, Publication Delay, and Certification Disclaimer (Graduate School Form 32), this thesis/dissertation adheres to the provisions of Purdue University's "Policy of Integrity in Research" and the use of copyright material.

Approved by Major Professor(s): Christoph Naumann

Approved by: Eric Long 12/5/2015

Head of the Departmental Graduate Program Date

PROBING CELLULAR MECHANO-SENSITIVITY USING BIOMEMBRANE-MIMICKING CELL SUBSTRATES OF ADJUSTABLE STIFFNESS

A Dissertation

Submitted to the Faculty

of

Purdue University

by

Yu-Hung Lin

In Partial Fulfillment of the

Requirements for the Degree

of

Doctor of Philosophy

December 2015

Purdue University

Indianapolis, Indiana

ACKNOWLEDGEMENTS

First of all, I would like to acknowledge Prof. Christoph Naumann and all members of Prof. Naumann's group who supported and who helped me accomplish all the works in IUPUI. Especially, Dr. Amanda Siegel, Dr. Daniel Minner, Ms Yifan Ge, and Mr. Kent Shilts. They provided special efforts on my thesis writing and discussion of the experiments. Also, I would like to appreciate the help I received from Mr. Eric Gao, Mr. Leandro Moretti, and Mr. Cameron Dawes in Prof. Naumann's lab.

Second, I would like to thank Prof. Ben Fabry , Prof. Wolfgang Goldmann and Biophysical group members who assisted me with research in FAU Erlangen, Germany, especially Dr. Lena Lautscham and Dr. Vera Auernheimer for their support.

And I would like to appreciate all the support from my Taiwanese friends, Ms. Demorah Chang, Ms. Carina Hsieh, Ms. Emily Liu, Dr. Jian-Yuan Li, Dr. Nai-Wei Kuo, Dr, Chi-Shuo Chen, Dr. Bob Lei, Ms. Shu-Ting Yang, and all other friends everywhere in this six year.

Special thanks to Mr. Donald Jeske, who provided me the support in many ways. Finally, I would like to appreciate the support from my family, my mom, Ya-Ching Lin-Wu, my dad, Fan-Ching Lin, my sister, Mei-Li Lin, brother in law, Po-Hsun Wu, my niece, Emily Wu and my nephew Kyle Wu and all other relatives.

TABLE OF CONTENTS

Page

Page

Page

Page

LIST OF TABLES

LIST OF FIGURES

Figure Page

Figure Page

Figure Page

Figure Page

LIST OF ABBREVIATIONS

2D	Two-dimensional.
3D	Three-Dimensional.
AFM	Atomic Force Microscopy.
APS	Ammonium Persulfate.
DGS-NTA	1,2-dioleoyl-sn-glycero-3-[(N-(5-amino-1-carboxypentyl)-iminodiacetic acid)succinyl] (nickel salt).
DIC	Differential interference contrast microscopy.
DLPC	1,2-dilauroyl-sn-glycero-3-phosphocholine.
DMEM	Dulbecco's Modified Eagle Medium.
DOPC	1,2-dioleoyl-sn-glycero-3-phosphocholine.
DODA-E85	Dioctadecylamine [poly(ethyloxazoline) 8988].
DPPC	1,2-dipalmitoyl-sn-glycero-3-phosphocholine.
DPTE	1,2-dipalmitoyl-sn-Glycero-3-Phosphothioethanol (Sodium Salt).
DSPC	1,2-distearoyl-sn-glycero-3-phosphocholine.
ECM	Extracellular Matrix.
EDC/NHS	1-Ethyl-3-(3-dimethylaminopropyl)-carbodiimide /N-hydroxysuccinimide.
EPI	Epifluorescence.
FA	Focal adhesion.
FAK	Focal adhesion kinase.
FBS	Fetal bovine serum.

FCS	Fluorescence correlation spectroscopy.
FRAP	Fluorescence recovery after photobleaching.
HA	Hyaluronic acid.
GFP	Green fluorescent protein.
GFP-actin	Green fluorescent protein tagged actin.
GMBS	(N-[g-Maleimidobutyryloxy]succinimide ester).
GPCR	G Protein-coupled receptors.
HEPES	4-(2-hydroxyethyl)-1-piperazineethanesulfonic acid.
LB	Langmuir-Blodgett technique.
LS	Langmuir-Schaefer technique.
NBD-PE	N-(7-nitrobenz-2-oxa-1,3-diazol-4-yl)-1,2-dihexadecanoyl-sn-glycero-3-phosphoethanolamine, triethylammonium salt.
N-Cad	N-cadherin.
NGF	Nerve growth factor.
PAA	Polyacrylamide gel.
PAM	pressure-assisted microsyringe.
PBS	Phosphate buffered saline.
PBrS	polybromostyrene
PDMS	Polydimethylsiloxane.
PEG	Polyethylene glycol.
PEG2000	1,2-distearoyl-sn-glycero-3-phosphoethanolamine-N-[methoxy-polyethylene glycol)-2000] (ammonium salt).

PEG2000-MAL	1,2-distearoyl-sn-glycero-3-phosphoethanolamine-N-[maleimide(polyethylene glycol)-2000] (ammonium salt).
PEG2000-NHS	1,2-distearoyl-sn-glycero-3-phosphoethanolamine-N-[NHS-Active Ester(polyethylene glycol)-2000] (ammonium salt).
PLA	Poly(L-Lactic Acid).
PMOX50	1,2-distearoyl-sn-gycero-3-phosphoethanolamine-N-polymethyloxazoline(50).
POPC	1-palmitoyl-2-oleoyl-sn-glycero-3-phosphocholine.
PS	Polystyrene
SDS	Sodium Dodecyl Dulfate.
SOPC	1-stearoyl-2-oleoyl-sn-glycero-3-phosphocholine.
Sulfo-Sanpah	N-Sulfosuccinimidyl-6-(4'-azido-2'-nitrophenylamino) hexanoate.
SUV	Small Unilamellar Vesicle.
TEMEM	N,N,N’,N’-Tetramethylethylenediamine.
TFM	Traction Force Microscopy.
TR-DHPE	Texas Red®1,2-dihexadecanoyl-sn-glycero-3-phosphoethanolamine, triethylammonium salt.
TRITC	Tetramethylrhodamine isothiocyanate.
TRITC-DHPE	N-(6-tetramethylrhodaminethiocarbamoyl)-1,2-dihexadecanoyl-sn-glycero-3-phosphoethanolamine, triethylammonium salt (TRITC-DHPE).

TYPE I	Biomembrane-mimicking Multiple Bilayer-based substrate.
TYPE II	Polymer-supported phospholipid bilayer-based cell substrate.
VSF	Ventral stress fiber.
VF	Vesicle fusion.

.

ABSTRACT

Lin, Yu-Hung. Ph.D., Purdue University, December 2015. Probing Cellular Mechano-Sensitivity Using Biomembrane-Mimicking Cell Substrates of Adjustable Stiffness. Major Professor: Christoph Naumann.

It is increasingly recognized that mechanical properties of substrates play a pivotal role in the regulation of cellular fate and function. However, the underlying mechanisms of cellular mechanosensing still remain a topic of open debate. Traditionally, advancements in this field have been made using polymeric substrates of adjustable stiffness with immobilized linkers. While such substrates are well suited to examine cell adhesion and migration in an extracellular matrix environment, they are limited in their ability to replicate the rich dynamics found at cell-cell interfaces. To address this challenge, we recently introduced a linker-functionalized polymer-tethered multi-bilayer stack, in which substrate stiffness can be altered by the degree of bilayer stacking, thus allowing the analysis of cellular mechanosensitivity. Here, we apply this novel biomembrane-mimicking cell substrate design to explore the mechanosensitivity of C2C12 myoblasts in the presence of cell-cell-mimicking N-cadherin linkers. Experiments are presented, which demonstrate a relationship between the degree of bilayer stacking and mechanoresponse of plated cells, such as morphology, cytoskeletal organization, cellular traction forces, and migration speed. Furthermore, we illustrate

the dynamic assembly of bilayer-bound N-cadherin linkers underneath cellular adherens junctions. In addition, properties of individual and clustered N-cadherins are examined in the polymer-tethered bilayer system in the absence of plated cells.

Alternatively, substrate stiffness can be adjusted by the concentration of lipopolymers in a single polymer-tethered lipid bilayer. On the basis of this alternative cell substrate concept, we also discuss recent results on a linker-functionalized single polymer-tethered bilayer substrate with a lateral gradient in lipopolymer concentration (substrate viscoelasticity). Specifically, we show that the lipopolymer gradient has a notable impact on spreading, cytoskeletal organization, and motility of 3T3 fibroblasts. Two cases are discussed: 1. polymer-tethered bilayers with a sharp boundary between low and high lipopolymer concentration regions and 2. polymer-tethered bilayers with a gradual gradient in lipopolymer concentration.

INTRODUCTION

1.1 Rationale and Objective

For decades, most research related to the physiology of cells and tissue focused on molecular structure and biochemical signaling mechanisms that impact cell function and pathology[1,2]. Meanwhile, it has been recognized that mechanical signals may also have a profound impact on cellular fate and function. Such mechanical cues may include shear stress, osmotic forces, mechanical load and stretch as well as stiffness provided by the extra cellular matrix that surrounds most cells[3,4]. External mechanical forces not only affect the morphology and intracellular organization of cells, but also their proliferation and migration. Like other critical mediators of the interactions between cells and their environments, such as steroids and hormones, mechanical properties of the surroundings are considered to be one of the key characteristics necessary for biological functions determining the fate of cells and tissues. Failure of the mechanical components of tissue and cells can cause various dysfunctions and disease states, including cardiac hypertrophy, cancer and so on[5,6]. Mechanical properties also appear to be relevant to the normal development of tissue during embryogenesis and growth. Understanding the nature of these mechanical forces and how cells sense and respond appropriately to them is a challenging problem that ranges in scale from protein conformation to cell organization and tissue function.

Cells plated on various substrates, or microenvironments, can sense the corresponding external applied force. Artificial cell substrates of adjustable viscoelasticity have been instrumental in demonstrating that substrate elasticity significantly impacts cellular mechanotransduction[5,7,8] (i.e., the ability to transfer mechanical signals into biochemical signals) including morphology, cytoskeleton organization and motility. For example, myoblasts grown on substrates with a materials compliance comparable to mature muscle tissue (~12 kPa) develop actomyosin striations characteristic of proper muscle differentiation, whereas those grown on softer or stiffer substrates have been shown to have a different mechanoresponse, and in turn different cytoskeleton organization. Research of artificial substrate design and fabrication for the investigation of mechanoresponse between cell forces related from cytoskeleton, such as F-actin, to focal adhesion structure can benefit the understanding of the mechanism in biochemistry, biophysical and pathological fields[7,9-11]. For example, force transduction via adheren junctions linked to actin on artificial substrates impact not only the cytoskeleton structure but also the cellular mechanoresponse via cadherin linkers. Furthermore, the mechanism of cellular differentiation and development is also able to be guided by appropriate mechanical signaling via changing physical properties of substrates[12-14].

2D and 3D polymeric gel substrates of adjustable stiffness represent the most broadly used substrates in exploring cellular mechanosensitivity[5,12-16]. Such artificial cell substrates mimicking an ECM environment have been a powerful tool with their variable stiffness ranging from 100 MPa to 100 Pa, which can mimic microenvironments from skeleton muscle to neuron cells. A hallmark of such substrates is that cell spreading critically depends on linker density, a parameter, which can be impaired by polymer

artifacts. Moreover, the linker immobilization may hinder the lateral assembly of cell adhesion proteins at cellular adhesion sites, such as focal adhesions and adherens junctions.[17-19] Consequently, polymeric cell substrates with immobilized linkers are not well suited to replicate the plasticity and rich dynamics found at cell-cell interfaces, which includes basal-to-apical movement and treadmilling of adherens junctions in polarized cells[20,21].

Herein, an alternative strategy for novel cell surface-mimicking cell substrates was employed, which is based on a linker-functionalized biomembrane-mimicking polymer-tethered lipid bilayer architecture of adjustable substrate stiffness. Unlike in traditional polymeric cell substrates, individual cell linkers are laterally mobile and free to assemble into largely immobilized linker clusters, thus enabling cell spreading and migration. Two types of linkers were employed, N-cadherin linkers forming cell-cell junctions with plated cells and ECM-mimicking laminin linkers. Substrate stiffness and lipid fluidity of biomembrane-mimicking polymer-tethered lipid bilayer substrates were altered in a complementary manner: (i) by varying the number of bilayers in a multi-bilayer stack and (ii) by modifying the concentration of lipopolymers in a single polymer-tethered lipid bilayer. In addition, polymer-tethered lipid bilayers with micro-patterned mechanical properties were built through a novel fabrication process. To examine cellular mechanosensitivity, cell spreading, migration, cytoskeletal organization, and cellular traction forces were investigated in response to the tunable mechanical properties of polymer-tethered lipid bilayer systems.

The research described within this dissertation focuses on the development of artificial biomembrane-mimicking cell substrates specifically designed to investigate the

impact of viscoelasicity on cellular mechanoresponse. This work has been divided into four main objectives:

Objective 1: Design and fabrication of two types of novel physisorbed polymer-tethered lipid single bilayers (TYPE I substrate) with micropattered lipopolymer concentrations: (i) TYPE Ia - Sharp Boundary Pattern; and (ii) TYPE Ib : Gradual Gradient Pattern.

Objective 2: Analysis of MEF Fibroblast cellular mechanosensitivity on linker-functionalized biomembrane-mimicking single bilayer systems (TYPE I, Ia, and Ib substrates) of different lipopolymer concentration.

Objective 3: Design, fabrication, and characterization of linker-functionalized polymer-tethered multi-bilayers (TYPE II) as cell substrates of adjustable viscoelasticity with the following linker systems: (i) cell-cell junction-forming N-cadherin linkers and (ii) cell-ECM-mimicking laminin linkers.

Objective 4: Assessment of C2C12 Myoblasts cellular mechanosensitivity on biomembrane-mimicking multiple bilayers of different degree of stacking with N-cadherin and Laminin linkages.

1.2 Organization

This dissertation is comprised of five chapters. The first chapter contains the introduction. The second chapter provides the scientific background. The third chapter describes the materials and methods. The fourth chapter outlines the results and discussions of this thesis work. The final chapter contains the conclusion and outlooks.

BACKGROUND

2.1 Methodology

Supported lipid bilayers are biomembrane-mimicking models[22,23] that can be combined with advanced biophysical detection methods to study the biophysical and biochemical properties of biological membranes[14]. Supported lipid bilayers[24,25] are also important tools for nanobiotechnological applications[26-29], such as for the design of a patterned biosurface with well-defined functionalities.

The most widely-used methods to fabricate supported lipid bilayers are by:

a. Langmuir-Blodgett (LB) and Langmuir-Schaefer (LS) deposition.

b. Fusion of lipid vesicles, such as small unilamellar vesicles or giant unilamellar vesicles.

c. Langmuir-Blodgett (LB) deposition and vesicle fusion.

Other techniques of supported lipid bilayer formation were also developed, such as the formation of supported lipid bilayer by spin-coating, in which homogeneous lipid films are formed on the solid supported material after solvent evaporation and by painting.

2.1.1 Langmuir-Blodgett (LB) and Langmuir-Schaefer (LS) Deposition Technique[24-26]

In the LB method, a monolayer of lipids is compressed on an aqueous subphase by the moveable barriers of a Langmuir trough made of Teflon (See Figure 2.1.1, top). A lipid

molecule mixture dissolved within solvents, such as chloroform/methanol or hexane/ethanol, are usually spread at the air-water interface. After total evaporation of the solvent on the surface, for 20-30 minutes depending on the temperature and humidity, the monolayer, also known as Langmuir monolayer, is compressed to the desired film pressure. During the compression and decompression of the monolayer, isotherms are obtained by plotting the surface pressure, which is acquired by a surface pressure detector, as a function of the area. The resulting pressure-area isotherm provides information about several monolayer parameters, such as phase state, lipid packing, and organization of lipid molecules. During LB deposition, the monolayer of amphiphilic molecules will be transferred by a computer-controlled dipper from the air-water interface to a solid support material, such as a coverslip of glass or mica thereby maintaining a constant surface pressure and constant lifting speed (See Figure 2.1.1 center). To avoid the dipping artifacts like holes or feature alignments to the deposition structures, it is necessary to carefully control surface pressure and dipper speed. The deposited monolayer can be stored in air, thereby maintaining its integrity of the film for two to three days.

To form a supported lipid bilayer by monolayer depositions, the LB deposition should be accompanied by a Langmuir-Schaefer (LS) deposition. During LS deposition, the LB monolayer-functionalized solid substrate is pressed like a stamp through the second Langmuir monolayer into the aqueous subphase (See Figure 2.1.1 bottom) The secondary (LS) monolayer can be composed of a different lipid mixture forming an asymmetric supported lipid bilayer. Again dipping speed and accurate pressure control are critical for

the quality of the resulting bilayer structure. Supported lipid bilayers built using subsequent LB and LS depositions can maintain their integrity under water for several days.

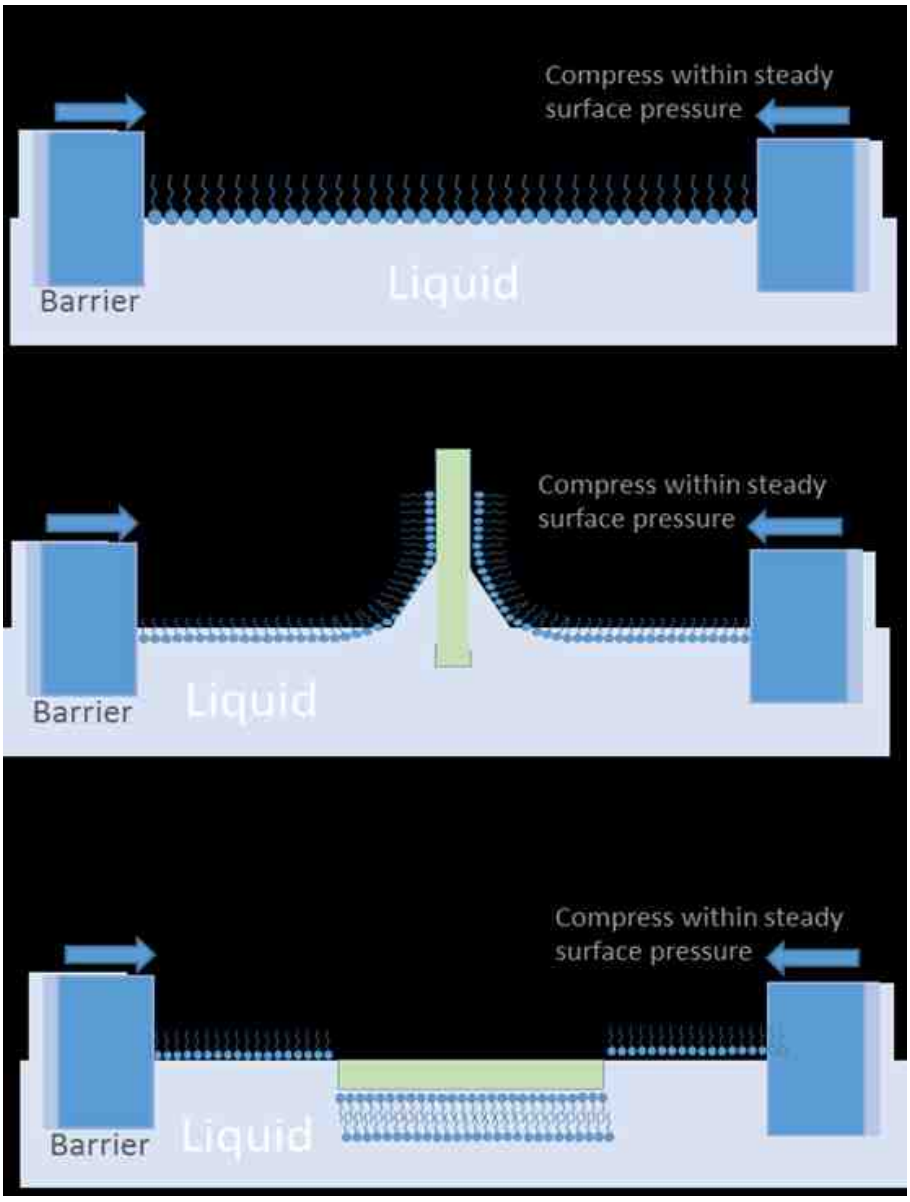

Figure 2.1. 1 Langmuir film, Langmuir-Blodgett deposition, Langmuir-Schaefer deposition and multilayers obtained after repeated deposition.

2.1.2 Multilamellar Vesicles and Multiple Bilayer Stacking via Giant Unilamellar Vesicles (GUVs) [24]

The most simple and broadly used method for preparing supported lipid bilayer is by fusion of small unilamellar vesicles (SUV) and giant unilamellar vesicles (GUV) on solid supported substrates. Lipids are first dissolved in an organic solvent for homogeneous mixing and dried under nitrogen purging and desiccated under vacuum. Lipid films are resuspended in an aqueous buffer yielding multilamellar vesicles.

For small unilamellar vesicle (SUV) formation[30,31], multilamellar vesicle solutions are sonicated using a rod sonicator, while keeping the sample container at a moderate temperature by a surrounding ice bath. The formation of SUVs is indicated by the opalescence of the sample solution. Prior to usage, it is necessary to remove the remaining large vesicles via centrifugation of the SUV solution or filtration of the solution on a nylon membrane. Next, the resulting SUV solution is added to the solid substrate of glass or mica, allowing formation of supported lipid bilayers following an incubation time of 45-60 minutes at 30-45 ˚C. Finally, lipid bilayers are rinsed with Milli-Q water to remove unfused vesicles. SUV rupture and roll out on a solid substrate is driven by attractive bilayer-substrate interactions and high bilayer curvature stress, which is a hallmark of these vesicular systems. This method allows formation of a continuous supported lipid bilayer.

To prepare GUVs[24,32], a lipid mixture is dissolved in organic solvent. Next the organic solvent is evaporated under nitrogen purging leaving a dried lipid film. Next, the dried lipid film is resuspended in an aqueous buffer, which can contain divalent cations

(particularly calcium), placed in hot water bath (75-90 ˚C) for 60-90 minutes to induce vesicle formation. After cooling to room temperature, GUV solutions are poured onto solid substrates or bilayer substrates. After rinsing off the unfused vesicles, multiple bilayer stacked substrates can be used as a biomembrane-mimicking substrate in biophysical and biochemical studies. Such multi-bilayer systems are typically stabilized using specific inter-bilayer tethers[33,34].

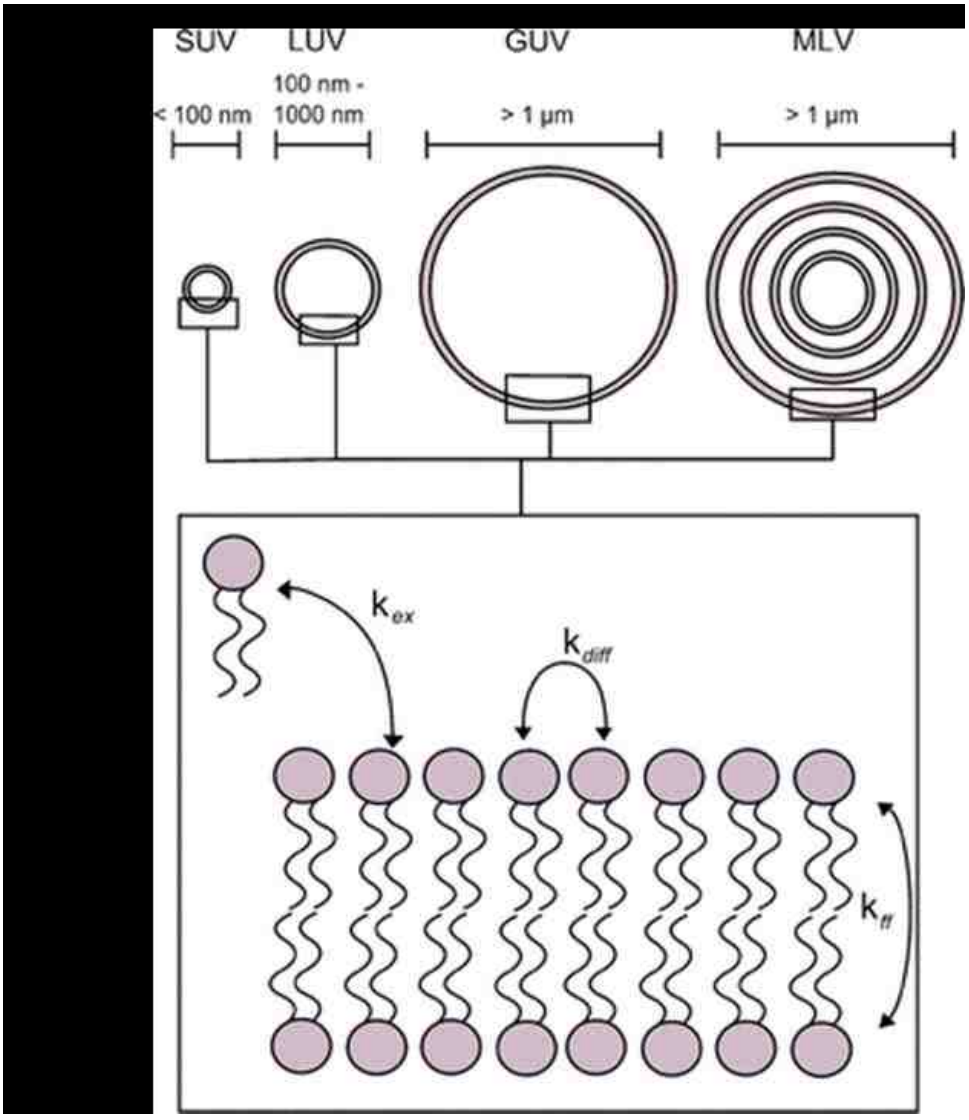

Figure 2.1. 2 Different types of vesicles in use nowadays[35]

Multilamellar vesicle are less suitable for the formation of supported lipid bilayers. While fabrication of supported lipid bilayers by vesicle fusion is rather straightforward, it is limited to the formation of bilayers of symmetric bilayer composition. In contrast, the layer-by-layer assembly of the LB/LS technique enables the design of biologically more relevant asymmetric bilayer compositions. Lipid packing and the lipid lateral mobility in a single supported lipid bilayers formed by vesicles (SUV, GUV) fusion and LB/LS transfers are comparable, resulting in similar lipid diffusivity[24].

2.1.3 Optical Microscopy Techniques

2.1.3.1 Epifluorescence Microscopy (EPI)

One of the most powerful tools for investigation of biological processes, as well as physical, mechanical or chemical mechanisms is fluorescence microscopy that detects the universal luminescence family of processes in which susceptible molecules emit light from electronically excited states. Excitation of a molecule by ultraviolet or visible light photons produce luminescent light that can be formally categorized as fluorescence and phosphorescence, depending upon the pathway of the light emission from excited state falling back to steady state. Fluorescence is a property of some atoms and molecules to absorb light at a particular wavelength and to subsequently emit light of longer wavelength after a brief interval, termed the fluorescence lifetime. On the other hand, phosphorescence has much longer excited state lifetime compared to fluorescence with similar relaxation process as fluorescence.

Advanced fluorescence microscopy combines the power of high performance optical components with computerized control of the instrument and digital image acquisition to achieve a high level of sophistication that far exceeds that of simple observation by the human eye. Microscopy now relies significantly on electronic imaging to quickly obtain information at low light levels or at wavelengths outside the visible spectrum. These technical improvements are not mere window dressing, but are essential components of the light microscope as a system. Nowadays, obtaining the optical image of a specimen is just the beginning toward data analysis. Microscopes help to achieve this first step in conjunction with electronic detectors, image processors, and displaying devices that can be viewed as extensions of the imaging system. With more improvements of the image detail analysis and quantitative exploration, EPI microscopy can help researchers and scholars in their investigation of various fields ranging from the characterization of polymeric molecule to imaging of tissue samples.

2.1.3.2 Differential Interference Contrast Microscopy (DIC)

Brightfield microscopy, which simply requires a basic light microscope, relies on differences in light absorption to produce contrast. In the 1930s, Dr. Zernike established phase contrast microscopy, which is often employed to image challenging specimens, which show a weak contrast in brightfield microscopy. However, the DIC technique has several disadvantages which includes halo artifacts, the restriction to ultrathin samples, and the inability of taking advantage of the full condenser and objective apertures. Living cells and other transparent, unstained specimens are often difficult to observe under

traditional bright field illumination using the full aperture and resolution of the microscope objective and condenser system.

Differential Interference Contrast (DIC) microscopy is a complementary technique applied to enhance contrast to cellular images, allowing organelles and other cellular components to be observed. DIC microscopy is a light-diffracting interference method in which the reference beam is filtered by a minuscule amount. Here, changes in light phase are accomplished by inserting a phase annulus (or phase ring) with a matched objective containing a phase plate into the light path. This optical technique establishes the image with a monochromatic shadow-cast that displays continuous optical paths from high to low spatial frequencies present in the specimen. The phase plate contains a centered, ring-shaped area, which matches the annulus and retards light exactly by a quarter-wavelength. A gradient pattern in the linear path length or refractive index of the specimen, which results in elliptical polarization for the recombined beam that exits the objective Wollaston prism, produces phase difference as the two orthogonal wave-fronts combine. Thus, optimum contrast, field brightness, and sensitivity can be adjusted though the light pathway and heights of the sample stages. In this method, the optical beam is directed through the annulus, the sample, and then the objective before hitting the phase plate.

Major imaging advantages of DIC microscopy include: (i) the ability to acquire an image of smaller specimen features which could be disregarded in the contiguous area with large optical gradients and (ii) the ability of DIC microscopy to enhance the image sensitivity of small specimens next to larger objects (a problem in traditional phase

contrast techniques). However, the disadvantage of DIC microscopy, depending on its application, is the formation of “phase halos” or glowing edges along the boundaries of specimen and background. These halos are a consequence of the phase-retarding ring of the phase plate also transmitting small amounts of the light diffracted from the specimen.

DIC microscopy is broadly used for the observation of biological related specimens, ranging from big living tissue cultures, to polymer samples. Furthermore, DIC microscopy is usually combined with EPI-fluorescence microscopy to investigate the cellular morphology with fluorescent immunostaining methods. When coupled to enhanced video techniques, DIC can be utilized to produce images of structures having dimensions below the optical resolution of the microscope.

2.1.3.3 Laser Scanning Confocal Microscopy [36,37]

Laser scanning confocal microscopy represents another widely used optical microscopy method in the biological, physical, chemical and physiological fields. A modern laser scanning confocal microscope can be considered as a sophisticated imaging system that integrates basic microscopy stand, a complex laser excitation system typically made of multiple lasers with wavelength selection devices, a beam scanning assembly, and a computer for image display, processing, output, and storage that the entire confocal microscope. Unlike an EPI fluorescence microscope, confocal imaging is accomplished using a combination of a monochromatic excitation source and a confocal aperture to aid in eliminating out of plane fluorescence. Here, coherent light emitted by the laser system passes via a pinhole aperture that is situated in a conjugate x-y plane

(confocal). It results in smaller excitation volumes which help to eliminate background noise by exciting only a thin plane at a specific scanning point of the specimen and by placing a second pinhole aperture positioned in front of the detector. A confocal image of high signal/noise is acquired by scanning point-by-point using a scanning stage. The resulting fluorescent image can be observed directly though the eyepieces of the microscope or via a CCD monitor or electronic array detector.

The primary advantage of laser scanning confocal microscopy lies in the ability to serially produce thin optical sections through fluorescent specimens that have a thickness ranging up to 50 mm or more. The ability to image optical sections with reduced background fluorescence results in clearer fluorescent images throughout a sample and allows for 3D rendering. Moreover, optical capability allows the acquisition of three-dimensional images (e.g. for the analysis of a cell) by building a stack of multiple fluorescent images. Modern laser scanning confocal microscopes also allow parallel image acquisition through different fluorescent channels, thus enabling analysis of multiple types of fluorescent probe molecules, while eliminating fluorophore interference much more efficiently than EPI microscopy. Confocal microscopes are used for various applications. They are utilized extensively in the biomedical sciences to study the structure of thick biological samples and in the engineering disciplines to analyze complex structures such as microelectronic circuits.

However, laser scanning confocal microscopy also has some limitations, such as the range of laser excitation wavelengths and laser induced sample damage. For example, narrow bands of UV excitation with a short lifetime are rather expensive to produce on a

confocal microscope system. In contrast, mercury or xenon lamp excitation on EPI fluorescence microscopes result in a broad range of excitation wavelengths from UV-visible to IR spectral regions. Furthermore the relatively high-intensity laser irradiation might damage the various specimens such as living cells and tissues.

In conclusion, confocal microscopy has several advantages over traditional EPI fluorescence microscopy, such as the abilities to reduce the background from the focal plane and capability to acquire 3D images of thick specimens. A further advantage of the confocal approach is that spatial filtering techniques can be employed to reduce out-of-focus light or glare in ultra-thick specimens. Not surprisingly, there has been a tremendous explosion in the popularity of confocal microscopy in recent years, due in part to the relative ease with which high-quality fluorescent micrographs can be acquired from specimens prepared for traditional fluorescence microscopy, and the growing number of applications in cell biology requiring images of cell and tissue samples. The field recently experienced a substantial boost with the emergence of super-resolution microscopy, which allows acquisition of fluorescence images with sub-diffraction limit resolution.

2.1.3.4 Fluorescence Recovery after Photobleaching (FRAP) [38]

Fluorescence recovery after photobleaching (FRAP) is well suited for the analysis of dynamic movement of biological samples For investigation of laterally mobile substrates, such as solid supported bilayers or vesicles, photobleaching techniques are broadly used to measure the transport of a molecule on the surface of and within living

cells and biomembrane-mimicking substrate systems. FRAP methods are based on the photobleaching of defined regions of the substrate to destroy the fluorescence emitted from the region; sequentially, the recovery of fluorescence into that region reflects the type of transport processes occurring. There are many factors to impact the recovery curve, such as the fluorescent molecule diffusion and the mechanism of the fluorescent molecule transport from unbleached area. In sum, the steeper the curve, the faster the recovery and therefore, the more mobile the molecules. Indeed, the FRAP technique has experienced a resurgence in popularity during the couple of decades, as it is quite suitable for analyzing the lipids and proteins. [39,40]

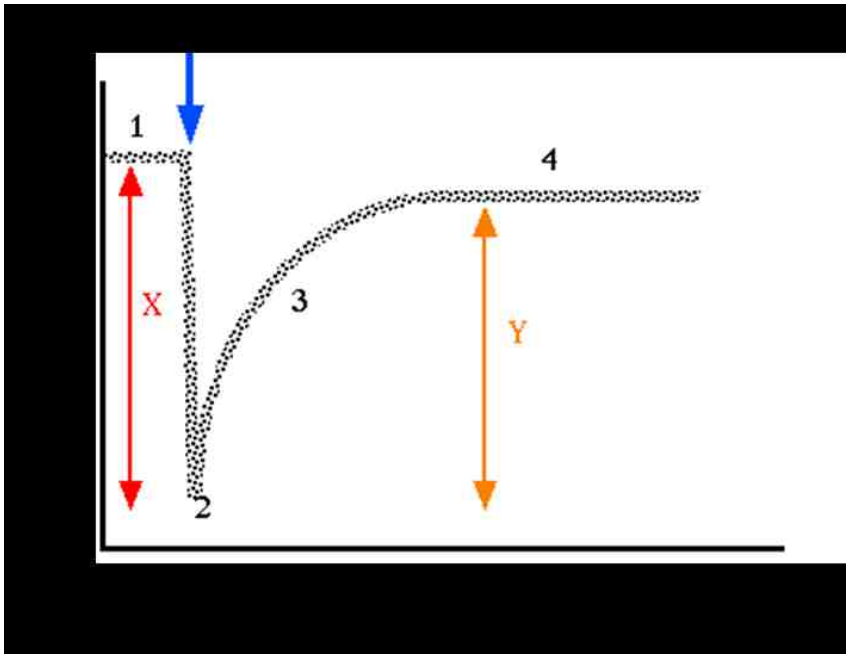

Figure 2.1. 3 Graphical representation of data collected during a FRAP experiment. A baseline of fluorescence is collected as following; (1) original intensity before the photobleaching (2). Over time, fluorescence increasing in the photobleached area from diffusion of fluorescent molecules from unbleached reservoir (3) then, stabilization of the amount of fluorescence recovery (4) and a steady flattop curve is observed. The percent recovery uses the formula: (Y/ X) x 100% = % recovery.

In the case of a bilayer substrate, the experimental data can be fitted using the following Gaussian diffusion equation (eq. [1]):

$$F(t) = F_{final}\sqrt{(1 - w^2(w^2 + 4\pi Dt)^{-1})} \quad [1],$$

where F(t) is the intensity as a function of time; t= 0 is the initial point ; F(final) is the final intensity reached to the after complete recovery; w is the width; and D is the diffusion coefficient constant. To switch from the 1D Gaussian model into a 2D model, the fluorescence intensity of the photobleached area can be described as:

$$I_{rn}(\mathrm{x.y}) = \frac{2\,I_{final}}{\pi r_n^2}\exp(\frac{-2(X^2+Y^2)}{r_n^2}) \quad [2],$$

where r_n^2 is the radius of the photobleached region. Then, the concentration of the fluorescent probe C(x, y, t) can be described by the diffusion equation:

$$C_t = D\ \Delta C \quad [3],$$

Here, D is a diffusion coefficient and $\Delta = (\delta^2/\delta x^2) + (\delta^2/\delta y^2)$, then the convolution of the fundamental solution of the diffusion equation can be expressed by:

$$C\ (x, y, t) = \iint C(x - x', y - y', 0)\emptyset_{Dt}(x', y')\,dx'dy' \quad [4],$$

where $\emptyset_{Dt}$(x,y) in Equation 4 is:

$$\emptyset_{Dt}(x, y) = \frac{1}{4\pi Dt}\exp(\frac{-(x^2+y^2)}{4Dt}) \quad [5],$$

and the fluorescent intensity of the lateral dye lipids is:

$$F(t) = q\ \iint \varepsilon\, I_{rn}(x, y)C(x, y, t)dx\,dy \quad [6],$$

Eq. 6,. has been simplified into Eq. 7 to [40]

$$F\ (t) = Fi\ \left\{1 - \frac{K}{1+\gamma^2+{}^{2t}/_{\tau_D}}\right\}M_f + \left(1 - M_f\right)F_0 \quad [7]$$

where $\tau_D = r_e^2/4D$ and $\gamma = r_n/r_e$ and $M_f = F_\infty - F_0 / F_i - F_0$; $F_{1/2} = (F_0 + F_\infty)/2$ and $F(\tau_{1/2}) = F_{1/2}$

$$F_{1/2} = \frac{(F_i - F_0)}{2} M_f + F_0 \quad [8]$$

Applying the $F_{1/2}$ back to Eq. 7 eventually provides the simplified equation for a confocal FRAP experiment, which is :

$$D_{confocal} = \frac{2r_n^2}{8\tau_{1/2}} = \frac{1}{4}\frac{r_n^2}{\tau_{1/2}} \quad [9]$$

Eventually, both Axelrod's method[41] using a Gaussian laser and Soumpasis' [42]method using a uniform laser, result in the following equation:

$$D_{Exp} = 0.224\frac{r_n^2}{\tau_{1/2}} \quad [10]$$

The simplified equation [10] enables quantitative analysis of confocal FRAP data from the 2D bilayer substrates, thus benefiting many biochemical and biophysical studies using laser scanning confocal microscopy.

2.1.4 Atomic Force Microscopy (AFM) [43]

During the past decades, atomic force microscopy (AFM) has developed into a powerful method of supported lipid bilayer characterization at the nanoscale[44]. AFM not only enables visualization of the nanoscale structures of a lipid bilayer under physiological condition, but also AFM allows monitoring of dynamic events such as bilayer modifications and remodeling. AFM is also a well-established method for imaging the lateral organization of phase separated supported lipid bilayers. In a previous AFM study[45], hydrated bilayers made of a mixed DMPE and DPPE (19:1) on DPPE-coated mica were imaged, revealing the coexistence of fluid and crystalline domains within the supported lipid bilayers via AFM images . In another example, two-phase coexistence was also observed in a supported lipid bilayer comprised of a binary mixture of DOPC/DPPC (1:1)

in buffer. In this case, the step height measured between the two phases is 1.1 nm, which results from a difference in the thickness and mechanical properties of the DOPC and DPPC films. Blanchette et al.[46,47] investigated the impact of cholesterol to the ternary system of DLPC/ceramides/cholesterol using AFM, these researchers observed that this ternary mixture only displayed L_d/S coexistence and no L_o phase even at elevated cholesterol level. Chiantia *et al.* [48] combined AFM, confocal fluorescence microscopy and fluorescence correlation spectroscopy to probe the supported lipid bilayers consisting of sphingolipid/DOPC/cholesterol/ceramides. The authors observed three coexisting phases within the bilayer: L_d enriched in DOPC, L_o enriched in sphinogolipid and cholesterol, gel enriched in ceramide.

Besides the investigation of nanoscale organization of lipid bilayers, AFM has also been used for investigating supported lipid bilayers in the presence of other important biological materials. For example, AFM was utilized to monitor the bilayer-detergent interaction for the fractionation and reconstitution of membrane components, with the aim to perform biophysical and structural studies of biological membranes and proteins. AFM has also emerged as a powerful tool for visualizing the interaction of a supported lipid bilayer with short peptides and proteins, which play essential roles in a number of biological events like membrane fusion and membrane lysis. AFM was also employed to investigate bilayer-drug interactions, in which the toxicity and activity of drugs could be demonstrated in terms of their impact on the structure and organization of biological membranes.

AFM is also suitable to explore membrane-nanoparticle interactions, thus enabling the design of nanoparticles for biomedical applications, such as medical imaging and drug/gene delivery.

Overall, AFM is now a powerful tool in biomembrane research, which is particularly well suited for monitoring coexisting micro- and nanoscale domains in supported lipid bilayers, and for observing membrane remodeling and alternation upon interaction with solvent, detergent, peptides and nanoparticles. AFM analysis also represents a viable strategy for characterizing other properties of supported lipid bilayer architectures, such as membrane elasticity and bilayer pore formation. AFM analysis can also be combined with other techniques, such as stimulated emission depletion far-field fluorescent microscopy, and secondary ion mass spectrometry, thus suggesting a wide range of new applications in future membrane research.

2.1.5 Traction Force Microscopy[49]

Traction force microscopy represents a powerful experimental tool that allows the analysis of cellular traction forces of migrating cells. Analysis of cellular traction forces is quite valuable as it provides important insight into cellular mechanosensitivity, with potential significance in biological processes including angiogenesis, inflammation, wound healing and metastasis formation. At the cellular and subcellular levels, the forces generated from a cell are just a few nN, which makes their accurate detection rather challenging. Yet, traction force microscopy provides a method for determining cellular traction forces with high accuracy.

Most of the cells in culture are typically adhering to a solid substrate to grow and survive. The adherent agrin of a cell develops tension via actomyosin interactions inside cells. The cellular tension is transmitted to the underlying substrate through focal adhesions (FAs) located on the substrates and linked with actin stress fiber inside the cells. The tensile force is referred to as cell traction force. It is well-known that the traction force at on single FA agrin to substrate is around 10 nN. However, the various factors of the microenvironment, such as substrate stiffness could impact the cell traction force and the cellular mechanoresponse.

Prior to the emergence of traction force microscopy, several alternative methods were used to estimate cellular traction forces. Among the earliest methods[50] was a cell-populated collagen gel (CPCG), which mixed cells with liquid collagen to form a polymerized gel disk. After the solidation of the gel, cells adhere to the collagen gel, thereby generating traction forces. Cellular traction force analysis by the CPCG method was accomplished by measuring the change in diameter of the gel disk. However, this method only allows semi-quantitative measurements of cellular traction forces. Furthermore, it is not accurate enough to allow single cell analysis. Another technique was applied by floating a PDMS membrane in growth medium. In this method, cells attach to the PDMS gel in medium [51] and caused the PDMS surface to wrinkle, which allows the traction forces to be measured quantitatively. The micro-patterned elastomer method was also developed for measuring cell traction force by the motion of the elastomer and stiffness of the substrates. However, this method does not provide a completely flat surface for cell adhesion.

Three major research groups, Dembo and Wang[52], Butler[49], and Yang[53] have been instrumental in developing the cellular traction force method which uses an elastic polyacrylamide gel (PAA) substrate with embedded fluorescent beads to measure cellular traction forces. Traction force microscopy involves three major steps. The first step is to fabricate elastic PAA gels substrates with a flat surface. In the second step, the researcher has to acquire a pair of "null force" and "force loaded" fluorescent microscopy images, from which the displacement field can be determined based on the movement of a fluorescent marker on the PG surface. Finally, the substrate deformation is used to calculate cell traction forces via software such as Matlab.

To fabricate PAA gel substrates, an acrylamide/Bis-acrylamide mixture is added to a pretreated glass coverslip of a circular dish after being mixed with micron sized fluorescent beads. Stiffness of PAA gel substrate is controlled by the percentage of the acrylamide in the PAA gel substrate, which can impact cellular traction force and cellular mechanoresponse. Following exposure to UV light and removal of excess Sulfo-SANPAH, the substrate can be coated with ECM proteins, such as fibronectin or collagen type I. Next, additional material can be coated on top of the ECM protein layer using specific crosslinker molecules. After preparation of the traction force microscopy assay, target cells can be placed above the substrates for incubation. Initially, "force loaded" images are acquired using an inverted microscope, followed by detachment of cells via trypsinization and acquisition of the corresponding "null force" image. Comparison of

bead positions in “force loaded” and “null force” images allow calculation of the displacement field as shown in Fig. 2.1.4.A.

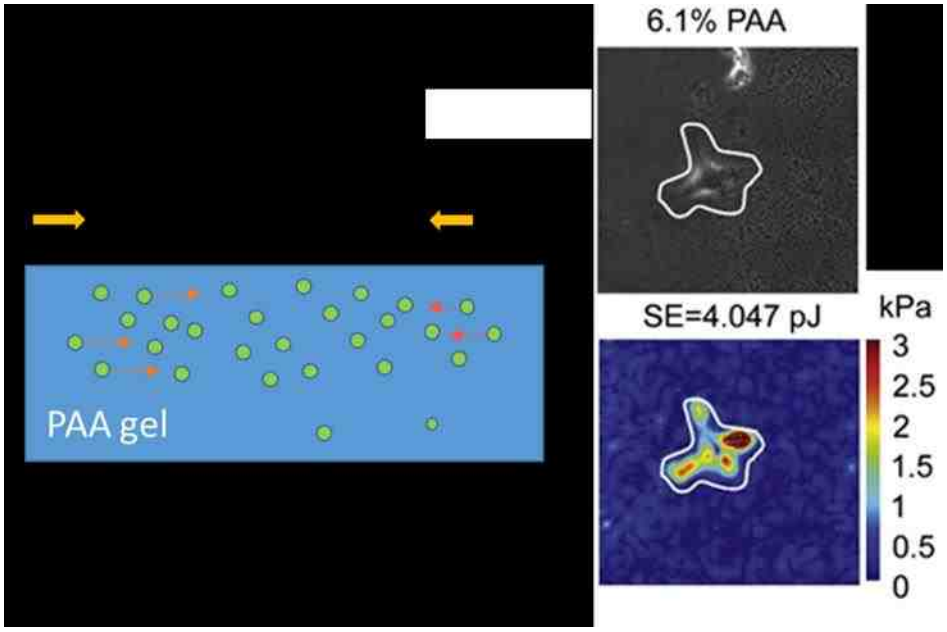

Figure 2.1. 4 Traction Force Microscopy for Fibroblast cells on PAA gels with fluorescent beads.[54]

The determination of cell traction forces can be described in a formula for elucidation of an inverse problem, which calculates for the cell traction force via bead displacement. Most of the research groups including Dembo and Wang[52], and Butler[49] use the Boussinesq analytical solution as the forward model, the expected displacement at any point, xj of an elastic substrate due to n cell traction force can be expressed in a general discrete convolution form as shown in Eq. [10]

$$d(Xj) = \sum_{i=1}^{n} G(Xi - Xj) * F(Xj) \qquad [10],$$

where F(*Xj*) is the point force acting at *Xj*, and G(*Xi-Xj*) represents the forward model that computes the displacement at *Xj* due to force at *Xi.* The convolution can also be elaborated as following:

$$[A] * \{F\} = [d] \text{ where } A\ i,j = G(\ Xi - Xj) \quad [11]$$

where [A] is a full rank matrix, [F} can be found by simple inversion based on the approach of the Butler group. Both force points and the displacement points to the reside on regular grid as standard samples can be conducted to the computation in the frequency domain. Thus, the back substitution of force can be resulted as iteration until the force in the interior of a cell converge.

On the other hand, the method employed and developed in Dembo and Wang's group[55,56] enable the computation of the force via Bayesian a posteriori statistics. In an FEM formulation based on Zienkiewicz's theory, the force can be computed based on the displacement on the known substrate system and the adoption of adequate involves two major factors: measured displacement of fluorescent beads [d} and the stiffness of matrix substrate [K] with the force vector as the equation below:

$$[K] *\ [d] = [F] \quad [12]$$

By expressing the displacement in traction-free nodes as a formula of those at the prescribed displacement node, the cell traction force can be modified through multiplication as the following:

$$[F'] = [K] * [d] \quad [13]$$

Where [d} represent the displacement and [F'] is the corresponding cell traction forces. Cellular traction force can be calculated based on Equation [13] via matlab software.

Finally, the cell traction force can be computed as illustrated in Fig. 2.1.4.C, thus providing valuable insight into cellular focal adhesion forces.

Traction force microscope technology provides automation and real-time tracking of cell traction force for observation of the cell mechanoresponse and cell migration. In that sense, it is also a useful tool for examining cellular biological processes, which are associated cellular actomyosin machinery.

2.2 Cell Migration & Cellular Mechanosensitivity

Cells can transduce mechanical signals into a biochemical response. The process is known as mechanotransduction[57]. But the subcellular mechanisms during cellular mechanotransduction are not well understood. Mechanical forces applied to a cell from surrounding microenvironments such as extracellular matrix, can cause the conformational change of membrane proteins at cell adhesion sites[58]. Such conformational changes can stimulate particular signaling pathways[29,30] and gene expressions[59]; thus, it can ultimately alter cell morphology[60], change cell migration speed and direction[61], and cause the alternation of binding proteins in focal adhesion sites[62].

2.2.1 Cell Migration

Cell migration analysis provides a simple strategy for observing many diverse cellular functions and behaviors such as cell motility, cell-cell adhesion and ECM

remodeling. Single cell migration allows us to study cell movement contribution to many physiological motility processes, such as development, immune cell surveillance, and cancer cell metastasis.

There are two major categories of cell migration: collective cell migration[63] and single cell migration[63]. Collective cell migration has been proven as one of the main steps of embryonic growth[64]; single cell migration is strongly addressed as a major process of metastasis[65], which is highly related to cancer cell invasion. Recently, there are several approaches to investigate the mechanisms of cell migration in vitro within different microenvironments. (Shown as Table 2.1.1)

Table 2.1. 1 Artificial substrates for investigation of cellular mechanoresponse[11]

Model	Cell Type	Substrates	Parameters assessed	Ref
2D scratch wound assay	Epithelial cells.	Plastic and Polymeric gel, supported lipid bilayer on glass slides	Stiffness of substrate, different adhesion linkage, and individual or collective cells.	[66]
3D sprouting and invasion assay on to a 3D ECM	Endothelial and epithelial cells.	3D ECM-coating hydrogels	Strand length, cell numbers and extracellular proteolysis	[67,68]
3D organ explant culture	Mammary ducts and primary cancer tissues	3D matrigel or 3D collagen	Strand length, branching and location of epithelial and stromal cells.	[69-71]

2D models include the popular scratch wound assay that allows polarization, force generation, and mechanisms of cell-cell junction and cell-ECM adhesion to be studied for cellular mechanoresponse and cell migration research[66,72]. Different mechanical

properties of substrates, like stiffness and plasticity, would impact the cell migration and its related cell behaviors. 3D ECM-coated scaffolds[67,70] were also employed for investigation of cell migration, in which vertical invasion of cells into a tissue matrix could be reproduced in 3D ECM culture. Cellular migration as a single invasion pattern or cancer invasion sprouting into tissue coating can also be studied using 3D matrigel and collagen models.

Single cell and collective cell migration modes serve mutually exclusive purposes during morphogenesis, tissue regeneration, and during pathological conditions[73,74]. Collective cell migration is essential for the establishment, shaping and remodeling of complex tissue and tissue compartments, such as ducts and vessels. Otherwise, single cell migration enables a cell to cover local distance, to integrate into tissues, also observed during neural crest cell migration, or to move from one location to another in the body and fulfill effector functions like immune cell trafficking and protrusion processes of cancer cells during metastasis. Although the complete mechanisms[15] of cell migration modes are not fully understood, some key factors have been identified , which maintain, or cause an increase or decrease of activity, or initiate transitions of cellular motility[75,76].

2.2.1.1 2D Cell Migration

2D models have been broadly used for investigation of cell migration due to convenience of observation and tracking of cells on a flattop surface[75]. In general, single cell migration can occur with amoeboid or mesenchymal shaped cells. Amoeboid migration commonly refers to the movement of a rounded or ellipsoid shaped cell that lacks mature focal adhesions and stress fibers during migration[77]. These cells with blebby

peripheral structure can migrate fast and lack the formation of the pseudopodia (temporary actin fiber formation). In 2D models with accessible adhesion sites, cells with terminal mature non-adhesion sites can migrate with their leading edge and form an entanglement with substrates to establish focal adhesion sites. As Figure 2.2.1 (1) cells polarize in response to a stimulus/signal and protrusions called lamellipodia (flat protrusions containing a network of actin filaments) and filopodia (containing parallel fibers of actin filaments) are formed at the leading edge of migrating cells[15]. The filopodia's role during the migration cycle is to sense the microenvironment and surroundings whereas formation of lamellipodia is associated with directional guidance of migrating cells. Cells with high levels of attachment and cytoskeletal contractility typically display mesenchymal migration, which involves localized cell-matrix interactions at focal adhesion sites, and movement in a fibroblast-like manner. Formation of cellular protrusions during cell migration is driven by actin polymerization, which happens underneath the cell surface regulated by specific actin-binding proteins. Lastly, cell motility also requires disassembly of focal adhesions at the cell's tail in Figure 2.2.1 [78] Interestingly, there are a few in vivo examples for observation of 2D cell migration, such as epithelial keratocyte migration across a flat 2D substrate using rapid spread-out cell gliding.

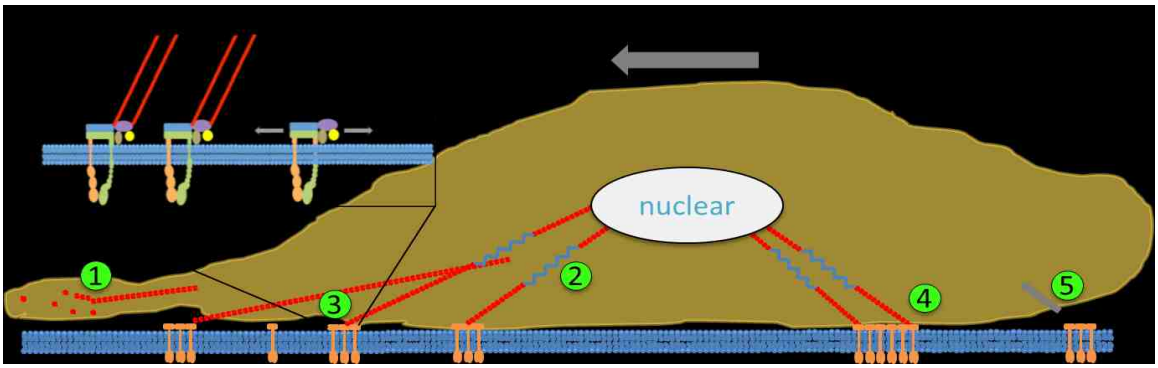

Figure 2.2. 1 Cell migration on a 2D substrate. [78]

Besides the single cell migration mechanism, collective cell migration of a cohesive cell group is particularly prevalent during embryogenesis and drive the formation of many complex tissues and organs. For example, mechanistically distinct types of cell movements in embryological development, tissue and cancer invasion are highly influenced with the collective migration regulated by surrounding microenvironments. On 2D substrates, collectively migrating cells move as 2D sheets single cell level or along to form a single-layered epithelium, and start subsequent proliferation and thickening as a multiple-layered epithelium. Actin-rich pseudopodia and lamellipodia lead the migration and follower cells, which are connected each other via adherens junctions. Cells interact with the basement membrane via integrins in focal contact sites. Cell-cell cohesion is mediated by adherens junction proteins, including cadherins, other immunoglobulin superfamily members and integrins, all of the proteins are directly or indirectly connected to F-actin or filament cytoskeleton structures. Cell-cell adhesions and coupling to cortical actin cytoskeleton structure are mediated with various cadherins,

such as E-cadherin for epithelium formation, N-cadherin for stromal cell-cell contacts, and VE-cadherin for angiogenesis.

Most mechanisms of collective cell migration are similar to single cell migrations, including principles of actin turnover and polarized force generation by moving cells. However, the group of cells are shared and coordinated between cells at different positions. The cortical actin network in the cell group shows multiple-cellular organizations, such as anterior protrusion activities and posterior retraction dynamics involving multiple cells. The mechanism controlling collective cell cytoskeleton organization is not very clear due to the difficulty of observation of cellular mechano-response on current artificial biomembrane-mimicking substrates.

2.2.1.2 3D Cell Migration

Most cells in vivo are embedded in a 3D environment[49,53]. Consequently, many scientists have focused on the design and characterization of artificial substrates that allow analysis of cell migration and growth in 3D matrices. In particular, it has been of interest to explore whether cell migration in 2D and 3D models can be described by comparable mechanisms. For example, in a 3D matrix, it has been observed that cells do not show distinct focal adhesions or with small focal adhesion sites lasting only a very short time period. Fraley *et al*[79]. reported that HT1080 cells in 3D matrix contain some pseudopodia, which were neither similar to filopodia or lamellipodia. They also investigated the same cell line in 2D and 3D models and compared the migration speed of wild type HT1080 and concluded that 2D migration behaviors were not correlated to 3D migration patterns. To illustrate the new mechanism in 3D models, Petrie *et al*[80]

proposed “lobopodial migration”. This theory states that lobopodia are large, blunt, and cylindrical protrusions used for cell migration in 3D models. They also claim that cells would alternate between the lobopodial-mechanism and the lamellipodia mechanism based on the linear elasticity of different ECM substrates. It was found that cells migrate via a lobopodial mechanism while attaching to linear elastic substrates.

In 3D environments[6], cells migrate between pores and holes and attach on the linear elastic substrates. It has been shown that cells start remodeling or getting deformed depending on the size of pores (physical properties) and the stiffness of 3D substrates (mechanical properties). The strength of adhesion sites between cell and substrate is a one of the major factors for cell migration speed in 3D models. With higher adhesion strength, cells move much slower and start degrading the substrate. Another main factor that impacts cell migration is related to cell shapes in 3D matrices; in mesenchymal shape, cells are able to degrade the substrate like fibroblasts; in amoeboid shape[81], cells move faster and do not damage the structure of substrates or surrounding matrix.

2.2.2 Cellular Mechanotransduction Mechanism

Analysis of cellular mechantransduction, the mechanism by which cells convert mechanical signals into a biochemical response, has focused on the identification of critical mechano-sensitive molecules and other cellular components[82]. Like behaviors of cell migration, differentiation and proliferation, there are several mechanical parameters in the physiological environment to investigate influence of cell behaviors from mechanical force, which cells respond to cell-microenvironment interaction. At the same

time, several advanced methods and technologies such as nanotechnology, micromanipulation[83], biological imaging[84], and computer modeling[85] have been applied for the analysis of cellular mechanotransduction between a cell and its surroundings.

The field of mechano-biology has been driven by a search for specialized proteins[86-89], which change their chemical activity state in response to mechanical cues, thereby converting mechanical energy into biochemical energy. However, the function of virtually every molecule[90] could potentially be altered by mechanical stimuli in the process of carrying out their biochemical activities. One major mechanical stimulus[19,91] for a cell can be the mechanical properties of the cell substrate, which cells are cultured in/on. Stiffness of the substrate is considered as one of the main mechanical substrate properties known as stimulus for cell behaviors. Wang and Pelham[92] in late 1990s showed that cells are impacted by the mechanical properties of the substrate, which is demonstrated on polyacrylamide gels with tunable stiffness via concentration of acrylamide/bis-acrylamide. Spreading area of cells on stiffer substrates is higher compared to cells on softer substrates; as well as the migration speed of cells on softer polyacrylamide (0.55 μm/min) is faster on comparable stiffer PAA gel (0.06μm/min). Furthermore, the focal adhesion size of cells on softer substrates is typically smaller and irregularly shaped compared to those on stiffer substrate.

Another source of mechanical stimulus for cell can be the external forces applied to cells[58,93,94]. Differentiation of force amplitude in different tissues may range from 10 nN to 10 kN. For instance, on bone and cartilage tissue, cells are under cyclic stresses of both tension and compression around 9kN[95]; During cardiac cycle, cells feel shear,

compressive, and tensile stresses, whereas cells on inner vessels experience shear forces from blood flow. There are many techniques for mimicking the externally applied mechanical stimulus to cells, such as magnetic tweezer[96], substrate stretching[94,97] and atomic force microscopy,[61,97,98]. The single-cell mechanoresponse is usually explored using artificial substrates with tunable mechanical properties.

Currently, it remains unclear how the whole cell processes this molecular scale mechanical information and orchestrates a physiologically relevant response in the context of the multiscale architecture at tissue level. To understand how cells react to mechanical stimuli in a tissue environment, the close cooperation of various complementary fields such as biophysics, molecular cell biology, physiology, anatomy, engineering, and computer science, is required. Major mediators for cellular mechanotransduction can be categorized into four fields: **a. Ion channels, b. Cell membrane, c. Nuclei, d. Focal adhesion and cytoskeleton.**

a. Ion channels[82,99,100]

In general, the plasma membrane is somewhat permeable with respect to smaller and more hydrophobic molecules. In contrast, transport of larger molecules and ions across the membranes is efficiently blocked by the lipid bilayer of the plasma membrane. Ion channels, which consist of protein complexes that are selective to specific ions, play an important functional role in that they are important regulators of controlled ion transport across cellular membranes. Interestingly, some of the ion channels have been found to be mechanosensitive[101] By using

patch-clamp techniques, it was observed that induced conformational changes of ion channels led to a modulation of their cation-transporting activity. Specifically, the change of ion channel conformation was found to alter the rates of opening and closing speed through the distortion of intramolecular gating domains.[102]

b. Cell Membrane[103]

G-protein coupled receptors (GPCRs) are cell membrane proteins, which are involved in signaling cascades associated with smelling, sight and tasting. Some of the signaling pathways depend on more than one receptor. For instance, adrenalin interacts with 9 different GPCRs, and some are known to be mechanosensitive related to their signaling cascades[104]. Conformational change of the protein receptors can be altered by applied shear force[105]; thus, GPCRs could be activated without ligand binding, or de-activated with bound ligands by mechanical stimuli. Properties of plasma membrane like fluidity and polarity can also be involved in mechanotransduction pathways on cellular membranes, in addition to mechanotransduction-related processes involving membrane protein receptors.[106]

c. Nuclei

Two types of methods have been pursued to investigate the impact of mechanical properties on the cell nucleus. In one case, the cell nucleus is examined in its natural state inside the cell. In the other case, experiments are conducted on an isolated nucleus[107] . With nucleus isolation performed by mechanical or chemical techniques, it was observed that the stiffness of the cell nucleus is higher than typical stiffness values of cell membrane and cytoplasm[108]. Interestingly, while adherent cells detach from substrates, their nuclei change shape and become rounder. Such a shape change has been attributed to changes in hydrostatic pressure or lack of stretching in the adherent state[109] It also has been reported that cell nuclei are under constant mechanical load and that the mechanical properties of cells are viscoelastic and highly nonlinear[107]. There is some experimental evidence[110-112] that externally applied mechanical forces can deform the nucleus and change the cell shape. In response to the applied force, such as a shear force, the cell nucleus can become notably stiffer. Under shearing force, 3T3 fibroblast were found to show cytoskeleton reorganization and increased nucleus movements. Thus, change of cell shape and nuclei can affect cell phenotypes[112] .

d. Focal adhesion and cytoskeleton

Focal adhesions are anchoring spots of cells to their substrate. According to recent research[113] , the main membrane proteins involved in focal adhesion binding site are “Integrins”, which form a connection between ECM and cytoskeleton. FAs are sophisticated mechanosensors as they change their size and connectivity to the cytoskeleton in response to mechanical stimuli. The linkage between integrins and actin filaments of the cytoskeleton is regulated by a large number of proteins, which include, vinculin, talin, FAK, and paxillin. As exemplified by paxillin, mechanical cues are associated with changes in the phosphorylation activity. Other proteins, like Rho and Rho A kinase, are also involved in the FA-associated mechanoresponse and mechanotransduction[114] . For example, by tuning substrate stiffness, human stem cells show altered levels of calcium ion concentration, a process which is strongly regulated via Rho A kinase[13]. External applied force[115,116] from substrates with various mechanical properties is another major factor to impact the focal adhesion assembly and disassembly. There is also a close relationship between mechanical stimuli and cytoskeleton organization. This is most strikingly demonstrated by the altered organization of actin filaments in response to changing substrate stiffness. Mechanical signals may also result in

changing actin polymerization during cell migration. Microtubules, another important component of the cytoskeleton, are also involved in the mechanotransduction pathway, as illustrated by altered actin filament formation and motor protein action.

2.2.3 Other Key Characteristics of Cellular Mechanosensitivity

Based on recent research, there are several major indicators for analyzing cellular mechanosensitivity in biophysics and physiology as described in the results and discussion section: **1. Migration behavior, 2. Cell spreading area, 3.Cellular cytoskeletons, 4. Focal adhesion size, 5. Cellular phenotype, 6. Cell stiffness, and 7. Cell proliferation.**

In 2000, Lo *et al.*[91] reported a substrate with tunable stiffness for the investigation of cell migration on 2D artificial substrates, known as durotaxis. Durotaxis was also used to analyze cell migration in 3D collagen matrices, demonstrating distinct cellular mechanoresponse. As reported[12,117], mesenchymal stem cells are able to detect the substrate stiffness gradients and migrate from the softer side to the stiffer side of substrate. Also the spreading area and proliferation of stem cells on polydimethylsiloxane (PDMS) substrates are much higher on stiffer substrates[118]. For example, unlike on the softer substrates, stem cells on stiffer substrates increasingly display biomarkers representative of osteogenic cells.

In 3D collagen model[61,98,119], cellular mechanoresponse of 3T3 fibroblasts is illustrated by a close relationship between substrate stiffness and cell stiffness, indicating organizational changes of the cytoskeleton. Here cell stiffness can be examined using

atomic force microscopy. According to research from Coughlin and Fredberg[120], metastatic kidney cancer cells have higher stiffness of cell membranes compared to the same cells with milder metastatic capability. Interestingly, Miron-Mendoza *et al.* [121] reported that 3T3 fibroblasts exhibit enhanced proliferation in 3D collagen gels of higher stiffness, whereas the spreading area and migration of 3T3 fibroblasts was not impacted by substrate stiffness. Ligand density represents another parameter that affects cellular mechanosensitivity. For example, smooth muscle cells placed on a substrate with patterned ligands have different migration speeds in regions of lower ligand density[122,123] and patterning[124] relative to regions of higher ligand density. In the case of mammalian epithelial cells, it was also reported that the ligand density influences the cell spreading and migration of different cell phenotypes[10]

2.2.4 Cellular Adhesions

Most eukaryotic cells have cytoskeleton organization, which not only maintains the shape of cell, but provides mechanical and supportive functions.[125] The three major types of filaments in the cytoskeleton are the following: intermediate filament, microtubule, and actin filaments. Actin filaments are flexible fibers consisting of actin monomers, which are highly related to the formation of focal adhesions and mechnotransduction. While mammal cells placed on ECM-coated substrates, motor protein, myosin, on membrane interact with actin filaments unknown as “stress fiber”. Cytoskeleton organization, such as the ratio of stress fibers, was proven to be correlated to surrounding microenvironment mechanical properties. Moreover, stress fiber were

shown to be attached to the complex of focal adhesion proteins on cell membranes illustrating the important role of cytoskeleton and focal adhesions in cell mechanisms.

2.2.4.1 Focal Adhesions

In 1971, focal adhesions were first discovered by Abercrombie *et al* [126] via interference reflection microscopy. While attached to ECM substrates, cells assemble particular adhesion proteins at focal adhesions, which represent complex and dynamic structures at the cell membrane[127]. As shown in the figure below, integrins play a key role within focal adhesion structures. These α and β heterodimers[128] elongate to extend from the cytoplasm to the extracellular region, thereby forming a linkage between cytoskeleton (via actin-binding proteins) and extracellular matrix (via ECM proteins like fibronectin and laminin) [129] Hereby, different types of integrins of the integrin family show distinct binding affinity to specific ECM ligands. For example, $\alpha_3\beta_1$ and $\alpha_5\beta_1$ integrins bind most commonly to collagen and laminin, while $\alpha_2\beta_1$ and $\alpha_3\beta_1$ preferably attach to fibronectin[130]

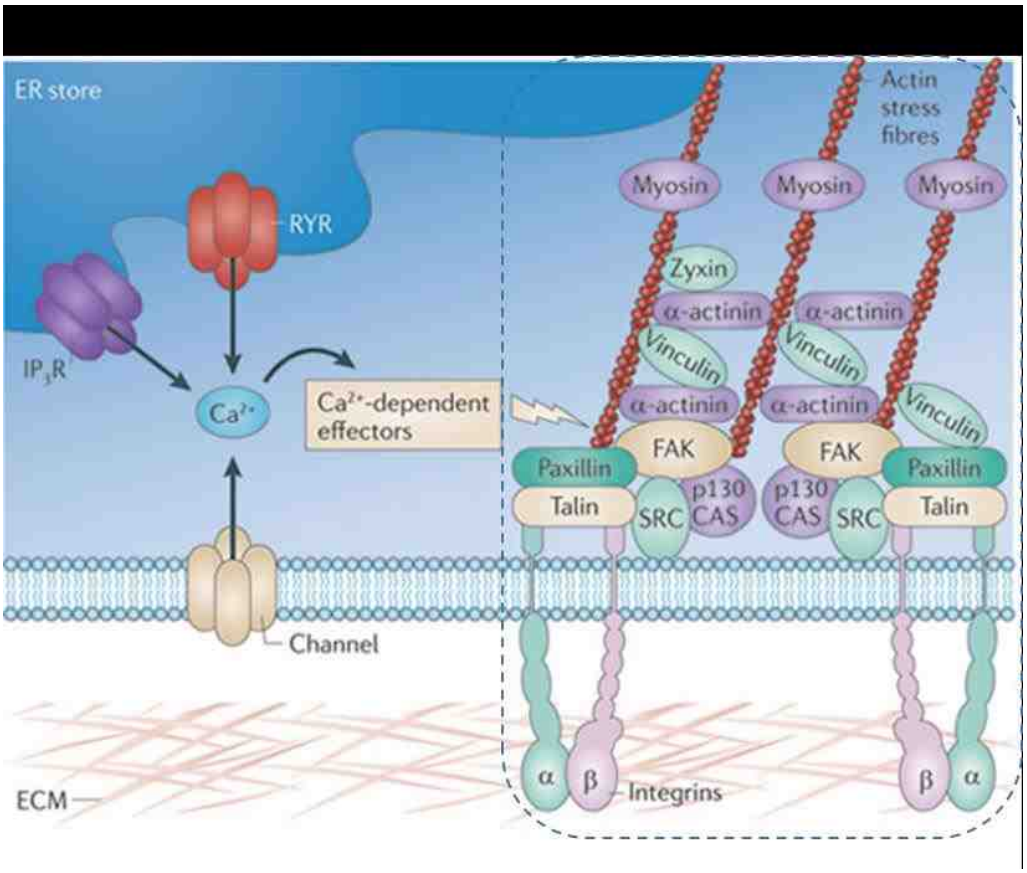

Figure 2.2. 2 Complex of Integrin and surrounding proteins on cell membrane[127,131]

Integrins are not only important adhesion proteins, but also play a pivotal role as signaling proteins in inside-out and outside-in signaling. During such signaling processes, integrins can not only collect information from microenvironments but also send the signal into the cell via their association with focal adhesions and linkage with the cytoskeleton. In fact, integrins can contribute to many different signaling cascades[132]. A hallmark of focal adhesion formation is the clustering of integrins. However, the functionality of focal adhesions not only depends on integrin assembly, but also on a wide range of regulatory, focal adhesion-associated proteins, such as vinculin, talin, and focal adhesion kinase (FAK) exemplified by FAK, protein functionality typically depends on the

presence of multiple adaptor proteins. All adaptor proteins are important for formation of focal adhesions as they form a bridge between integrins and actin filaments. For example, fibroblasts deficient of talin cannot form stable focal adhesion sites and are unable to maintain lamellipodial structures[82].

Focal adhesion formation and maturation is associated with several stages. First, dot-like small initial adhesions are formed in the cell membrane; then the integrin binding to ECM ligands and attachment to the cytoskeleton leads to focal complex formation[133,134]. Eventually, focal complexes mature into larger focal adhesions, which is accompanied by a stronger connection to the cytoskeleton. Paxillin plays a key role in the maturation of focal complexes. A stable focal adhesion site can extend and gather more material like zyxin. Interestingly, the size of focal adhesions depends on substrate stiffness, illustrating the functionality of focal adhesions as mechanosensors. In fact, the process of focal complexes maturation into focal adhesions reflects the presence of mechanical forces, which can be either intracellular forces caused by actomyosin contraction or external forces from the outside environment. Interestingly, it was shown that cells show a different mechanoresponse on substrates of different mechanical properties present, even though myosin activity was blocked[110]. It is worth noting that cells can apply forces to the substrates via focal adhesion sites, thereby remodeling the surrounding matrix.

2.2.4.2 Adherens Junctions

As outlined above, there is a close interplay between cellular traction forces and external environmental forces, which are transmitted across focal adhesions. Intracellular traction forces mediated via integrins to the ECM are proven to be regulated with the

ECM mechanical properties and external forces, which also impact cytoskeleton organization. Similarly, intercellular and external mechanical signals also play an important role in a number of collective cell migration processes, such as cell rearrangement and tissue reshaping during embryonic morphogenesis. Intercellular forces also influence cell migration, inflammatory processes, and cell differentiation. Cadherins[135] are the linker proteins for force transmission through cell-cell junctions as they constitute a universal family in the animal kingdom.

A whole family of cadherin proteins was recognized and named after the tissue type they were found in, for instance, E-cadherin in epithelial cells and N-cadherin in neural tissue. The extracellular part of the cadherin N-terminus consists of 5 Ig-like repetitive subdomains, known as extracellular cadherin (EC1 to EC5)[136]. To prevent the hinges between each repeat from flexing, calcium ions are essential to maintain the more or less rigid cadherin structure for engaging in homotypic interactions. The main proteins of adheren junctions in cytoplasmic plaques, which form a bridge between cadherin and cytoskeleton, are α-, β- , and P-120 catenin. P-120 catenin associates with the juxtamembrane domain of cadherin, and functions as regulator of cadherin turnover. β-catenin binds further to the C-terminus of cadherins, thereby interacting with α-catenin to form the complex that links to F-actin filaments[137-139]. Furthermore, a large number of additional cytosolic proteins have been found to bind to cadherins in adheren junction sites that mediate the link between the cadherin complex and F-actin complex[139].

There are three major types of cadherin junction structures which are focal adherens junction, linear adherens junction, and Zonula adherens junction as shown in Figure 2.2.3[140,141].

In 2D cell culture models, cadherin cell-cell adhesions have been identified in three types of cadherin-cadherin contacts. Myosin II dependent focal adherens junctions are formed upon initial cadherin contact with the appearance of calcium ions. Tension-dependent presence of vinculin has been recognized in association with cell-cell junctions[142]. During maturation of adherens junctions, the cell will form linear cell-cell junction structures, which colocalize with thin F-actin and align with thicker parallel F-actin bundles. In this conformation, vinculin is absent from cadherin complexes, which indicates the presence of an α-catenin non-stretched model without applied force. In the final stage of maturation, the cell-cell junction is called a Zonula adherens junction in which an apical F-actin belt binds to the cadherin complex in the presence of vinculin; recruitment of vinculin indicates the tension force applied and the stretching mode of α-catenin in the cadherin complex[20,143,144]. Measurement of α-catenin activity indicates the tension in cells and tissues as confirmed by Schwartz and coworkers[145,146], who used a FRET probe to investigate cell-cell adhesion force in the loop region of a focal adhesion site. Despite these efforts, the mechanism of cellular mechanorespose at cadherin-F-actin interface is still not well understood, in part due to the limitation of existing artificial models.

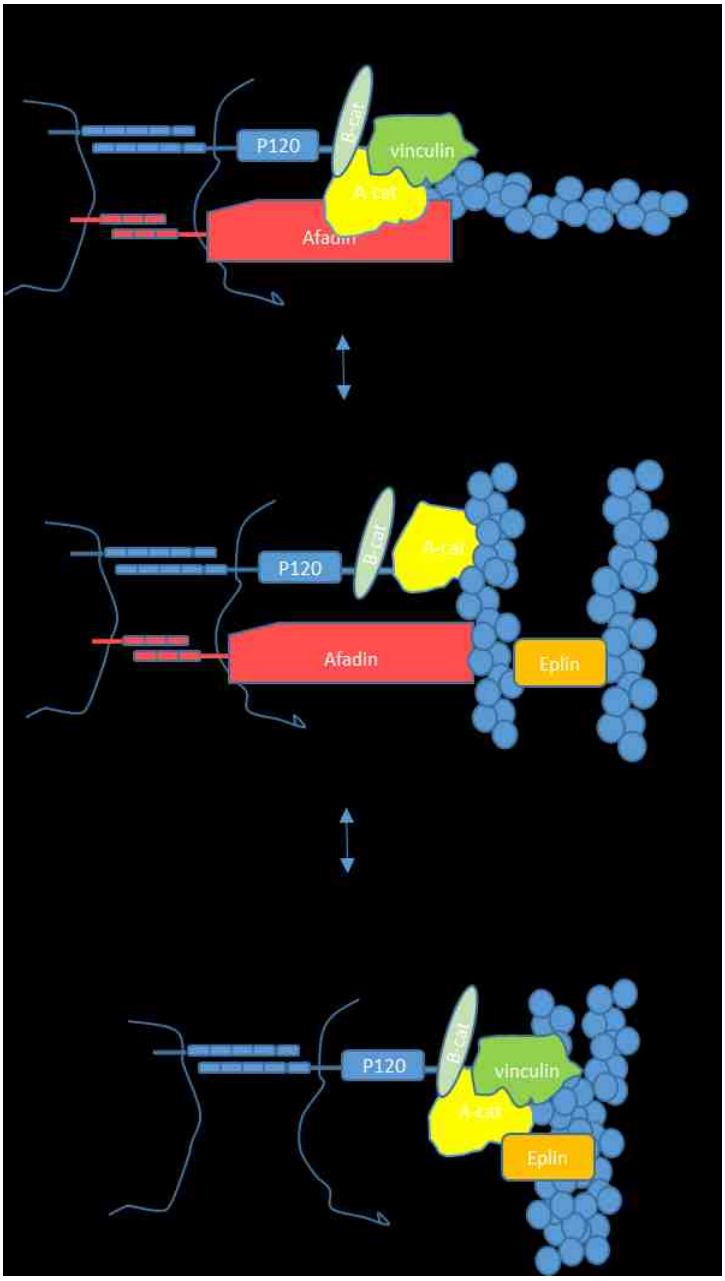

Figure 2.2. 3 Different Types of cadherin junction structures.[147,148]

Forces at cell-cell junctions in single cells and cell clusters impact cellular mechanoresponse differently, especially in morphogenesis and physiology[149-151]. Cells in whole tissue can reorganize cytoskeleton and its shape due to the change of applied force

from focal adhesions. Thus, both actomyosin-based forces and coordinated cohesive forces via cadherin junctions regulate collective cell movements in embryogenesis and wound healing. For example, Chen et al.[152] showed that cell migration is significantly influenced by the stiffness of substrates through a cadherin dependent mechanism. It is worth noticing that α-catenin plays a central role in mechanosensitive processes as well as to investigate for impact from exact molecular machineries involved. At the single cell level, the tension of cadherin-F-actin linkage also affects α-catenin and the associated actin machinery to feed back into cortical actin organization and cell sorting. Actomysin-based tensile forces at cell-cell junctions are an important role for tissue morphogenesis, in which cellular morphology change is apical constriction that derives[153]. For instance, cells with knocked-out α-catenin expression display in a disconnection between actomysin cytoskeleton and cell-cell junctions, which impact the cell morphology and cellular mechanoresponse[154]. According to these results, α-catenin is hypothesized as the key mechanosensor to trigger the force-induced actin remodeling and reshaping[155,156].

To understand the cellular mechanism of adherens junction and their mechanoresponse, there are several studies[157,158],which employ cadherin chimera in artificial substrates mimicking the cell-cell junctions. For example, Groves and coworkers[17] observed that trans-interaction of E-cadherin molecules regulates initial stages of junction formation in this hybrid system, and proceed via a nucleation process in which protrusion and retraction of filopodia play an important role.

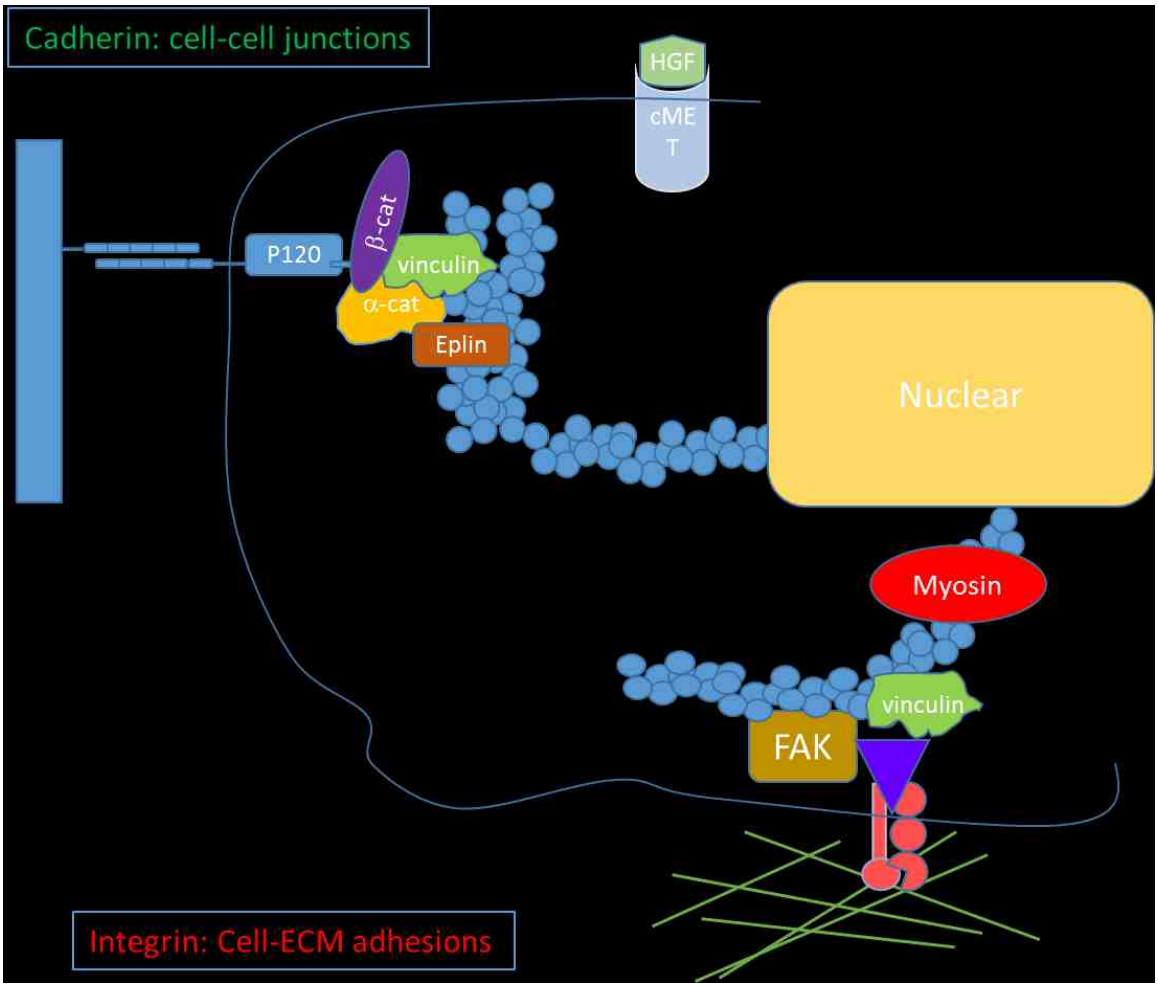

Figure 2.2. 4 Map of interaction between integrin and cadherin mechanotransduction[135]

2.3 Artificial Cell Substrates

In biological systems, boundaries between many phases are defined by "soft interlayers", such as membranes and biopolymers, which are immersed in physiological electrolytes. For instance, biological membranes are vital components that define the outer boundary of living cells to the surrounding environments as well as that of cell compartments (organelles) in cytoplasmic space. For physiological and biophysical

studies[22,34,159-161], artificial cell substrates of well-defined, tunable physical properties are used to investigate mechanical between cells and their surroundings. To accomplish such cellular studies, artificial substrates need to fulfill following specific properties: **1. Biocompatibility, 2.Existence of suitable cell attachment sites, and 3. Tunable mechanical properties.**

1. **Biocompatibility:** Biocompatibility illustrates the ability to mimic natural conditions and to exhibit low cytotoxicity. A model system must be able to allow cells to grow on the top of (2D substrates) or within (3D substrates) the substrates without impairing substrate integrity.
2. **Suitable cell attachment sites:** Substrates need to carry specific anchoring sites for cell adhesion. For example, with several modifications to activate the substrate surface, PAA gels can be functionalized with heterobifunctional crosslinkers, which allow linkage of ECM ligands.
3. **Tunable mechanical properties:** A hallmark of artificial cell substrates for the analysis of cellular mechanosensitivity is the ability to adjust substrate stiffness. Artificial substrates may for example have tunable elasticity and viscosity, or may be patterned with regions of different viscoelasticity. For example, NIH 3T3 fibroblasts are placed on PEG-coated hydrogel substrates, in which viscoelasticity is adjusted by crosslinking density within the gel.

To find a proper artificial substrate for studying the mechanism of cellular mechanoresponse, scientists have been developing polymeric substrates to mimic the specific aspects of natural microenvironments by manipulating specific properties[102-110].

To illustrate this, we will discuss in the following chapter different types of substrates, which are designed for particular demands.

Table 2.3. 1 Polymeric substrates for investigation of cellular mechanoresponse.

Dimensions	Method	Materials	Elasticity (Young's Modulus)	Biological application		Reference
				Surface coating	Cell line	
Flat 2D		Silicone rubber (PDMS)			Heart Fibroblast, liver cells	139
Flat 2D	Soft lithography, Direct e-beam writing, microcontact printing.	PDMS, PMMA	15 kPa	Fibronectin	Foreskin Fibroblast, Cardiac Fibroblast.	140-142
Flat 2D	Replica molding with embedded microbeads	PDMS	~2.5 MPa, 1600-2.7 nN/mm depending on diameter and height of the posts	Fibronectin and Collagen IV	Bovine artery smooth muscle cells, NIH3T3 mouse fibroblasts	142-145
Flat 2D		Polyacrylamide	~5-8.5kPa	Collagen I	Dictyostelium discoideum	146
Flat 2D	LB/LS, Multi-unilamellar vesicles	Lipid and polymeric lipids		Laminin, Cadherin	MEF Fibroblast, C2C12 Myoblast	147,148
TOPO 2D	Replica molding	PDMS	32nN/mm	Fibronectin	NIH 3T3	143,144
3D	Microfabrication and soft lithography	PDMS			Connectu tussyre origenitor cells	149-151
3D	Two photon laser scanning photolithography	PEG		RGD	Human dermal fibroblast	152,153
Gradient 2D	Photolithography	Styrenated gelatin	10-400 kPa		3T3-swiss albino	154
Gradient 3D	Compressing of wedge-shaped collagen matrix	Collagen 1	1000-2300 kPa	Collagen I	Human Dermal fibroblast	155,156
Gradient/Topo 2D	LS/LB	Polymer-supported membranes		Laminin	MEF & 3T3 Fibroblast	147

2.3.1 Polymeric Substrates

Due to their ability to combine biocompatibility and adjustability of mechanical properties, polymers are broadly used in biomedical studies as a template for tissue engineering, shells for drug delivery, and coating for medical implants such as

cardiovascular stents. As already outlined, cells sense the underlying substrate with respect to mechanical properties such as elasticity, topography, gradients, and geometrical change. Polymer materials are great biomaterials because they allow the controlled adjustment of important mechanical properties, such as **surface topography, roughness, elasticity, and adhesion**[180] For instance, not only substrate roughness provides adhesion and alignment cues for endothelial cells, but also substrate elasticity induces change in cellular fate and functions, as exemplified by altered cell morphology and migration speed. Therefore, polymeric substrates could benefit researchers to understand how mechanical properties of substrate influence cellular mechanoresponse. In the following sections, not only the impact of polymeric substrates as cell substrates will be described, but also their potential and limitation towards practical use in *in vitro* biophysical studies will be discussed[181]

2.3.1.1 Artificial Polymeric Substrates

In the late 1990s, Pelham and Wang[182,183] used polyacrylamide (PAA) gel as the first template to investigate cellular mechanotransduction. Fabrication of gels was initiated with tetramethylethylenediamine (TEMED) and ammonium persulfate for polymerization of monomeric acrylamide and cross linker bis-acrylamide. Sulfo-SANPAH was added to the gel for activation of PAA gel surface under ultraviolet light, and then ECM proteins could be applied on the substrate. The advantages of the PAA gel as a template for studying cellular mechnoresponse are the following: (1) ease to adjust the versatile properties by adjusting the concentration of acrylamide, (2) optical clearness (relevant in

optical experiments), (3) chemical inertness, and (4) linear elasticity over a wide range of stress forces. However, the PAA gel technique also has its disadvantages, such as the rather rough surface and the frequently occurring monomeric residues. While changing the elasticity of the substrate, porous architectures are formed on the surface of the gel altering the surface density of ECM molecules affecting cell spreading. Furthermore, monomeric acrylamide has a high cytotoxicity to most mammalian cells. Despite these potential problems, PAA gels are considered as a good polymeric cell substrate of tunable elasticity for basic control experiments and traction force microscopy [184].

Surface roughness relates to the texture of the uppermost layer of material and is quantified by measuring the protrusion or depression at the surface. Owing to the improvement of biomaterials in nanofabrication, poly (dimethylsiloxane) (PDMS) gels were developed as a good template with tunable surface properties such as roughness and topography[185]. Shadpour et al.[186] established a technique to polish PDMS surface with alumina particles to achieve similar smoothness as obtained using epoxide-based photo-resists with SU-8 and 1002F reagents. The roughness value (Ra) of PDMS substrates treated by particle polish was observed to be 7.7-19.8 nm. Three different cell lines, (Rat basophilic leukemia, HeLa and 3T3 fibroblast) were seeded on such polished substrates. These experiments showed that cell adhesion sites on rough substrates increased 20-fold compared to smooth surface PDMS substrates of comparable elasticity.

Not only flat 2D PDMS gels have been used to investigate cellular mechanoresponse, but also 3D PDMS gels with different topographic features, such as micro-pillar and microstructure patterns, have been employed as cell substrates. In Ghibaudo group's

work[187,188], fibroblast cell adhesion and migration were observed on PDMS substrates with micro-pillar structure of 2 to 10 mm height and 5 to 10 μm diameter. Their experiments showed that cellular morphology and cytoskeleton organization are dependent on the size of micro-pillar, which also impacts cell migration if compared to cellular mechanoresponse on corresponding flat PDMS substrates. Interestingly, fibroblast with fewer focal adhesion sites on micro-pillar patterned substrates have enhanced focal contact on the edge of pillars[188].

Poly-lactic-co-glycolic acid (PLGA)[189,190] is another widely utilized polymeric biomaterial and known for its high biocompatibility and degradability. In most biomedical applications, PLA polymer is used in the replacement of diseased bladder tissue as buffer materials between smooth surface and rough surface of the native bladder. The mixture of polystyrene (PS) and polybromostyrene (PBrS)[191] was utilized as template for studying cellular mechanoresponse of human fetal osteoblastic cells. Cell adhesion size and morphology was analyzed with different stiffness and topographic scaffold of PS/PBrS substrate.

In summary, artificial polymeric substrates have advantages such as ease of tunable mechanical properties and fabrication of various topographies. However, most artificial polymeric substrates need extra coating procedures to activate the surface for cellular adhesion. Immobility of cell adhesion sites on the polymeric substrate barely mimic authentic cellular ECM systems. Furthermore, such substrates fail to replicate the rich dynamics found at cell-cell junctions.

2.3.1.2 Natural Polymeric Substrates

3D collagen matrix gels were first developed to explore the effect of dimensionality on cellular mechanoresponse[192,193] . Like biochemical composition and mechanical properties, dimensionality plays an important role in cell behavior, such as proliferation, biosynthesis and migration. However, due to the biodegradability of polymers, it remains challenging to utilize them in the quantitative and qualitative analysis of cellular mechanoresponse to dimensionality. To overcome such challenges, other 3D scaffolds were applied with different materials, such as synthetic polymers, ceramics and even metals. Current methods and techniques[194-199] provide a micrometer or sub-micrometer 3D scaffold functionalized with ECM materials to monitor the cellular mechanoresponse in the defined 3D environments. There are several fabrication strategies discussed in the following section: **Photolithographic resins of 3D structure, Microfabrication and soft lithography, and Tough 3D structure.**

Photolithographic resins of 3D structure[187,200]: This direct laser writing method is one of the popular methods for manufacturing 3D scaffolds (typically accomplished by exposure to a laser operated in two photon absorption mode). Scanning of the laser with respect to the material of interest results in a 3D structure, which can be functionalized with ECM ligands for cell growth. According to Klein and coworkers, this method offers a highly controllable 3D scaffold to mimic in vivo conditions, advantageous to the 2D planar environments commonly used[201].By employing this method, chicken fibroblast cells could be seeded on a fibronectin-coated 3D scaffold consisting of polyethylene glycol diacrylate and pentaerythritol tetra-acrylate. Another method for manufacture of ECM-mimicking

3D scaffolds comprised of hydrogel and biodegradable polymers is called pressure-assisted microsyringe (PAM). This method has been utilized to investigate the influence of defined 3D topography and stiffness to cellular mechanoresponse**.**

Microfabrication and soft lithography[196]: As already mentioned[188], , PDMS is a well-known polymeric biomaterial that is suitable as an artificial cell substrate for the analysis of cellular mechanoresponse. Recently, 3D scaffolds comprised of PDMS with precise micro-pattern and micro-texture have been developed by soft lithography. Mesenchymal stem cells were placed onto 3D PDMS scaffolds, which were molded with a mechanical jig for alignment and stacking of subsequent PDMS layers. Within the textured scaffold, cells can grow, differentiate, and migrate freely on the surface compared to those cultured on a smooth surface. For example, fibroblasts were cultured on the novel 3D biopolymer scaffold, which was fabricated via the combination of microfabrication and soft lithography methods. To enable cell spreading, the surface of the biopolymer scaffolds was coated with laminin, to which the cells adhere in both static and dynamic conditions. Interestingly, cell migration and morphogenesis, which are highly significant parameters in tumor invasion and metastasis, are influenced by scaffold architecture and pore size of the scaffold[202].

Tough 3D structure[199,203]: The tough 3D scaffold was broadly used in the medical field and was built with photopolymers or metals. For example, biomaterials like polypropylene fumarate were utilized as there are few elastic substrates to mimic mechanical properties of bone tissues. Most of the tough materials are usually mixed with other soft biomaterials to establish a hybrid scaffold for better cell adhesion and growth.

It is worth noticing that cellular mechanoresponse in 2D and 3D scaffolds is different. However, in contrast to 2D substrates, it remains challenging to conduct quantitative experiments related to cellular mechanosensitivity. This challenge is exemplified by the complex impact of mesh size of polymer gels on cell migration. Here mesh size not only influences cell migration in terms of steric conditions, but also in terms of mechanical properties. Consequently, 2D cell substrates will remain to be important as artificial cell substrates for the examination of cellular mechanoresponse.

2.3.1.3 Substrates with Elastic Gradient and Patterns

Substrates with gradient patterns in terms of elasticity and texture have emerged as an attractive experimental tool to probe cellular mechanosensitivity. Such substrates are interesting because different parts of a cell are located or attached on various points of a continuous gradient substrate thus receiving different mechanical inputs. Cellular mechanoresponse should reflect the parallel exposure to different mechanical cues.

Recently, several methods were introduced to prepare continuous and patterned gradient substrates for the analysis of cellular mechanoresponse. The original method to control the gradient of polymerization was achieved by physical strategies like pressing a gel or inter-diffusion of two components[204].Most of the gels were generated by defined photo-irradiation to control the process of polymerization or degradation of photosensitive polymers [205]. Another strategy has been to design a PAA gel composite comprised of two regions of different concentrations of acrylamide monomers, and a boundary region consisting of several gel strips of continuous stiffness. While placed on

continuous gradient gels, 3T3 fibroblasts were found to migrate from the softer region to the stiffer region, displaying a process known as durotaxis. In Crowe-Willoughby's research[206] two elastic polymers, PDMS and Polyvinylmethylsiloxane, were mixed, thereby forming a substrate with a continuous gradient stiffness ranging from 20 to 400 kPa.

To optimize the manufacturing process of substrates with gradient elasticity, photopolymerization was applied, in contrast to the mixing method above. The variables here are the distribution of the photo initiators and the irradiation intensity and time. Wong's group presented a method to use the photo masks with linear or gradual transmittance to establish PAA gels with gradient elasticity from 2 to 11 kPa. Meanwhile, Kiodoaki *et al.*[207] manufactured the styrenated gelatin with gradient elasticity form 10 to 400 kPa.

2.3.2 Biomembrane-Mimicking Substrates

One of the main purposes of the biological membrane is to provide an outer boundary of living cells and internal cell compartments to keep toxic materials away and bring in essential materials [208,209]. Biomembranes are also the sites of membrane channels, which regulate the transport of ions, and adhesion proteins like integrins and cadherins, which organize in specialized cell adhesions, thus enabling cellular attachment to the ECM and formation of cell-cell linkages[209]. Thus, the lipid bilayers of the plasma membrane are probably nature's most important two-dimensional fluid, forming the underlying architecture of cell membranes. The character of the lipid bilayer as a 2D fluid enables the mobility of embedded membrane proteins, unless membrane proteins are attached to

the cytoskeleton. Proteins embedded in the plasma membrane and carbohydrates attached to its surface facilitate communication and transport across the membrane. Due to the complexity of biological membranes, it has been difficult to design mimetics of such sophisticated supramolecular assemblies. Nevertheless, multiple efforts have been made to develop models of biological membranes for biophysical studies and bioanalytical applications.

In particular, planar supported model membrane systems, such as solid-supported phospholipid bilayers and polymer-tethered lipid bilayers, are potentially interesting as artificial biomembrane-mimicking cell substrates. In 1985, Tamm and McConnell[34] reported the first fabrication method of a solid-supported lipid bilayer using two successive monolayer transfers. Currently, such bilayer architectures are used as model systems in a wide range of different fields, including chemistry, biology, and physiology[210].

Stable solid-supported lipid bilayers can be established by multiple techniques which include: spin-coating, micro-contact printing, solvent-exchange deposition, lipid-surfactant micelles, evaporation induced assembly, lipid dip-pen nanolithography, vesicle fusion and Langmuir-Blodgett/ Langmuir-Schaefer (LB/LS) methods. The most commonly used methods to fabricate solid-supported bilayer are perhaps LB/LS deposition and vesicle fusion.

Bilayer formation by vesicle fusion typically occurs by adsorption of lipid vesicles to a substrate, followed by vesicle rupture, fusion and bilayer spreading. Among all techniques, vesicle fusion is the most simple and versatile one since it does not require any sophisticated instruments to produce high quality lipid bilayers. Due to these advantages,

vesicle fusion still plays a pivotal role in advancing solid-supported bilayer research platforms particularly with respect to complex, multi-component supported lipid bilayers. However, the underlying mechanisms of vesicle fusion are not fully-understood and the process is influenced by many factors including vesicle composition, size, and surface charge, roughness of substrate, pH value, and ionic strength. In contrast, bilayer formation by LB/LS deposition is achieved through subsequent LB and LS monolayer transfers from the air-water interface to the solid substrate. During LB transfer, lipids are transferred from the air-water interface to a glass substrate mounted on a moving dipper. The LS monolayer is added by pushing the LB-functionalized glass substrate horizontally through another phospholipid monolayer at the air-water interface. The LB/LS methods not only allows the fabrication of high quality symmetric bilayer systems, but also enables the design of asymmetric lipid compositions.

Due to lubrication effect of the thin water layer between bilayer and hydrophilic substrate, solid-supported bilayer can exhibit substantial long-term lateral mobility, thus mimicking the functionally important membrane fluidity in biomembranes. To make supported lipid membranes available for the analysis of membrane proteins, a hydrophilic polymer layer has been introduced between lipid bilayer and solid substrate. Current supported membrane designs include bilayers with: a. hydrated polymer “cushion” b. functional lipopolymer “tethers” and C. Lumazin synthase (LuSy). Previously, solid-supported lipid bilayers have been employed as biomembrane-mimicking cell substrates[24] For example, solid-supported lipid bilayers have been employed to explore processes of immunological synapse formation[160]. However, such relatively simple model

membrane architectures are not well suited for the analysis of cellular mechanosensitivity, as they lack the ability to adjust substrate mechanical properties in a systematic way. In fact, cell spreading and migration on a fluid lipid bilayer is typically suppressed [171]As shown in this thesis, polymer-tethered lipid bilayers comprised of phospholipids and lipopolymers overcome these limitations. Here the polymer moiety of lipopolymers forming a polymer cushion between lipid bilayer and solid substrate prevents the protrusion of cells through bilayer defects. More importantly, lipopolymers enable the controlled adjustment of membrane viscoelasticity, which is a key requirement for artificial cell substrates for the analysis of cellular mechanosensitivity. The fascinating properties of these biomembrane-mimicking materials are described in more detail in the following sections.

2.3.2.1 Polymer-tethered Phospholipid Single Bilayers (TYPE I)

Polymer-tethered phospholipid single bilayers comprised of phospholipids and lipopolymers are attractive biomembrane-mimicking materials because their dynamic, organizational, and mechanical properties can be adjusted by the concentration of lipopolymers. Throughout this thesis, such membrane systems are referred to as TYPE I bilayers. For example, changes in lipopolymer concentration were found to have a profound influence on the lateral mobility of lipids and membrane proteins in a physisorbed polymer-tethered lipid bilayer[24]. Similarly, tuning of lipopolymer concentration causes changes in mechanical and topographic properties of the polymer-

tethered lipid bilayer system. In the sub-section 2.3.2.1, the mechanical and topographic properties of polymer-tethered single bilayers will be discussed in more detail.

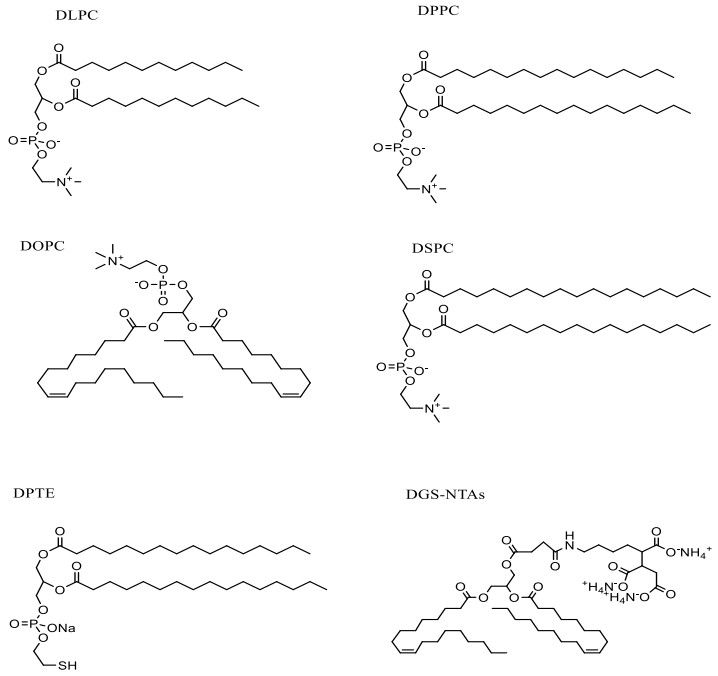

Figure 2.3. 1 Common Chemical structure of phospholipids employed on biomembrane-mimicking bilayer substrates

DSPE-PEG(2000)

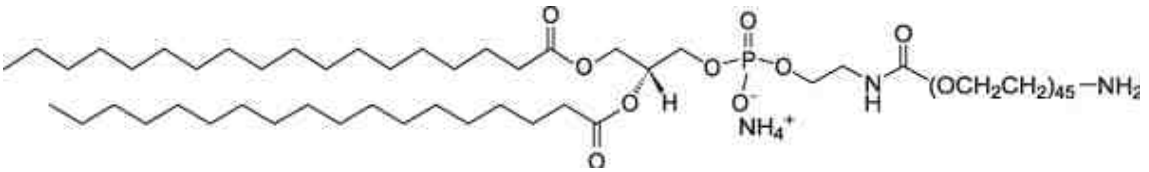

DSPE-PEG(2000) Maleimide

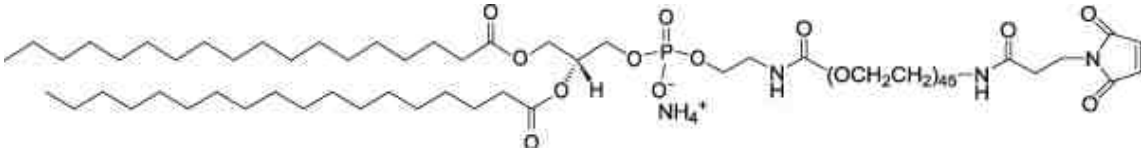

Sulfo-GMBS

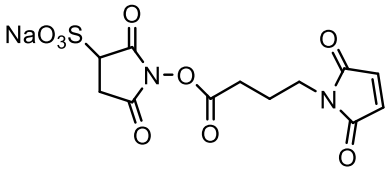

Pmox 50

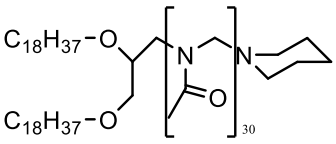

POPC

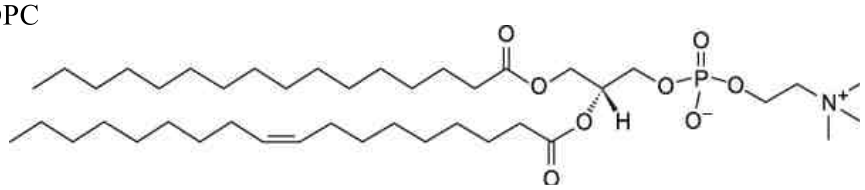

SOPC

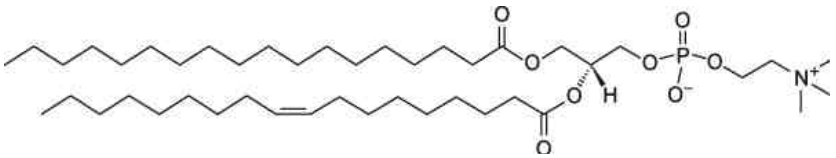

Figure 2.3. 2 Chemical structure of Lipopolymers employed on Biomemebrane mimicking bilayer substrates

2.3.2.1.1 Design and Fabrication of TYPE I Substrates

To design polymer-supported lipid bilayers, different types of polymer supports have been employed, including poly(ethylene glycol), polyacrylamide, polyethylenimine, or different types of lipopolymers. In this work, most TYPE I substrates, which consist of physisorbed poly (2-ethyl-2oxazoline) and poly(ethylene glycol) (PEG) lipopolymers, were built using the LB/LS techniques. Alternatively, lipopolymers can also be chemically linked to the glass substrate (e.g., by silanized polyethylene glycol lipids or benzophenon silane)[211]. To use TYPE I bilayers as artificial cell substrates, an additional surface modification with ligands for cell adhesion proteins is necessary to facilitate the formation of specific cell-substrate linkages, thus enabling cell spreading and migration. To achieve this, the top leaflet of all bilayer substrates contain a mixture of 1-palmitoyl-2-oleoyl-sn-glycero3-phosphocholine (POPC) and 5 mol% 1,2-Dipalmitoyl-sn-Glycero-3-Phosphothioethanol (DPTE), which acts as bridge between substrate and ECM coating; the bottom leaflet is comprised of different concentrations of lipopolymer from 5-40 mol% in a POPC lipid matrix. In our previous works, formation of physisorbed polymer-tethered lipid bilayers was characterized by a stable lateral gradient in lipopolymer concentration (TYPE I) substrate. TYPE I substrates are typically analyzed using atomic force microscopy (AFM), fluorescent (EPI) microscopy and FRAP.

2.3.2.1.2 Role of Lipopolymer on Membrane Stiffness

By altering the concentration of lipopolymers, properties of polymer-tethered lipid bilayers of TYPE I can be tuned in terms of compressibility and bending stiffness. Previous

mean-field calculations of polymer-tethered membranes have demonstrated that mechanical properties of such model membranes, including bending modulus and compressibility, can be altered by the type, molecular weight and concentration of lipopolymer in the membrane. Bivas *et al*.[212-214] have shown that lipopolymers are able to alter the mechanical properties of lipid vesicle membrane using the micropipette techniques. Both artificial lipid monolayer and bilayer membrane systems mimicking elastic properties can be altered with the concentration of the lipopolymer such as DSPE-PEG5000 or poly (2-ethyl-2-oxazoline) lipopolymers. The increase in bending stiffness with increasing lipopolymer concentrations reflects the superposition of the lipid layer and the increasing polymer layer thickness (polymer chains stretch at elevated lipopolymer concentrations). The increased repulsive inter-polymer interactions at increasing lipopolymer concentrations give rise to fascinating stress relaxation phenomena, such as membrane buckling, which are discussed in the next section.

2.3.2.1.3 Membrane Buckling in TYPE I Bilayer

It is now widely recognized that thin elastic films can show stress relaxation phenomena, such as wrinkling and buckling. While wrinkling is observed for elastic thin films on compliant substrates, their counterparts on rigid substrates display buckling delaminations[215] .For example, wrinkling patterns have been reported in monolayers of phospholipids and lung surfactants. In this case, the lung proteins not only induce the wrinkling pattern as surfactant, but also prevent phase separations among the lipids during compression. Our group recently reported the formation of buckling patterns in

mixed LB monolayers of phospholipids and lipopolymers [poly (2-ethyl-2oxazoline)-lipopolymers and DSPE-PEG5000] over a wide range of lipopolymer concentrations[216]. Here buckling width, 2b, and buckling amplitude, w_{max}, were analyzed using AFM. Table 2. 3. 3. below provides a summary [217] of the buckling analysis from 3 mol% to 40 mol% lipopolymer of polymer-tethered lipid monolayer substrate using atomic force microscope in 5 x 5 μm^2 area.

Table 2.3. 2 The characteristics of TYPE I substrates with various lipopolymer concentrations in ratio of buckling area[202]. From the quantitative data of buckling structure in the table above, the empirical relationships between buckling area and the lipopolymer concentration are illustrated. It is worth noting that the histogram is divided into two regimes. While $0 \leqq X_p \leqq 0.2$ %, the relationship between buckling area and Xp is linearly correlated; it shows nonlinear scaling in the range of $X_p \geqq 0.2$.

X_p	b(nm)	W_{max} (nm)	Buckling Area (%)
0.03	203±59	9.0±1.0	3.3±0.2
0.05	230±75	8.2±0.8	5.9±0.3
0.1	350±104	9.4±1.1	14±0.7
0.2	660±170	10.4±0.9	31.5±1.5
0.3	907±384	7.9±1.5	38.2±2
0.4	1149±390	7.0±1.5	39±2

Importantly, experimental analysis of buckling structures in polymer-tethered lipid monolayers can be combined with buckling theory of an Euler column (straight-sided blister), to link buckling structures to membrane elasticity. Here values of membrane thickness and bending elasticity can be obtained from mean-field calculations of polymer-tethered membranes and applied to simplified buckling theory, which dates back to the analyses by Foeppl and Karman of the buckling of thin plates in the late 1990s. For an

Euler column, the bending stiffness is related to Young's modulus (E_f) and the plane strain modulus (E^*_f) of the film as follows:

$$K_c = \frac{E_f h^3}{12(1-v^2)} = \frac{E^*_f h^3}{12} \quad [15],$$

where K_c is the bending modulus; *v* is Poisson ratio of the film; and *h* represents the film thickness. Buckling theory provides a relationship between non-dimensional loading parameter, which is the ratio of the film stress σ_o and the film stress at onset of buckling σ_c and the experimentally accessible buckling parameters w_{max} and b:

$$\frac{W_{max}}{h} = \sqrt{\frac{4}{3}\left(\frac{\sigma_o}{\sigma_c} - 1\right)} \quad [16]$$

The critical stress at the onset of buckling can be related to bending modulus buckling width, and film thickness:

$$\sigma_c = \frac{\pi^2 K_c}{b^2 h} \quad [17]$$

Table 2. 3. 3. Summarizes results, in which the concentration of DSPE-PEG5000 was varied from 3-40 mol% (X_p: 0.03- 0.4)to modify the lateral stress in a polymer-tethered SOPC monolayer. The table compares elastic properties of the film for different values of X_p and h. The gradual change of mechanical film properties with lipopolymer concentration is exemplified by a linear relationship between E^*_f and X_p in the range of $0.05 \leqq X_p \leqq 0.4$.

Table 2.3. 3 the characteristics of TYPE I substrates with various lipopolymer concentrations[202].

X_p	h (nm)	E_f*(MPa)	s_c/E_f^*	s_c/s_o
0.05	13.1	1.95	26.5×10^{-4}	1.30±0.08
0.10	15.6	2.22	16.4×10^{-4}	1.27±0.06
0.20	18.4	4.07	6.37×10^{-4}	1.17±0.04
0.30	19.8	6.14	3.93×10^{-4}	1.12±0.03
0.40	20.7	7.96	2.66×10^{-4}	1.09±0.03

2.3.2.1.4 Obstacle-Induced Obstructed Diffusion in TYPE I Bilayers

By building TYPE I bilayers layer-by-layer using LB/LS deposition technique, one is able to vary lipopolymer concentration over a wide concentration range. Previously, Deverall *et al*[218] demonstrated that lipopolymers (polymer-tethered lipids) act as diffusion obstacles of lipid and membrane protein diffusion. In these wide-field single molecule fluorescence microscopy experiments, TRITC-DHPE and monomeric bacteriorhodopsin mutants were used as lipid and membrane protein tracers, respectively, in a bilayer of 1stearoyl-2-oleoyl-*sn*-glycero-3-phosphocholine (SOPC) of varying concentrations (0-40 mol%) of physisorbed dioctadecylamine [poly (ethyloxazoline) 8988] (DODA-E85) lipopolymers in its inner monolayer. These experiments not only revealed the largely homogeneous distribution of obstacles in the bilayer, but also showed their immobilization as percolation thresholds of tracer diffusion could be observed. Previously, obstructed lipid diffusion was also observed in binary phospholipid-cholesterol systems[219] and in mixtures of fluid and gel-phase domains[220].

Table 2.3. 4 Diffusion coefficients Dlipid listed at different molar concentrations of tethered lipids X_p[202].

X_p (mol%)	D_{lipid} [mm^2/s]
0	2.1
5	1.8
10	1.6
15	1.3
20	0.9
30	0.6
40	0.03

Experiments of obstacle-induced obstructed diffusion with known concentrations of obstacles help us understand how lipid and proteins in biomembranes may be obstructed by very small obstacles consisting of one or a few molecules. Furthermore, the impact of the membrane lateral mobility by interaction of lipids and membrane proteins can be theoretically illustrated using established models.

2.3.2.2 Biomembrane-Mimicking Polymer-Tethered Multi-Bilayer Substrate (TYPE II)

As mentioned above, the tunable mechanical properties of biomembrane-mimicking substrates are important for research in biology, physiology and biophysics. In TYPE I bilayers, this was achieved by altering the concentration of lipopolymer in the bilayer. However, single bilayer substrates are limited in terms of their mechanical properties and their susceptibility for substrate-induced bilayer artifacts. Therefore, several groups have pursued the design of solid-supported multi bilayer systems[25]. Tamm *et al.* [26,34] presented a well-defined method for establishing a double bilayer system by using biotin-

streptavidin coupling. In this case, the double bilayer system was stable and showed good lateral fluidity of lipids in the second bilayer. Chung and coworkers[28,221] built a solid-supported double bilayer system by DNA hybridization using NHS/EDC coupling chemistry. However, their double bilayer system lacked stability, as established by the reduced bilayer fluidity observed by FRAP method [40].

2.3.2.2.1 Design and Fabrication of TYPE II Substrates

In order to fabricate a stable polymer-tethered multiple bilayer substrates, the following three major components were used: (a) 1-palmitoyl-2-oleoyl-*sn*- glycero-3-phosphocholine (POPC) (b) 1,2-distearoyl-sn-glycero-3-phosphoethanolamine-N-[maleimide(polyethylene glycol)-2000] [ammonium salt](DSPE-PEG2000-maleimide) (c) 1,2-dipalmitoyl-*sn*-glycero-3- phosphothioethanol [sodium salt] (DPTE). In the first step, a mixture of 95 mol% POPC and 5 mol% DSPE-PEG2000-maleimide was deposited to glass coverslips through subsequent LB/LS depositions. In the second step, GUVs consisting of 95 mol% POPC and 5% DPTE lipids were formed within 0.1 mM glucose/1 mM $CaCl_2$ aqueous solution and added into the first bilayer substrate immersed within 0.1 mM sucrose/ 1 mM $CaCl_2$ stock solution. Here, a sugar gradient difference helps the GUVs to sink down to the underlying bilayer thus promoting GUV rollout and double bilayer formation using maleimide-thiol coupling chemistry. Compared to other previously employed methods of double bilayer formation, the resulting double bilayer shows good stability and homogeneity, as evidenced by AFM and fluorescent microscopy.

Assembly of double bilayers can be analyzed in terms of bilayer fluidity using methods like FRAP and single molecule tracking. This is because the diffusivity of the top bilayer is expected to be higher relative to the bottom bilayer. Remarkably, the double bilayer substrate from Han and Evan's research[222] using NHS/EDC shows the opposite effect compared to other coupling method. Tamm and coworkers reported[26,34] that a double bilayer with different biotin-strepatavidin linker densities exhibits a slower diffusion coefficient (<1$\mu m^2/s$) compared to a GUV system (~3.5 $\mu m^2/s$).

2.3.2.2.2 Linker Density in TYPE II Substrates

Different compositions of the biomembrane-mimicking substrates impact the mechanical properties such as diffusion coefficient and elasticity. Among all multiple lipid bilayer substrates, the density of the linker lipids act as a bridge in the gap between bilayers were varied. For example, the concentration of lipids with NHS/EDC coupling reagents was changed from 5% to 18 mol% by Evan's group[222]. Thus, the diffusion coefficient of the bilayer decreases with increasing concentration of linker lipids on the inner bilayers. Tamm's lab[26] varied the density of biotin-streptavidin linkages between 0.1-1 mol% biotin-PEG-DPPE lipids, resulting in bilayer diffusivities from 0.25 to 0.03 $\mu m^2/s$. Interestingly, these linker density changes were associated with changes in the thickness of double bilayer substrates ranging from 14.6 to 16.6 nm. Linker density between double bilayers was also varied in the presence of DNA-lipid conjugate linkers[221,223]. In our previous work[24,170,171] linker concentration was altered from 0.1 to 5

mol% in a multi-bilayer system stabilized maleimide-thiol coupling chemistry. In this case, the multi-bilayer substrates remain homogeneous and laterally mobile.

2.3.2.2.3 Inter-Bilayer Coupling in TYPE II Substrate

There are three major methods for establishing multiple lipid bilayer substrates: (a) by DNA-lipid tethered via hydrogen bonding, (b) by functionalized lipids via covalent bonding, such as EDC/NHS coupling, and (c) by charged polyelectrolyte lipids with opposite charges via electronic bonding. The different methods for fabricating multiple lipid bilayer substrates are summarized in Table 2.3.5. One key feature of lipid multi-bilayer substrates is the ability to alter substrate thickness and bilayer fluidity by changing the degree of stacking. Multiple lipid bilayer substrates interconnected by lipopolymer tethers can have adjustable thickness by utilizing lipopolymers with different polymer chain lengths

Table 2.3. 5 summary of current methods to fabricate multiple lipid bilayer substrates

Number of bilayers	Lipids	Force between lipid bilayer	First bilayer Diffusion coefficient	Top bilayer Diffusion coefficient	Ref.
Double	DOPC/DMPC/DOPS	electrostatic adhesion	0.3		25
Double	POPC/ DPPE/ Biotin-PEG-DSPE	Biotin/ Streptavidin	0.52	0.88	4a
Double	DMPC/ DHPC/	DNA-tethered	3.1	5.1	142
Double	Egg PC/ DHPE/ DNA-lipids	DNA-tethered	3.2 (GUV)/ 3.4 (Vesicle Fusion)	6.5 (Immobile tethered) /4.8 (mobile tethered)	4c, 140
Double	Egg PC/ DOTAP	NHS/EDC	1.3 (18%)/ 1.7(9%)/ 1.9(5%)	0.9(18%)/ 1.0(9%)/ 1.5(5%)	143
Quadruple	POPC/ DSPE-PEG2000 Maleimide/ DPTE	NHS/ Thiolethanol	0.9	1.94	106

2.4 Solid-Supported Phospholipid Bilayer Systems with Various Linker Systems

There are two major common linker strategies to mimic the linkage between cell and artificial substrates: a. Cell-ECM mimicking linkage and b. cell-cell junction-mimicking linkage. In the Cell-ECM linkage, ECM proteins or ECM-mimicking peptides are specifically linked to the model membrane system. Linkages may be based on: collagen [147,224,225], RGD-functionalized short peptide[209,226], and fibronectin[92a, 103c, 120b]. In cell-cell junction linkage[3,17,147,165,227], different kinds of cadherin proteins can be employed. Because cadherins are membrane-spanning proteins, cadherin-based linkers have been typically designed by binding cadherin constructs (lacking transmembrane and cytosolic domains) with a histidine tag coupling to Ni-chelator lipids in the planar bilayer system.

In our previous work[24,170,171], membrane proteins, such as fibronectin and laminin, were added onto solid-supported lipid bilayers and associated via N-γ-maleimidobutyryl-oxysulfosuccinimide ester (GMBS) and DPTE (thioethanol-functionalized) lipids. However, extracellular membrane proteins usually form sheets of networking structure above biomembrane-mimicking substrates at 37°C, resulting in their immobilization. In contrast, bilayer--bound cadherin constructs remain laterally mobile, unless they are assembled in linker clusters underneath cellular adhesions.

MATERIALS AND EXPERIMENTAL PROCEDURES

3.1 Materials

3.1.1 Biomemebrane-Mimicking Bilayers Substrates

All lipids and lipopolymers were purchased from Avanti Polar Lipids (Alabaster, AL). Laminin and fibronectin were purchased from Invitrogen Life Sci. (Temecula, CA). The fluorescent probes: TRITC-DPPE, NBD-PE and Texas Red DHPE were acquired from Molecular Probes (Eugene, OR). The HPLC grade solvents and other chemicals were purchased from Fisher Sci. Sulfo-GMBS was purchased from Sigma Aldrich (Milwaukee, WI). Water utilized was purified using a Milli-Q Water Purification System (Millipore, Millford, MA). All glass substrates used were cleaned using sonication for 30 minutes in each of the following solutions: 1% SDS, methanol saturated with sodium hydroxide, and 0.1% HCl. Following each sonication step, the slides are rinsed and stored in Milli-Q water.

3.1.2 Cell Culture Materials

3T3 Fibroblasts, purchased from ATCC Virginia, and MEF Fibroblasts, provided by Profs. Fabry and Goldmann at University of Erlangen, were both cultured in DMEM medium (Invitrogen life science, CA) with 10% fetal bovine serum (Thermo Fisher Sci., MA), 100 U/mL Penicillin/Streptomycin (Thermo Fisher Sci., MA), and incubated at 37 °C in a humidified 5% CO_2 atmosphere (Prixar Air). For cell passaging, 2.5% trypsin (Therm

Fisher Sci., MA) was used to detach C2C12 myoblasts and 3T3 fibroblasts from 75 mL or 25 mL culture flasks (BD BioScience, CA). For rinsing off residues of cells, phosphate buffer solution (PBS) 10X (Thermo Fisher Sci., MA and IBI Scientific, Iowa) was diluted to 1X and sterilized via autoclave treatment. All aspirator pipettes and micropipettes were purchased from Thermo Fisher Sci. MA and sterilized with an autoclave from Primus Sterilze Co. Omaha NE.

3.1.3 Traction Force Microscopy Materials

All chemicals used in the preparation of PAA gels were purchased from Sigma-Aldrich and they include: sodium hydroxide powder: (3-Aminopropyl)trimethoxy silane, 97%; ammonium persulfate (APS); glutaraldehyde, 25%; acrylamide/bis-acrlamide, 40% (PAA); electrophoresis-grade N,N,N,N'-tetramethylethylenediamine, >99.0% (TEMED); electrophoresis-grade ammonium persulfate, >98%; and 4-(2-hydroxyethyl)-1-piperazineethanesulfonic acid (HEPES). Dulbecco's PBS without Ca^{2+} and Mg^{2+}, Fibronectin, and yellow-green 0.5µm carboxylate fluorospheres were obtained from Invitrogen CA. The crosslinkers utilized in these experiments, *N*-Sulfosuccinimidyl-6-(4'-azido-2'-nitrophenylamino) hexanoate(Sulfo-Sanpah) and *N*-[g-Maleimidobutyryloxy]succinimide ester (GMBS) were purchased through Pierce Biotechnology MN. Basic glassware and supplies including: 1x3in glass slides, 1x1cm gene frames, and 24x67 four-well multidishes were purchased from Fisher Scientific.

3.2 Experimental Procedures

3.2.1 Fabrication of Bilayer via Langmuir Blodgett (LB)/Langmuir Schaefer (LS) Deposition Techniques

Lipid bilayer-based cell substrates were constructed by using Langmuir-Blodgett and Schaefer techniques or by using Langmuir-Blodgett and vesicle fusion. A film balance with a dipper (Labcon, UK) was used to transfer the inner layer of the supported bilayer model to a glass substrate. A film pressure of 30 mN/m was used because this pressure is significantly above the plateau region of the pA isotherm that represents the submerging transition of polymers from the air-water interface into the water phase. The lipid mixture for the inner layer consists of lipopolymers to provide a cushion between the lipid bilayer and the solid substrate, and in the case of patterned substrates, can be used to tune mechanical properties. The outer layer of the lipid bilayer systems was completed using either a Schaefer transfer technique or vesicle fusion.

All first bilayers within the multiple-bilayer substrates were fabricated on a glass slide using Langmuir-Blodgett (LB) and Langmuir-Schaefer (LS) techniques with stock solutions of lipids at a concentration of 1mg/mL in chloroform and containing 95 mol% 1-palmitoyl-2-oleoyl-sn-glycero-3-phosphocholine (POPC) and 5 mol% 1,2-distearoyl-sn-glycero-3-phosphoethanolamine-N-[maleimide(polyethylene glycol)2000] (ammonium salt) (DSPE-Maleimide PEG-2000).

3.2.2 Giant Unilamellar Vesicles (GUV) and Small Unilameller Vesicles (SUV)

Stacks of multiple polymer-tethered lipid bilayers were fabricated as described previously[24,170]. In short, the layer-by-layer assembly of the polymer-tethered multi-bilayer stacks was accomplished through subsequent rollout of giant unilamellar vesicles (GUVs) consisting of either 1-palmitoyl-2-oleoyl-sn-glycero-3-phosphocholine (POPC) and 5 mol% 1,2-dipalmitoyl-sn-glycero-3-phosphothioethanol (DPTE) or POPC and 5mol% 1,2-distearoyl-sn-glycero-3-phosphoethanolamine-N-[maleimide(polyethylene glycol)2000] (ammonium salt) (PEG2000-Maleimide). All lipids and lipopolymers were purchased from Avanti Polar Lipids (Alabaster, AL). Here, maleimide-thiol coupling between DPTE and PEG200-Maleimide lead to stable linkages between adjacent lipid bilayers. To assist this process, GUVs contained 0.1mM sucrose/1mM$CaCl_2$, thus promoting their transport to the substrate via gravitation. For each planar bilayer addition, GUVs were allowed to bind and unfold for 2-4 h and then rinsed with Milli-Q to remove excess GUVs. To facilitate the formation of cadherin-cadherin linkages between multi-bilayer substrates and plated cells, GUV's forming the top bilayer also contained 0.5 mol% of the Ni chelator lipid 1,2-dioleoyl-sn-glycero-3-[(N-(5-amino-1-carboxypentyl)iminodiacetic acid)succinyl] (nickel salt) (DGS-NTA Ni) (Avanti Polar Lipids, Alabaster, AL); In this case, GUV addition was conducted in calcium ion-free buffer. In a subsequent step, an equimolar ratio (relative to DGS-NTA Ni) of His-tagged N-cadherin chimeras (R&D Systems, Minneapolis, MN) was added and allowed to bind to DGS-NTA Ni within the top bilayer of the multi-bilayer system (incubation time: 30 min), thus forming N-cadherin linkers. Next, the bilayer sample was rinsed with PBS to remove unbound N-cadherin. To confirm the distribution

and lateral mobility of bilayer-bound cadherin linkers in the absence of plated cells, Alexa 555-labeled anti-cadherin antibodies (Thermo Fisher Sci. Waltham, MA) were added in excess and allowed to bind to N-cadherin linkers using an incubation time of 1.5 h followed by rinsing off excess (unbound) antibodies with PBS. Dye-labeling of antibodies using an Alexa 555 antibody labeling kit (Life Technologies/Invitrogen, Carlsbad, CA) followed standard procedures[228]. Laminin linkers were formed by linking mouse laminin (Invitrogen, Carlsbad, CA) to DPTE within the top bilayer of the multi-bilayer substrates via the heterobifunctional maleimide-NHS esther crosslinker N-gamma-Maleimidobutyryl-oxysulfosuccinimide (Sulfo-GMBS) (Thermo Scientific, Rockford, IL), as described before[170]. To confirm the presence and integrity of the bilayer system in the presence of plated cells, top bilayers typically contained 0.5 -0mol% of the fluorescently labeled lipid Texas Red-1,2-dihexadecanoyl-sn-glycero-3-phosphoethanolamine (TR-DHPE) (Invitrogen, Carlsbad, CA). NBD-DHPE (Avanti Polar Lipids, Alabaster, AL) was also used together with labeled cadherins in the fabrication of multiple bilayer substrates. Formation of GUVs containing lipid or lipid-lipopolymer mixtures has been described elsewhere[24]

3.2.3 Cell-Substrate Linkage Systems on Boimembrane-Mimicking Substrates

3.2.3.1 Cell-ECM Mimicking Linkage

To bind ECM proteins to the biomembrane-mimicking substrate, 1 mg (in 100 µL Milli-Q water) of the thiol-NHS heterobifunctional crosslinker Sulfo-GMBS (Aldrich-Sigma) was added to the DPTE-containing bilayer. Here the thiol group of the crosslinker enables

linkage to the DPTE in the bilayer, whereas the NHS group allows binding to ECM proteins. Following an incubation time of 40 mins, samples were rinsed twice with PBS and 5 mg of Laminin (Invitrogen Carlsbad CA) (incubation time: 40 mins) followed by subsequent rinsing with PBS.

3.2.3.2 Cell-Cell Junction Mimicking Linkage

To enable the formation of cell-cell mimicking linkages, polymer-tethered single and multi-bilayers were fabricated largely following procedures described for the design of laminin-functionalized substrates. However, in this case, the cell-exposed bilayer also contained 0.5 mol% 1,2-dioleoyl-*sn*-glycero-3-[(N-(5-amino-1-carboxypentyl)iminodiacetic acid)succinyl] (nickel salt) (DGS-NTA Ni) (Avanti polar lipid Inc.). Here the DGS-NTA lipid was added to allow binding of His-tagged N-cadherin chimera (R&D systems Cat. No.: 748-EC-50) to the bilayer. Specifically, the GUV's forming the top bilayer of the multi-bilayer system were comprised of 94.5%mol POPC, 5%mol DPTE and 0.5% 1,2-dioleoyl-sn-glycero-3-[(N-(5-amino-1-carboxypentyl)iminodiacetic acid)succinyl] (nickel salt) (DGS-NTA Ni) (Avanti polar lipid Inc.). These GUV's were added to the planar membrane system in calcium ion free buffer. After addition of the DGS-NTA-Ni-containing top bilayer to the multi-bilayer system, the sample was rinsed several times with Milli-Q water, followed by addition of N-cadherin chimera (R&D systems Cat. No.: 748-EC-050). Following an incubation time of 2 hours to 2.5 hours, excess N-cadherin was rinsed off, thus allowing plating of C2C12 myoblasts.

3.3 Image Acquisition Systems

3.3.1 Zeiss Axiovert 200 Microscope and Accessories

An Axiovert 200M (Carl Zeiss, Oberkochen, Germany), equipped with a Zeiss C-Apochromat objective (water immersion, 40 x NA=1.2) and a Zeiss AxioCam MRm monochrome digital camera was utilized to analyze the distribution, aggregation state, and lateral mobility of Alexa 555-antibody-labeled cadherin linkers bound to the bilayer systems (prior to cell plating). The microscope, which is part of a Confocor 2 fluorescence correlation spectroscopy system, not only allows epifluorescence (EPI) microscopy analysis, but also enables the acquisition of differential interference contrast (DIC) micrographs. The microscope is equipped with a stage incubator for live cell imaging experiments at 37°C.

3.3.2 Olympus FV-1000 Confocal Microscope and Accessories

Live cell imaging experiments on C2C12 myoblasts were mostly conducted 20 h after plating using confocal microscopy system (FV1000, Olympus USA, Center Valley, PA) equipped with an active z-axial drift correction system (ZDC, Olympus USA, Center Valley, PA) to facilitate long-term studies. To enable live cell imaging experiments, the microscopy system was equipped with a stage cell incubator (Takashi Thermo., Japan) operated at 37°C and 5% CO_2. Confocal micrographs of plated cells were acquired through a 20x objective (Olympus USA, UPlanSAPo 20x/0.75) using Olympus FV10-ASW imaging software (Olympus USA, Center Valley, PA). Micrographs were analyzed in terms of cell spreading area and extent of stress fiber formation using FV10-ASW viewer software (Olympus USA, Center Valley, PA). To determine cell migration speed, confocal

micrographs of plated cells were acquired every 5 mins over a time period of 2h. Cell motility data were obtained by tracking the nucleus of migrating cells over time using ImageJ and the plugin “object tracker and manual tracking” [ImageJ, U. S. National Institutes of Health, Bethesda, Maryland, USA, http://imagej.nih.gov/ij/, 1997-2014 date last access 12/10/2015.].

3.4 Immunostaining of Multiple Cell Lines

3.4.1 Cell Culture

3.4.1.1 3T3 and MEF Fibroblasts

3T3 Fibroblasts, purchased from ATCC Virginia, and MEF Fibroblast provide by Profs. Ben Fabry and Goldmann from the University of Erlangen, were both cultured in DMEM medium (Invitrogen life science, CA) with 10% fetal bovine serum (Thermo Fisher Sci., MA), 100 U/mL Penicillin/Streptomycin (Thermo Fisher Sci., MA), and incubated at 37 °C in a humidified 5% CO_2 atmosphere. For cell passaging, 2.5% trypsin (Thermo Fisher Sci., MA) was used to detach C2C12 myoblasts & 3T3 fibroblasts from 75 mL or 25 mL culture flasks (BD BioScience, CA)

In typical experiments, cells were plated with a density of 80/mm^2. Cells were analyzed on the different experimental substrates 20 and 40 h after plating. After incubation at 37℃ and 5% CO_2 for 20 and 40 hrs, 200 μL of LIVE/DEAD viability stock solution (Invitrogen Life Science, Carlsbad, CA) was added into the sample to cover all cells. Incubating for 40 mins under 37 °C or room temperature, the samples were rinsed with PBS buffer and observed using Confocal EPI microscopy. (FV 1000, Olympus USA,

Center Valley PA) In this case, the images were acquired through FITC and Alexa 555 channel to monitor live (FITC) and dead cells (Alexa 555) using the LIVE/DEAD Assay[229].

3.4.1.2 C2C12 Myoblasts

C2C12 myoblasts was purchased from ATCC Virginia, cultured in DMEM medium (Invitrogen life science, CA) with 10% fetal bovine serum (Thermo Fisher Sci., MA), 100 U/mL Penicillin/Streptomycin (Thermo Fisher Sci., MA), and incubated at 37℃ in a humidified 5% CO_2 atmosphere. For cell passaging, 2.5% trypsin (Thermo Fisher Sci., MA) was used to detach C2C12 myoblasts & 3T3 fibroblasts from 75 mL or 25 mL culture flask (BD BioScience, CA).

3.4.2 Immunohistochemical Staining of Cellular Adhesions Target Proteins

3.4.2.1 F-Actin

Immunofluorescence experiments were conducted to characterize actin network organization and AJs by adapting procedures described before[171]. Typically, about 8.5 cells/mm^2 were cultured for 20 h at 37°C and 5% CO_2 on laminin-coated glass or multi-bilayer substrates with laminin or N-cadherin linkers inside of a 35 mm petri dish with a 15 mm diameter glass bottom. Cells were fixed in 4% formaldehyde and treated with 0.5% Triton X-100 (incubation time for each step: 10 min) followed by rinsing with PBS and 1h incubation in PBS with 1% BSA and the subsequent addition of secondary IgG1 antibody (Biolegend, San Diego, CA), and phalloidin-TRITC (Sigma Aldrich, St. Louis, MO). Primary and secondary antibodies were added for one hour using 1:500 for phalloidin- TRITC, respectively. Samples were washed with PBS and 3% BSA in PBS and stored at 4°C until

used. Fluorescently labeled cells were imaged using confocal microscopy (FV1000, Olympus USA, Center Valley, PA) and analyzed using Olympus FV10-ASW imaging software and Image J.

3.4.2.2 β-Catenin

For the immunostaining of β-catenin on C2C12 Myoblasts, cells were fixed with 4% formaldehyde and rinsed twice with 1% BSA solution. After a 10 min incubation time with 0.5% Triton X-100, samples were rinsed with BSA buffer and the primary β-catenin antibody (eBioscience, San Diego, CA) was added for direct labeling with Alexa 488 for 2 hours. After rinsing twice with BSA and PBS buffer, samples were imaged using confocal microscopy (FV 1000, Olympus USA, Center Valley PA) or stored in a refrigerator for up to 2 days followed by imaging.

3.5 Acquisition and Analysis of Cellular Mechanosensitivity

3.5.1 Cell Spreading Area and Morphology

DIC and EPI images of C2C12 Myoblasts and MEF/3T3 Fibroblasts placed on biomembrane-mimicking substrates were obtained with 20x and 40x objectives on both Zeiss Confocor 2 microscope and Olympus FV1000 confocal microscope described in section 3.3. For cell spreading area analysis, fluorescently labeled cells were imaged using confocal microscopy (FV1000, Olympus USA, Center Valley, PA) and analyzed using Olympus FV10-ASW imaging software and Image J. For cellular morphology, cells were imaged with using the DIC channel of the Confocor 2 Microscope and analysis was performed with Image J.

3.5.2 Cytoskeleton Organization

Analysis of actin stress fiber formation has been a useful measure to probe the extent of cell-generated forces on substrates of different stiffness. By building on this general concept, we recently reported that the percentage of fibroblasts with visible ventral stress fibers on different laminin-functionalized bilayer substrates decreases from about 20% on a single bilayer to less than 5% on a quadruple bilayer, thus validating the ability to alter substrate stiffness by altering bilayer stacking on linker-functionalized multi-bilayer substrates[230].

3.5.3 Cellular Adhesions

For analysis of size of cellular adhesions on biomembrane-mimicking substrates, the biomarkers of the focal adhesion protein were labeled with specific antibodies and fluorescent dye as described: C2C12 myoblasts on substrates for linkage of cell-cell junction mimicking were supplied with β-catenin antibodies with Alexa 488 for one hour incubation and rinsed off excess adhesion peptides with PBS buffer; MEF and 3T3 Fibroblasts were supplied with IgG protein antibodies labeled with rhodamine phalloidin to colorize focal adhesion kinase. Image data of labeled cellular adhesion agrin sites would be obtained from EPI microscopy and analyzed with Matlab software and ImageJ with a plugin compatible for an Olympus image format.

3.5.4 Cell Migration

To determine cellular migration speed, confocal micrographs of plated cells were acquired every 5 mins over a time period of 2h. Cell motility data were obtained by tracking the nucleus of migrating cells over time using ImageJ and the plugin “object

tracker and manual tracking" [ImageJ, U. S. National Institutes of Health, Bethesda, Maryland, USA, http://imagej.nih.gov/ij/, 1997-2014.date last accessed 12/10/2015].

3.5.5 Traction Force Microscopy

A modified traction force microscopy assay was employed to probe cellular traction forces in a PAA gel underneath biomembrane-mimicking cell substrates using procedures described previously[56]. In short, after preparation of PAA gels, with a Young's modulus of 11.3 kPa, that contained embedded fluorescent particles and a fibronectin surface coating (described in 2.3), linkage between lipid bilayer and fibronectin layer was accomplished by subsequent addition of heterobifunctional NHS-maleimide cross-linker Sulfo-GMBS (Thermo Fisher Sci. Rockford, IL) (concentration: 10mg/mL in DMSO; incubation time: 30min) and lipid bilayer containing POPC and 5 mol% DPTE. Formation of multi-bilayers and design of bilayer-cell linkers followed procedures described in 2.1. C2C12 myoblasts were placed on the bilayer-functionalized gels at a density of 80 cells/mm2 and incubated at 37 ℃ and 5% CO_2. Bright-field images of plated cells were acquired together with fluorescent micrographs (through FITC channel) of bead positions 20 hours after plating using an inverted optical microscope (Axiovert 200M, Carl Zeiss, Oberkochen, Germany) with EC Plan-NEOFLUAR objective (20 x, NA=0.5) (Carl Zeiss, Jena, Germany). Following the treatment of cells with a 100μl cocktail of 80 μM cytochalasin D (BD BioScience, CA) in 0.25% trypsin solution, fluorescent micrographs of the bead positions were taken again. The displacement of beads between gel relaxations due to the cells traction were estimated and analyzed with an unconstrained deconvolution algorithm. Both of the traction force and the displacement field were calculated using the

Fourier transform traction cytometry method described in ref[49]. Furthermore, strain energy, U, of each cell was estimated with the methodology within the reference[56] .

3.5.5.1 Fabrication of Traction Force Microscopy Assay

Polyacrylamide gels (PAA gel) were built on pretreated glass slides. Pretreatment of glass slides included subsequent incubation in aqueous solutions of 0.1 M NaOH, 2.0% 3-aminopropyltrimethoxysilane, and 2.5% glutaraldehyde and rinsing with Milli-Q water after each incubation step. Formation of the PAA gel followed established procedures[56]. In short, aqueous solutions with 40% acrylamide/bisacrylamide with embedded 0.5μm green fluorescent beads (505/515) (Invitrogen/ Life Science, Carlsbad, CA) were made to achieve final concentrations of 4.1% or 6.1% acrylamide. The solution was centrifuged at 1500 rpm for 30 mins at 4 ℃ and 0.2% N.N.N'N-tetramethylethylenediamine (TEMED) was added as a crosslinker and mixed with the initiator 0.5% ammonium persulfate (APS) to start the polymerization and crosslinking reactions resulting in the PAA at room temperature (1 h for polymerization). For activation of the gel surface, 150 μl of the photocrosslinker Sulfo-SANPHA (Thermo Fisher Sci. Rockford, IL) was added and allowed to bind to the gel using UV light irradiation for 5 mins. After extensive rinsing with PBS to remove unbound Sulfo-SANPHA, 120 μl of 1.5% fibronectin solution (Thermo Fisher Sci. Rockford, IL) was added and incubated overnight to allow fibronectin binding to the gel via Sulfo-SANPHA linkers. Prior to usage, the gel was stored in PBS buffer at 4℃ for up to 4 days.

Sulfo-GMBS (Thermo Fisher Sci. MA) was added onto PAA gel traction force assays for bridging to fibronectin above PAA gels with NHS functional group for 40 mins incubation. For single bilayer substrate on traction force microscopy analysis, GUVs solution consisting of POPC, DPTE and DGS-NTA Ni lipids was manufactured as section 3.2.2.2 describes and added to the fibronectin-coated PAA gel with Sulfo-GMBS linker molecules. For multiple lipid bilayers stacking, GUVs solutions were added to PAA gels via the fusion of GUVS containing 5 mol% DPTE, and 95 mol% POPC forming the first bilayer substrate and the subsequent fusion of GUV's comprised of 5 mol% DSPE PEG-2000 Maleimide and 95 mol% POPC for the secondary bilayer. The third bilayer was built by fusion of GUVs containing 0.5 mol% DGS-NTA Ni /5 mol% DPTE/94.5 mol% POPC. In a last step N-cadherin Chimera was added to the DGS-NTA Ni-containing bilayer, thus creating a modified traction force microscopy gel, which is surface of N-cadherin-functionalized multi-bilayer system.

Polyacrylamide gels (PAA gel) were built on pretreated glass slides. Pretreatment of glass slides included subsequent incubation in aqueous solutions of 0.1 M NaOH, 2.0% 3-aminopropyltrimethoxysilane, and 2.5% glutaraldehyde and rinsing with Milli-Q water after each incubation step. Formation of the PAA gel followed established procedures[56]. In short, aqueous solutions with 40% acrylamide/bisacrylamide with embedded 0.5μm green fluorescent beads (505/515) (Invitrogen/ Life Science, Carlsbad, CA) were made to achieve final concentrations of 4.1% or 6.1% acrylamide. The solution was centrifuged at 1500 rpm for 30 mins at 4 °Cand 0.2% N.N.N'N-tetramethylethylenediamine (TEMED) was

added as a crosslinker and mixed with the initiator 0.5% ammonium persulfat (APS) to start the polymerization and crosslinking reactions resulting in the PAA at room temperature (1 h for polymerization). For activation of the gel surface, 150 μl of the photocrosslinker Sulfo-SANPHA (Thermo Fisher Sci. Rockford, IL) was added and allowed to bind to the gel using UV light irradiation for 5 mins. After extensive rinsing with PBS to remove unbound Sulfo-SANPHA, 120 μl of 1.5% fibronectin solution (Thermo Fisher Sci. Rockford, IL) was added and incubated overnight to allow fibronectin binding to the gel via Sulfo-SANPHA linkers. Prior to usage, the gel was stored in PBS buffer at 4℃ for up to 4 days.

Sulfo-GMBS (Thermo Fisher Sci. MA) were added ontoPAA gel traction force assays for bridging to fibronectin above PAA gels with NHS functional group for 40 mins incubation. For single bilayer substrate on traction force microscope, GUVs solution consisted with DPTE lipids and DGS-NTA Ni lipids manufactured as section 3.2.2.2 section heated in 75℃ water was added to the assay substrates for single bilayer formation with thiol linker to Sulfo-GMBS. For multiple lipid bilayers stacking, GUVs solutions were then added to atop PAA gels via the fusion of GUVS containing 5%mol DPTE, and 95%mol POPC forming the first bilayer substrate, and then 5%mol DSPE PEG-2000 Maleimide and 95% POPC for the secondary bilayer. GUVs solution with 0.5%mol DGS-NTA Ni /5%mol DPTE/94.5%mol POPC was added to the third bilayer substrate for linkage to N-cadherin Chimera as descripted as coated system as descripted in section 3.2.2.2.for cadherin system or 5%mol DPTE/95%mol POPC for Laminin coated system.

3.5.5.2 Process of Image Acquisition and Data Analysis

C2C12 Myoblasts and other cells were placed on the traction force microscopy assay and incubated in 37℃ and 5% CO_2 for 24 hrs and 48 hrs. Assays were imaged with both DIC and EPI-FITC channel for recording the cell shape, location and bead displacements between treatment with the 100 µL cocktail of 80 mM Cytochalasin D (Sigma-Aldrich) in 0.25% trypsin. With no cellular force applied, the gel relaxes back to its stress-free configuration, and the second image was taken. The displacements of the bead due to the cell tractions are estimated with Matlab software using an unconstrained deconvolution algorithm, and the cell tractions are computed using the Fourier transform traction cytometry method described in reference[49]. From the displacement field and the traction force, the strain energy U were calculated as the following formula

$$U = \frac{1}{2}\int (traction\ x\ displacement)\ dxdy \qquad [14]$$

RESULTS AND DISCUSSION

4.1 Design and Characteristics of Cell-Cell Junctions Biomembrane-mimicking Multi-Bilayer Substrates (TYPE II) with N-cadherin Linkers

Previously, cadherin linkers were employed in artificial cell-cell mimicking substrates, which were mainly comprised of polymeric gels such as PDMS[186,215] and PAA[57,118,231]. In this work, we successfully design and fabricate a cadherin system on polymer-tethered multi-bilayer substrates with DGS-NTA lipids (4.1.1) (Type II substrates). These novel cell surface-mimicking cell substrates represent a significant advance over existing polymeric systems with polymer-conjugated linkers because they enable the free assembly of linkers at cell-cell-junctions without impairing cell spreading and migration. In that sense, this biomembrane-mimicking substrate better replicates the rich dynamics found at cell-cell interfaces. Moreover, recent magnetic tweezer experiments on magnetic beads bound to laminin-functionalized single, double, triple, and quadruple bilayers demonstrated the largely elastic nature of these supramolecular assemblies with respect to adsorbed 4.5mm size particles mimicking cellular adhesions and the ability to alter substrate mechanical properties by changing the number of bilayers in the stack[171] These remarkable, tunable materials properties can be attributed, at least in part, to the fascinating coupling phenomena in polymer-tethered membranes, which include

coupling of lipopolymer-enriched interbilayer connections, percolation of linker clusters, and strong interleaflet coupling of immobilized linker clusters [218,232-234]. As part of this thesis, the characteristics of TYPE II substrates with cadherin linkers was examined using complementary microscopy methods (4.1.2). After placing C2C12 myoblast cells on TYPE II substrates with N-cadherin linkers, the cellular mechanoresponse of myoblast cells was analyzed on such substrates (4.1.3). Results from these experiments will be presented in the following subsections.

4.1.1 Fabrication of TYPE II Substrates with N-Cadherin Linkers

Fabrication of TYPE II substrates with N-cadherin linkers was successfully accomplished by multi-bilayer formation using subsequent LB/LS and GUV deposition techniques (see schematic of multi-layer assembly in Fig. 4.1.1 [A]). Here the first bilayer was built by the LB/LS method using a membrane composition of 5 mol% DSPE-PEG2000-Maleimide lipopolymer and 95 mol% POPC. Cadherin linkage to the cell-exposed bilayer was accomplished by incorporating 0.1 mol% DGS-NTA into the lipid mixture, enabling binding of his-tagged N-cadherin chimera. While building multiple bilayer substrates, GUV deposition techniques were employed forming a substrate with two to four lipid bilayers. The GUV fusion method is the same as described in previous experiments and utilizes 0.1 mM sucrose/1 mM $CaCl_2$-filled GUVs containing 95 mol% POPC and 5 mol% DPTE in the presence of 0.1 mM glucose/0.1 mM $CaCl_2$ buffer. The sugar gradient, which causes the sinking of the GUVs, assists in the formation of the second planar bilayer. In contrast, the third bilayer was composed of 95 mol% POPC and 5 mol% DSPE-PEG2000 Maleimide with the same buffer to form GUVs and utilizing sugar gradient to help the process of third

bilayer stacking. The fourth bilayer on a quadruple bilayer substrate consists of 95 mol% POPC and 5 mol% DPTE with only 0.1 mM sucrose buffer to form GUVs to avoid the of replacement of Ni^{2+} ions on DGS-NTA lipids; there are no calcium ions added into the final GUV solution to enhance the process of vesicle formation. Thus, formation of GUV solution requires 15-30 minutes more to complete in calcium-free glucose buffer compared to glucose buffer with 0.1 mol% calcium chloride. Figure 4.1.1 [B, C] show representative fluorescence micrographs, which demonstrate the homogeneous distribution of dye-labeled lipids (NBD-DHPE) [B] and N-cadherin chimera (labeled with Alexa-555tagged anti-N-cadherin antibody) [C] in the polymer-tethered lipid bilayer prior to cell plating.

In the planar model membrane system, lipopolymers with a terminal maleimide functional group act as specific linkers to lipids with a sulfhydryl group in the adjacent lipid bilayer, resulting in the formation of a stable polymer--tethered multiple bilayer stack. In such a system, lipopolymer density not only impacts the degree of obstructed lipid diffusion, but also affects membrane curvature and surface roughness with direct implications on membrane tension and interleaflet coupling of lipid lateral mobility.

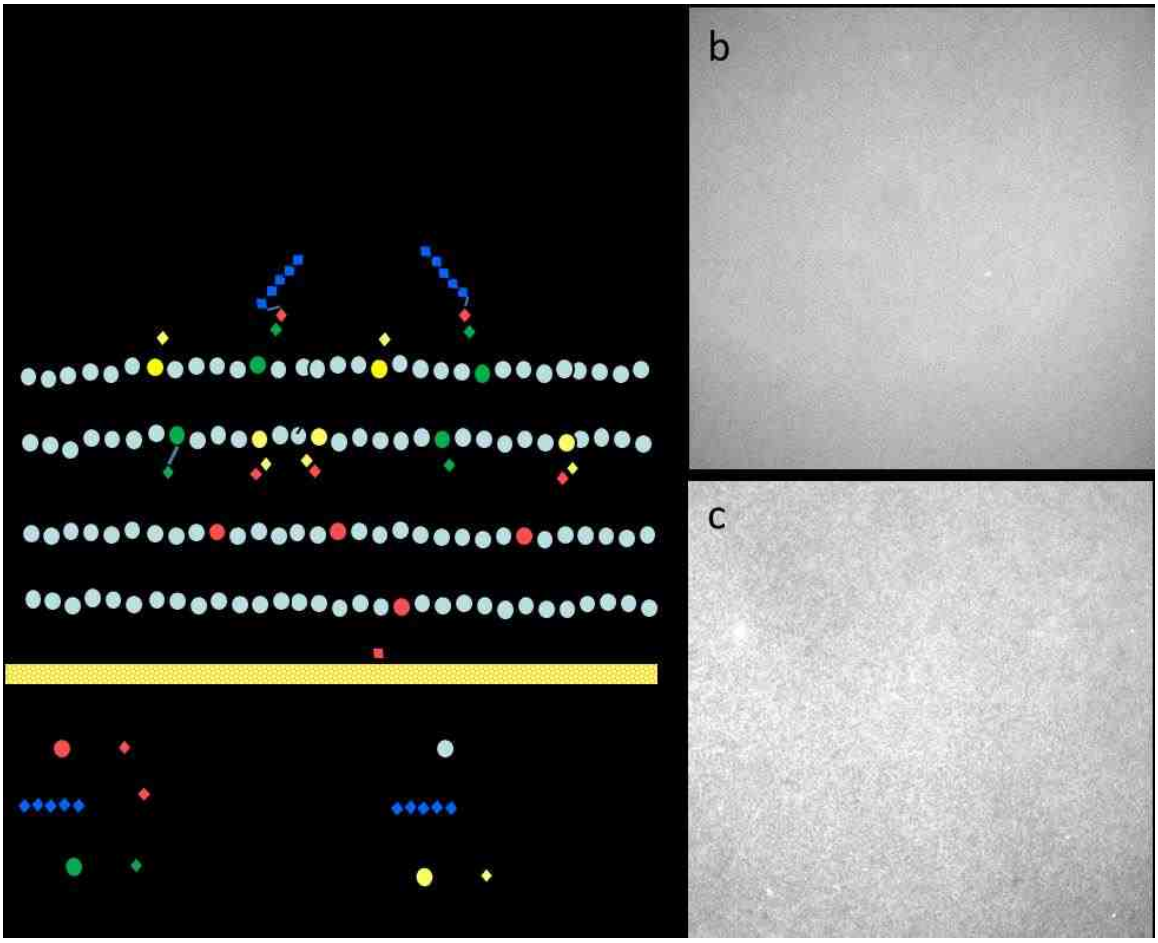

Figure 4.1. 1 a: the scheme of multiple stacking bilayer containing N-cadherin chimera via His-tag chemistry. b: Single bilayer containing 0.01% DGS-NTA and 0.1% NBD-PE. c: Single bilayer containing 0.01% DGS-NTA and N-cadherin chelating with antibodies labeled with Alexa-555. Size of b and c are 200 µm x 200 µm

The other role of the lipopolymer on TYPE II substrates is to allow the facile adjustment of bilayer bending stiffness with different molar concentrations, also acting as efficient crowding agents[170]. Interestingly, a polymer-tethered single bilayer substrate with 95 mol% POPC and 5 mol% of DSPE-PEG 5000 has a bending modulus (K_c) of about 50 K_bT, which is similar to that of a red blood cell membrane[208].

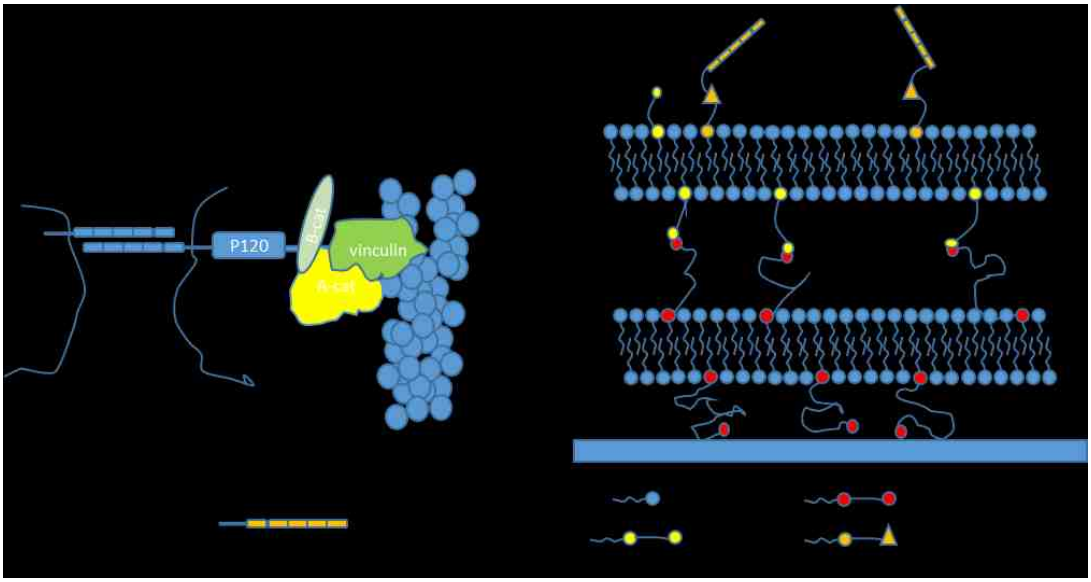

Figure 4.1. 2 Cadherin-functionalized lipid bilayers were built by incorporation of DOGS-NTA-Ni into the bilayer and subsequential binding of His-tagged cadherin chimera.

Figure 4.1.2 illustrates the cell-cell junction formation via N-cadherin homotypic binding, by which the extracellular domain of opposing N-cadherin proteins bind to each other. Here, the cellular cadherins form a complex with proteins, such as P120, β-catenin and α-catenin, which facilitate the linkage with actin filaments of the cytoskeleton structure. As mentioned in the previous chapter, fluorescent intensity of cadherin-catenin complexes after immunostaining indicates the degree of force of the cytoskeleton system on artificial substrate such as PDMS gel and PAA gels. Fluorescent intensity of β-catenin immunostaining on the periphery of the cell membrane also increases with increasing stiffness of artificial cell substrates [235,236]. In our work, C2C12 Myoblasts were placed on TYPE II substrates tethered with cadherin linkers as shown above.

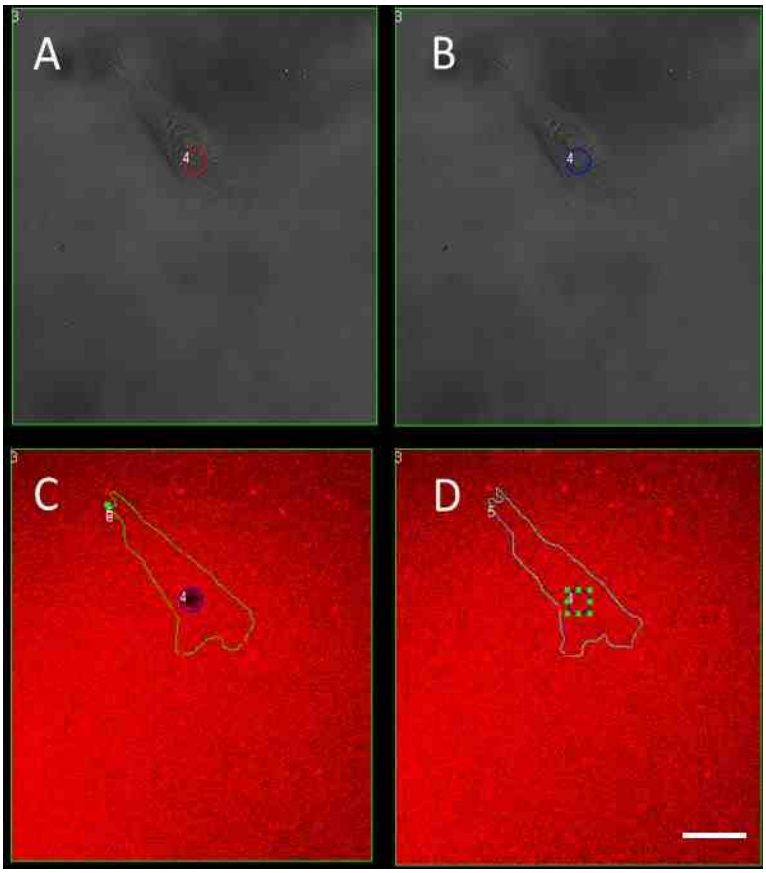

Figure 4.1. 3 [A] and [B] are DIC images before and after recovery with FRAP technique; [C] and [D] are EPI images before and after recovery with FRAP. Scale Bar: 20 µm

Integrity of the biomembrane-mimicking substrate was examined 48 hours after cell plating using confocal fluorescence analysis of DHPE-Texas Red distribution underneath plated cell together with FRAP analysis of dye-labeled lipid diffusivity. Figure 4.1.3, A and B illustrate representative DIC images of C2C12 myoblasts above the bleaching spot (indicated by circle) generated by the confocal laser system; C and D are corresponding EPI micrographs of the same area of the sample illustrating the distribution of DHPE-Texas Red in the top bilayer of a N-cadherin-functionalized double bilayer substrate immediately after bleaching (C) and 2min after bleaching (D). No optically

visible bilayer defects can be observed in these micrographs, demonstrating the stability of the multi-bilayer system in the presence of plated cells. Similarly, FRAP analysis revealed a lipid diffusion coefficient of D = 2.2 ± 0.2 $\mu m^2 s^{-1}$ and a 90 % intensity recovery (2 min after bleaching), confirming the integrity of TYPE II bilayer system underneath plated cells

4.1.2 Key Characteristics of TYPE II Substrates with N-Cadherin Linkers

To further characterize the properties of the cadherin linker system, we next determined the lateral mobility of TRITC-DHPE and N-cadherin chimera (labeled with Alexa-555 anti-N-cadherin antibody) using fluorescence correlation spectroscopy. Figure 4.1.4 shows representative results from these experiments, which demonstrate the lateral mobility of both fluorescently-labeled lipids and N-cadherin chimera in the polymer-tethered bilayer. It should be pointed out that compared to previous artificial cell surface-mimicking substrates [111,208], the current biomembrane-mimicking system is one of only a few models, in which individual cadherin linkers maintain their lateral mobility, thus better replicating a biomembrane-like environment.

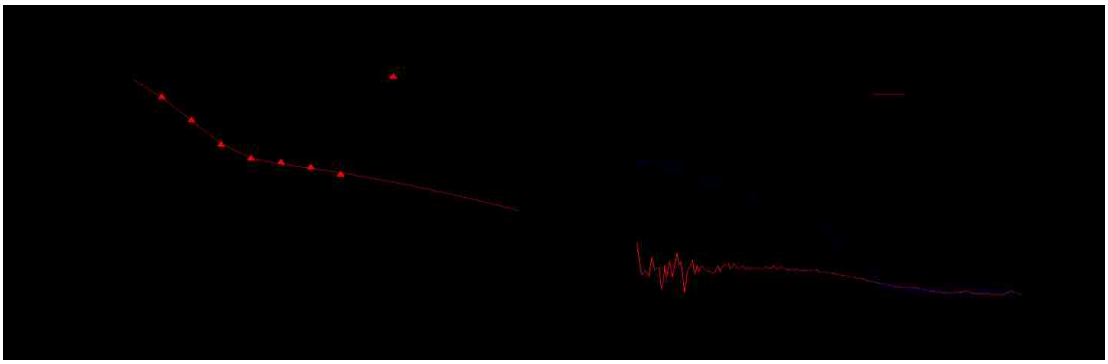

Figure 4.1. 4 Dye labeling (Alexa 555) of N-cadherin linkers allows analysis of linker distribution in the absence and presence of plated cells. FCS autocorrelation analysis confirms the lateral mobility of individual N-cadherin chimera in TYPE II Substrate prior to cell plating

In order to further investigate the properties of N-cadherin clusters in TYPE II substrates, we functionalized fluorescent beads with N-cadherin and let them bind to a single polymer-tethered bilayer with N-cadherin linkers (Figure 4.1.5 left). Binding of fluorescent beads functionalized with N-cadherin on the TYPE II bilayer was in the presence of calcium ions (Figure 4.1.5 right). Importantly, results from time lapse images (Figure 4.1.5 right) revealed that all bilayer-bound N-cadherin beads were immobilized, illustrating the immobilization of N-cadherin linker clusters in TYPE II bilayers.

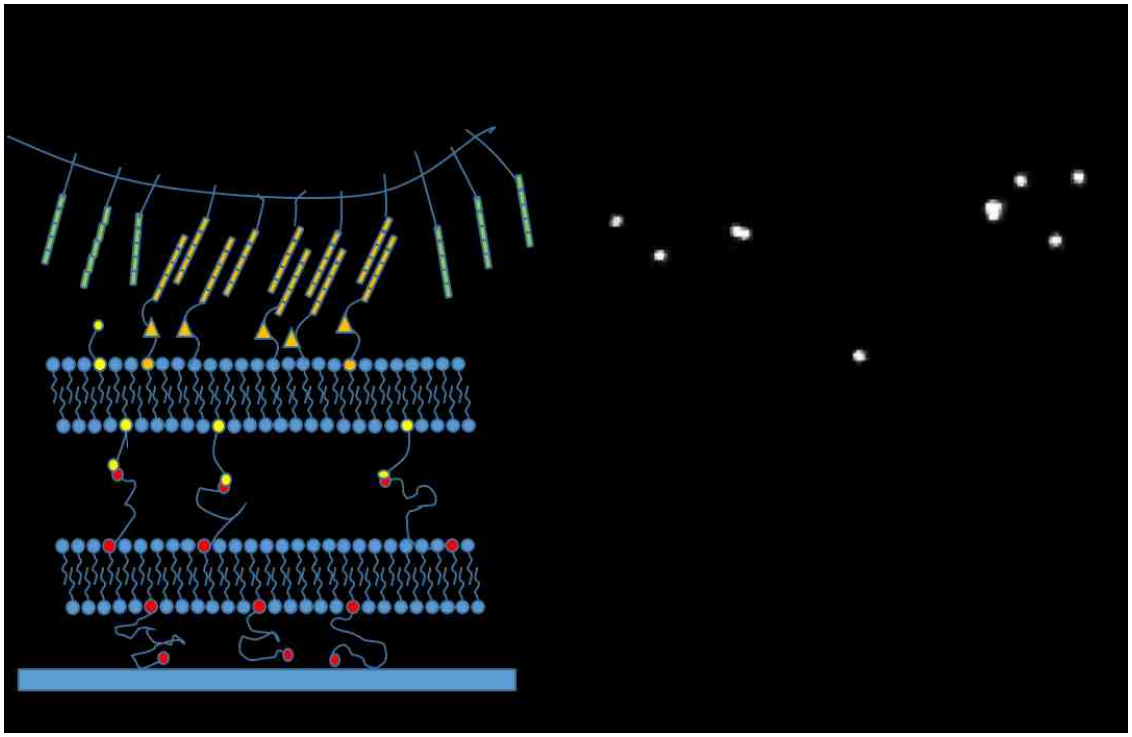

Figure 4.1. 5 N-cadherin functionalized bead placed on TYPE II polymer-tethered substrates shows linker clusters are immobilized

The analysis of N-cadherin linkers and linker clusters suggested that N-cadherin linkers are able to assemble into linker clusters underneath plated cells. To confirm this, we explored the distribution of dye-labeled N-cadherin linkers in the presence of plated

C2C12 myoblasts. Figure 4.1.6 illustrates a representative fluorescence intensity distribution of Alexa-555 labeled N-cadherin on a TYPE II substrate underneath a C2C12 myoblast. Most importantly, Figure 4.1.6 confirms the accumulation of N-cadherin linkers underneath the adsorbed cell. Moreover, quantitative fluorescence analysis (through confocal line scans) at 24, 48, and 72 hrs demonstrates the gradual accumulation of bilayer bound N-cadherin chimera underneath plated cells, indicating the linkers' ability to freely assemble into linker clusters in such membrane architectures. Figure 4.1.6 also shows that N-cadherin linkers are heterogeneously distributed underneath the plated cells.

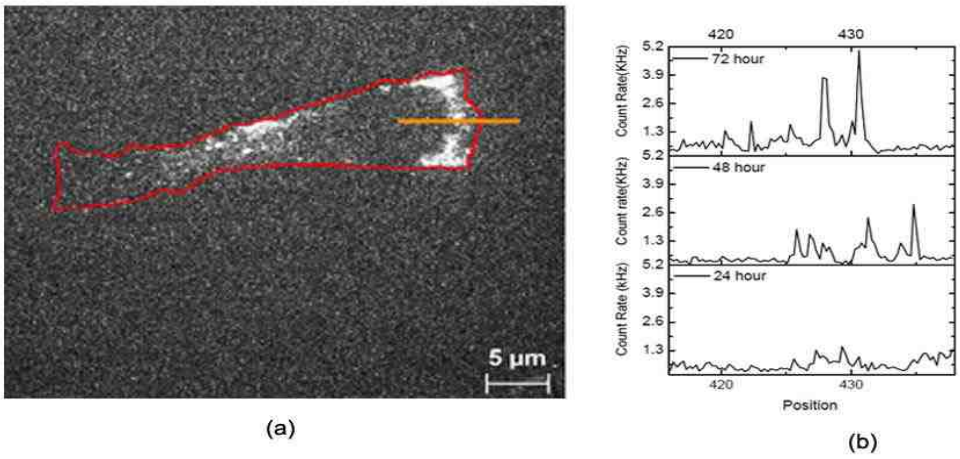

Figure 4.1. 6 Analysis of Alexa 555-labeled N-cadherin chimera distribution underneath C2C12 Myoblasts placed on TYPE 1 Bilayers: Fluorescence micrograph (a) demonstrates the accumulation of N-cadherin chimera at the leading edge of a migrating cell. Time evolution of confocal fluorescence intensity line scans (b) illustrates the gradual dynamic assembly of N-cadherin linkers underneath plated C2C12 Myoblasts.

Taken together, TYPE II bilayers display intriguing properties. Individual N-cadherin linkers are laterally mobile and free to assemble into immobilized N-cadherin

linker clusters, enabling the gradual accumulation of such linkers underneath plated cells over time. The ability of cells to spread on such a biomembrane-mimicking substrate (see Fig. 4.1.6) suggests that linkers underneath adsorbed cells are assembled, at least in part, into linker clusters, which are unable to diffuse freely.

4.1.3 Cellular Mechanoresponse of C2C12 Myoblasts on Multi- Bilayer Substrates (TYPE II)

The work in this section supports the central hypothesis that cellular mechanoresponse can be tuned by altering the number of bilayers in a polymer-tethered multi-bilayer of TYPE II. Previous reports demonstrated that mechanosensitive cells behave differently on substrates of different stiffness, thereby altering properties such as spreading area[237] migration speed, cellular traction forces, and cytoskeleton organization.

For example, fibroblasts on multi-bilayer substrates displayed increased migration velocities, migration directionality and heightened shape fluctuations[170]. Corresponding traction force microscopy experiments demonstrate the lubricating effect of the bilayer substrates that lead to a reduction of cellular traction forces [171]. Furthermore, a series of control experiments confirmed the integrity of the multi-bilayer systems underneath plated cells, thus excluding potential bilayer defects as possible explanation for the observed differences in cellular response on biomembrane-mimicking substrates.

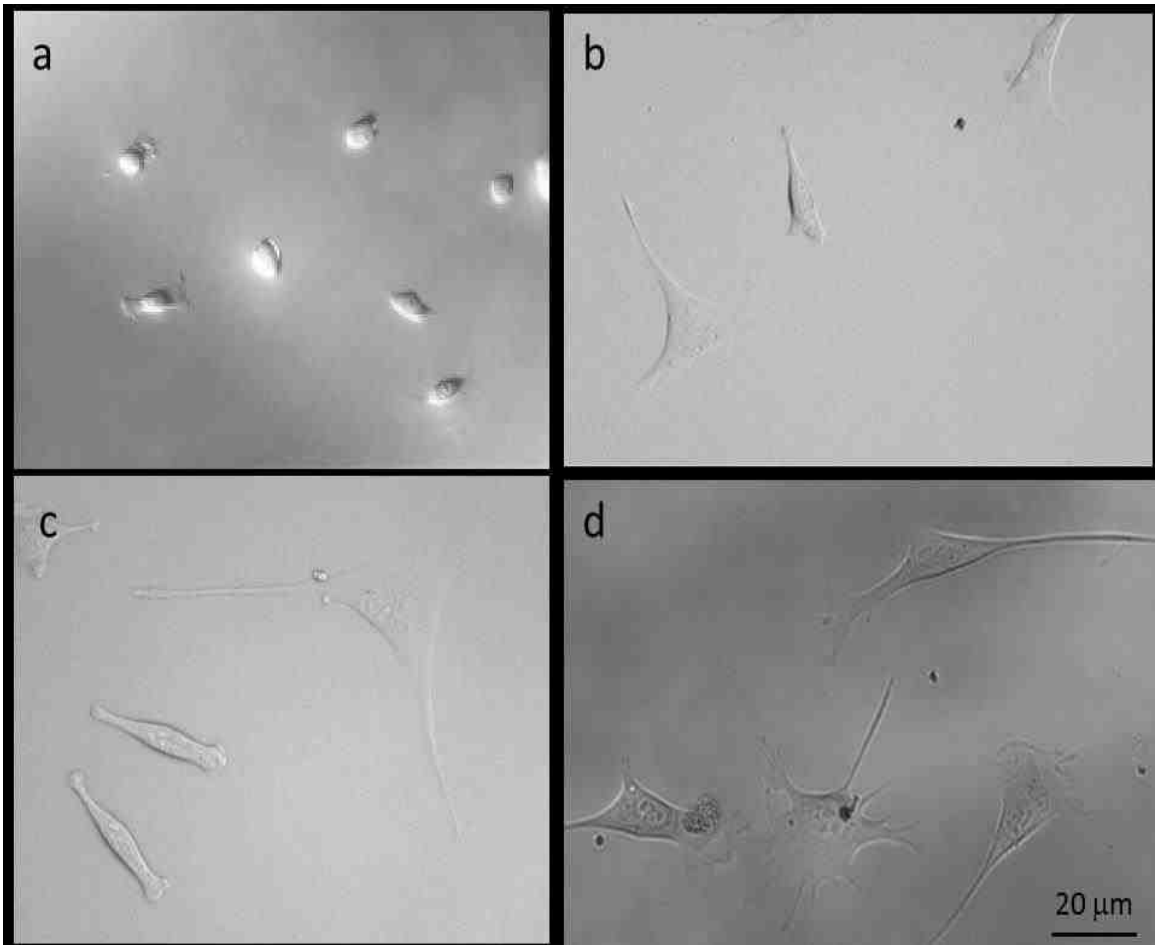

Figure 4.1. 7 Myoblast cells on double bilayer coated with different ligands a: No Linker b: 0.04 mol% N-cadherin c: 0.1 mol% N-cadherin d: Laminin.

In Figure 4.1.7, C2C12 myoblasts on double bilayers coated with different density of linker conditions are shown. As illustrated in Fig. 4.1.7 [a], most cells cannot spread out or remain in a spherical shape on double bilayers without any linker. In contrast, cells on double bilayers with high (0.1 mol%) and low density (0.04 mol%) of N-cadherin linkers show good cell spreading, thereby not displaying any notable differences in terms of shape and spreading area. According to figure 4.1.7 [b] and [c], linker density on TYPE II substrates contributes little to impact cell spreading and morphology. Interestingly,

myoblasts on TYPE II bilayer substrates coated with laminin show a somewhat larger spreading area[60] (if compared to the value obtained on an N-cadherin substrate of comparable linker density).

4.1.3.1 Cell Spreading Area and Morphology

As reported in Figure 4.1.8, the cell area decreases with increasing number of bilayers of a TYPE II multi-bilayer system. Cells are also smaller on the softer 4.1% PAA gels compared to cells on stiffer 6.1 and 6.8% PAA substrates. The relationship between bilayer stacking and cell area is characterized by a statistically significant correlation if one considers PAA gels and TYPE II substrates coated with laminin linkers. This correlation is less pronounced for TYPE II substrates with 0.1 mol% N-cadherin. As mentioned before, C2C12 spreading areas are moderately increased on TYPE II bilayers with laminin linkers versus N-cadherin linkers of the same degree of stacking.

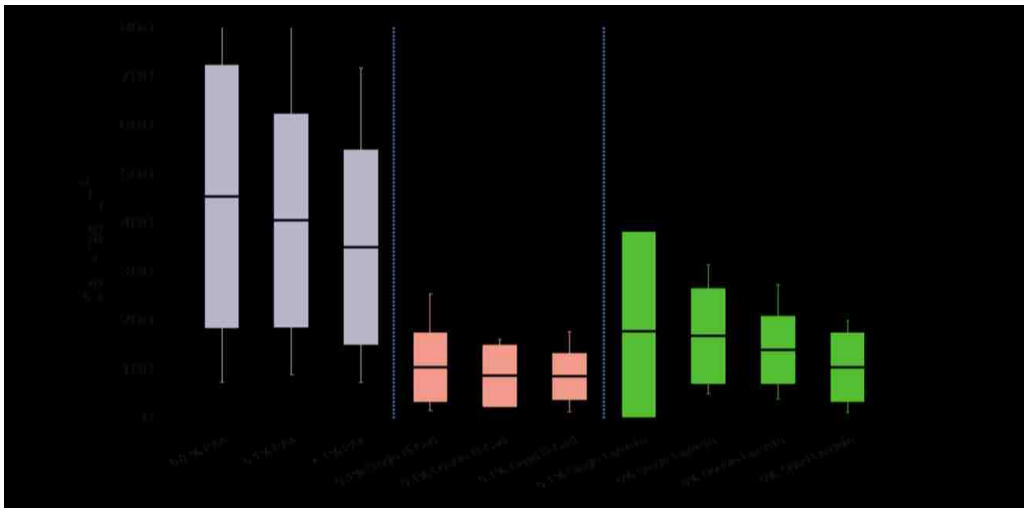

Figure 4.1. 8 C2C12 myoblast cell area on various substrates as. Blue strips: Poly acrylamide gel coated with fibronectin; Red strips: Multiple bilayer system coated with N-cadherin linker (N-Cad); Green Strips: multiple bilayer system coated with laminin.

4.1.3.2 Cytoskeleton Organization and Adheren Junctions Formation

There is a close correlation between cellular contractile forces and substrate stiffness. At the same time, the strength of cellular contractile forces is typically reflected by the extent of actin stress fiber formation and the size/distribution of cellular adhesions. For example, we have previously shown that increasing bilayer stacking in a laminin-functionalized TYPE II bilayer is associated with more dynamic and irregularly shaped focal adhesions. Similarly, Figure 4.1.9 illustrates that increases in bilayer stacking of N-cadherin-functionalized TYPE II bilayers reduce adherens junction size (visualized by β-catenin distribution).

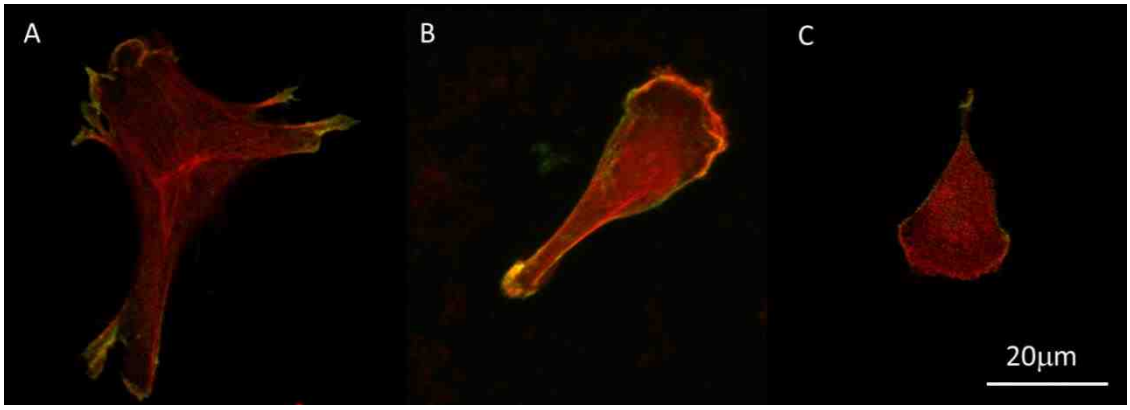

Figure 4.1. 9 β-catenin Immunostaining (in green) of C2C12 myoblast on stacking bilayer system 24 hours after placement. Average fluorescent intensity on Olympus Confocal microscopy of antibodies β-catanin decreases with additional bilayer stacking: A: Single bilayer (2364), B: Double bilayer (1577), and C: Quadruple bilayer (867).

Cytoskeletal organization is another indicator of cellular mechanoresponse on substrates with different mechanical properties. Fig. 4.1.9. already illustrates that increasing bilayer stacking of N-cadherin functionalized multi-bilayer system of TYPE II causes reduced formation of visible ventral actin stress fibers. The influence of bilayer

stacking on cytoskeletal organization is illustrated more quantitatively in Figure 4.1.10. Herein, Figure 4.1.10 shows that notable static stress fiber formation can be observed in single bilayers regardless of linker type (laminin versus N-cadherin). However, compared to laminin-functionalized TYPE II substrates, a smaller percentage of the C2C12 myoblasts showed formation of visible ventral actin stress fibers on N-cadherin coated substrates. Figures 4.1.9 and 4.1.10 are both important for the illustration of cytoskeletal organization since they can be well interpreted in terms of the cells' ability to adhere efficiently to both TYPE II and single bilayers coated with laminin and cadherin. The result of Figure 4.1.10 suggests that defect-mediated cell adhesion to the glass substrates appears to be only potentially significant on single bilayer substrate, but not on double or quadruple bilayer substrates. Similar results were previously obtained with 3T3 fibroblasts on laminin-coated TYPE II substrates[170]. That is to say, polymer-tethered multiple bilayer substrates with specific bilayer-cell linkers maintain their integrity in the presence of plated cells.

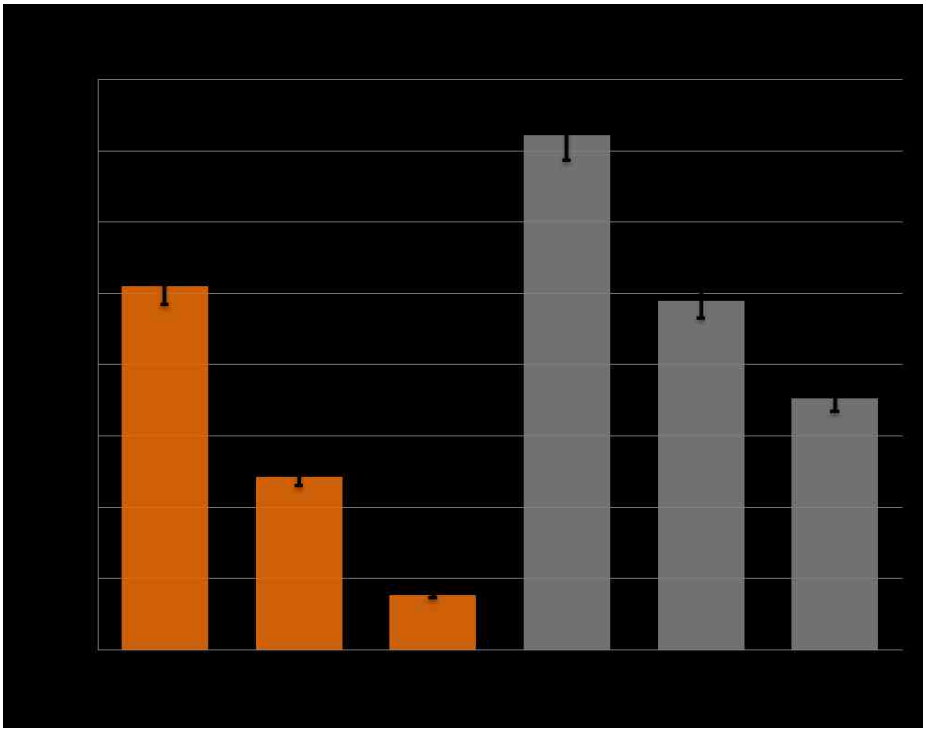

Figure 4.1. 10: Stress fiber ratio of C2C12 myoblast cells on multiple bilayer system coated with N-cadherin (gold) and laminin linkers (gray) demonstrates fewer stress fibers found for N-cad linked cells than laminin cells using single, double and quadruple bilayers

4.1.3.3 Cell Migration

To further investigate the impact of bilayer stacking on the cellular mechanoresponse of C2C12 myoblasts above TYPE II substrates coated with N-cadherin linkers, we next analyzed cellular migration speed. Cellular motility on N-cadherin and laminin-coated TYPE II substrates;(i.e, single, double and quadruple bilayers) were examined using time-lapse DIC imaging (time lag = 5 mins). In Figure 4.1.11 nuclear displacement over time demonstrates that cellular migration speed of myoblasts on TYPE II substrates gradually increases with bilayer stacking. Cellular motility results echo the

findings of cytoskeletal organization obtained on TYPE II substrates with N-cadherin and laminin linkers, respectively. Again, migration data obtained on TYPE II bilayers with N-cadherin and laminin linkers are slightly different for the same degree of bilayer stacking.

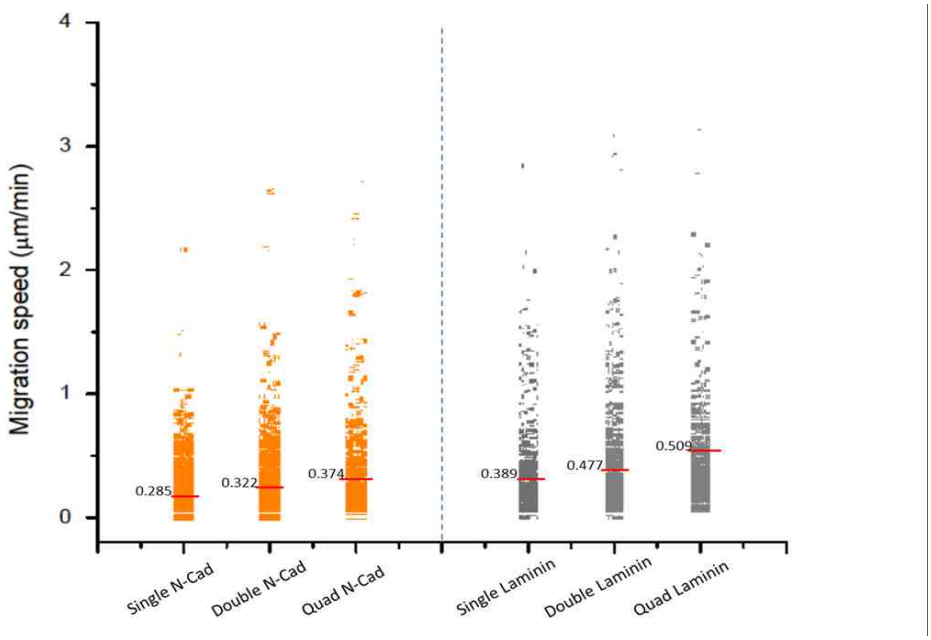

Figure 4.1. 11 Cell migration speed of C2C12 myoblasts on substrates functionalized with N-cadherin (gold) and laminin linkers (gray). N-cadherin and laminin linkers are histograms where each data point represents a measurement between sequential frames. All data poines within a given column represent the movement of the same cell over a 2 hour period. Average values are displayed as horizontal red line.

4.1.3.4 Cellular Traction Force

Cellular traction force microscopy is significant because traction forces are related to contractile cytoskeletal prestress [171]In this work, cell contractility changes on TYPE II substrates coated with N-cadherin were measured using traction force microscopy. C2C12 myoblast cells were placed directly on 6.1% PAA gels or on single or triple bilayers that were coupled to the activated 6.1% PAA gels via fibronection and Sulfo-GMBS linker.

After detaching the cells from substrates, the cell traction forces are counter-balanced by an equal and opposite substrate force, which is measured by bead displacement at the top of the elastic PAA layer, and which can be analyzed and estimated as cell traction. Furthermore, the strain energy stored in the substrate for each cell can be computed as in previous experiments[171]. Figure 4.1.12 demonstrates the calculation of the traction force of myoblast cells on different substrates; the data illustrates that the cell tractions and strain energy gradually decrease with bilayer stacking.

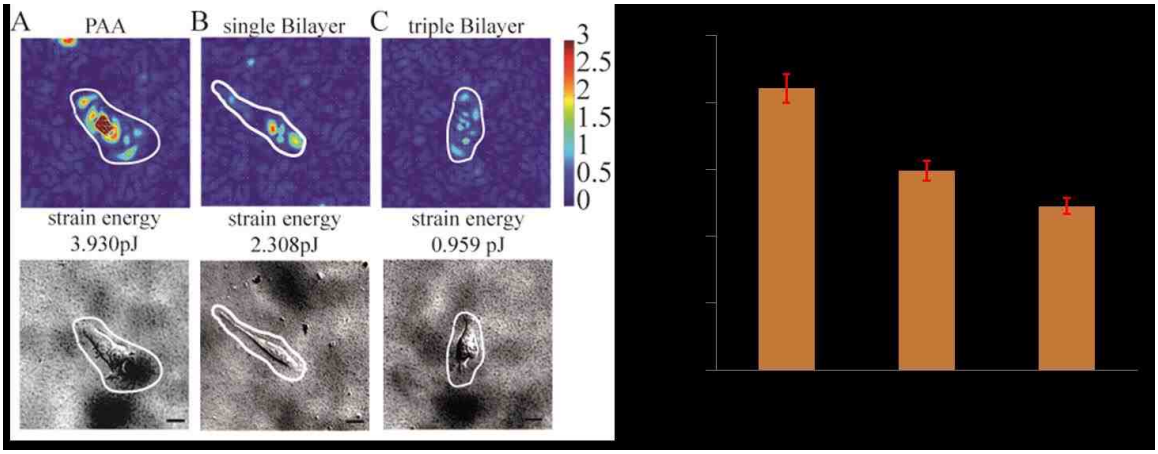

Figure 4.1. 12 Traction Force Microscopy of C2C12 Myoblasts on different biomembrane-mimicking substrates: A. PAA gel. B. Single bilayer. C. Triple bilayer.

4.2 Design and Fabrication of Biomembrane-mimicking Single Bilayer Substrates with Various Lipopolymer Concentrations. (TYPE I)

Mechanical properties of polymer-tethered membranes can not only be adjusted by varying the degree of stacking in a polymer-tethered multi-bilayer stack (TYPE II), but also by changing the concentration of lipopolymers in a single polymer-tethered lipid bilayer (TYPE I). Hereby, TYPE I and TYPE II substrates exhibit complementary substrate

viscoelasticity, enabling experiments of cellular mechanosensitivity on biomembrane-mimicking substrates over a wider range of substrate stiffness. TYPE I substrates were successfully built using the Langmuir-Blodgett (LB) and Langmuir-Schaefer (LS) techniques. Previous experiments[216] showed that TYPE I bilayers show buckling structures, a stress relaxation phenomenon, at medium to elevated lipopolymer concentrations. Furthermore, systematic analysis using AFM demonstrated that increasing lipopolymer content (increasing film stress) in the TYPE I bilayer results in increasing buckling amplitude and buckling width. Moreover, by combining experimentally determined buckling parameters with mean-field calculations of polymer-tethered membranes and buckling theory of an Euler column (straight-sided blister), a metric between elastic properties and buckling parameters in polymer-tethered monolayer and bilayer substrates can be derived[217].

4.2.1 Homogeneous Polymer-Tethered Single Bilayer of Tunable Viscoelasticity

4.2.1.1 Analysis of Mean Field and Impact of Lipopolymer Concentration on Stiffness of TYPE I Membrane Substrates

Previous research[217] on TYPE I substrates containing DSPE-PEG 5000 showed that there is a linear relationship between lipopolymer concentration and the plane strain modulus (E_f^*) (Figure 4.2.1). Similarly, previous micropipette experiments showed that increasing concentrations of PEG lipopolymers in vesicular systems are associated with increasing membrane bending elasticity[238,239] . And more experiments illustrate that the film thickness of lipid and lipopolymer mixtures, built as solid-supported substrates, were

gradually increasing with the polymer thickness from lower to higher concentration of lipopolymer compatible with mean-field and scaling calculations of polymer physics.

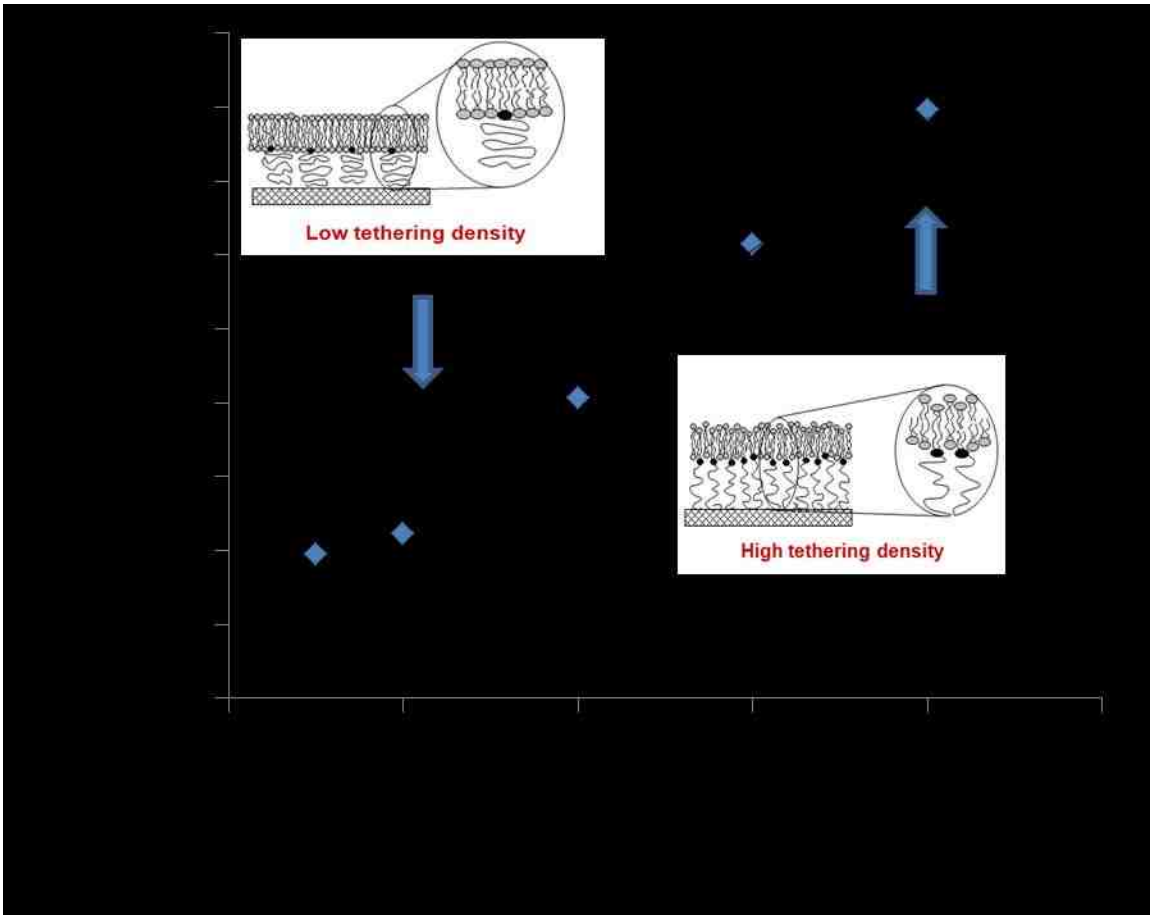

Figure 4.2. 1 Buckling Pattern and Structures with Various Polyethyleneglycol (PEG)-Based Lipopolymer Concentrations[202].

Figure 4.2.2 illustrates representative atomic force microscope micrographs of solid-supported monolayer (a) and bilayer (b) substrates consisting of elevated lipopolymer DSPE-PEG5000 concentration (20 mol%). The enhanced film stress caused by elevated lipopolymer levels cause formation of buckling patterns in LB monolayers (Figure 4.2.2a) and bilayer compartmentalization in corresponding LB/LS bilayer systems (Figure

4.2.2b). Buckling structures in LB monolayers represent a stress relaxation phenomenon, also known as buckling delamination, whereas the bilayer compartmentalization is caused by the inability of bilayer formation on top of buckling structures (presumably, surfaces of buckling structures are somewhat hydrophilic, due to penetrated/flipped polymer chains). As described before, polymer-tethered monolayers with buckling structures are obtained using LB deposition, whereas the compartmentalized polymer-tethered bilayer of TYPE I is accomplished using LB/LS depositions. Note that the LB deposition technique is essential to build polymer-tethered membranes with lipopolymer concentrations higher than 10 mol%, which is the reported saturation concentration of these amphiphiles in vesicular systems[14]. Interestingly, the buckling-associated bilayer compartmentalization in TYPE I bilayers acts as efficient lipid/protein diffusion boundary, resulting in fascinating length scale-dependent diffusion properties of membrane constituents, similar to those observed in cellular membranes[216]. Systematic analysis of buckling structures in polymer-tethered monolayers also revealed a gradual increase of buckling regions with increasing lipopolymer content, illustrating the film stress-inducing effect of lipopolymers in such model membrane systems.

Overall, this earlier work demonstrated that mechanical properties of TYPE I bilayers, which can be altered by lipopolymer concentration, can be determined by mean-field calculations and analysis of buckling structures combined with buckling theory of a straight-sided blister. Another intriguing outcome from these experiments was the discovery that such model membranes show complex length-dependent diffusion properties with remarkable parallels to those found in plasma membranes. Such tunable

properties are also interesting because they allow cell migration experiments in patterned membrane environments.

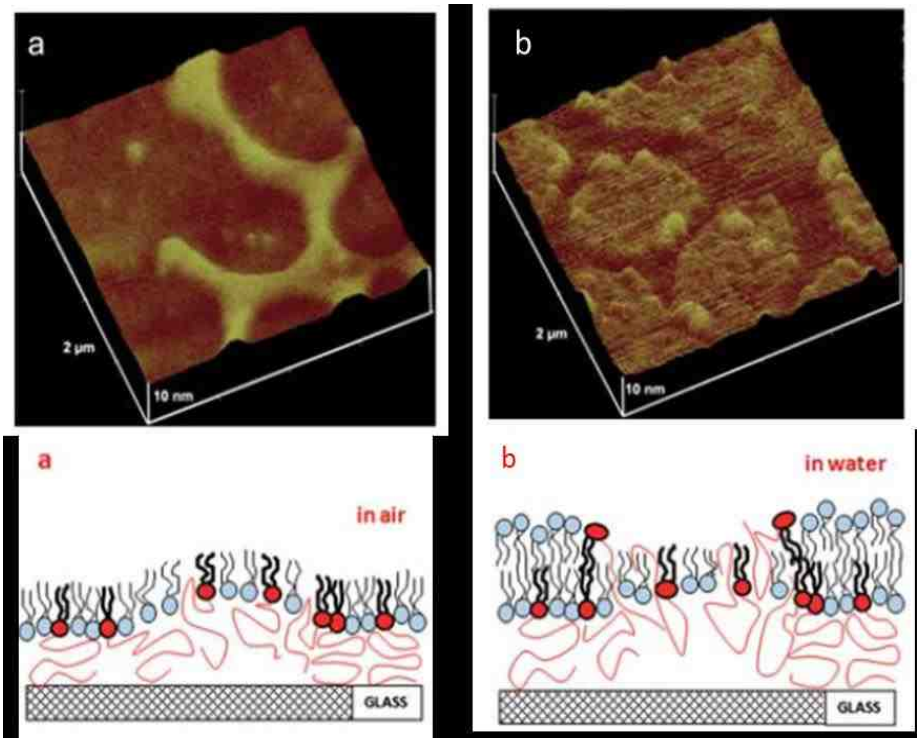

Figure 4.2. 2 Atomic force microscope micrographs of Single Monolayer (a) and Bilayer (b) comprised of mixture of 80 mol% phospholipid and 20 mol% lipopolymer[202.]

4.2.1.2 Polyethyleneglycol (PEG) and Poly(2-Methyl-2-Oxazoline) (Pmox)-Based Single Bilayers of TYPE I Substrates

TYPE I substrates can also be built using LB/LS techniques by replacing DSPE-PEG5000 with more hydrophilic Poly(2-Methyl-2-Oxazoline) (Pmox) lipopolymers. Interestingly, in this case, buckling structures are much smaller (only observable by AFM) and no bilayer compartmentalization is detected[216] . Figure 4.2.3 illustrates that enhanced lipopolymer concentrations not only cause membrane buckling, but also lead to increased

membrane roughness at a smaller length scale. At low tethering density, a polymer-tethered bilayer has a relatively smooth bilayer surface and polymers between bilayer and solid substrate are organized in a mushroom conformation. In contrast, at high tethering concentration, the bilayer shows enhanced roughness (membrane tension) and rather stretched polymer chains. Importantly, our group previously demonstrated that the polymer-induced roughening of the bilayer leads to a strong interleaflet coupling of lipid diffusion in TYPE I bilayers [232]. Furthermore, single molecule tracking experiments of dye-labeled lipids suggested that tethered lipids exist as randomly distributed obstacles of individual molecules at lipopolymer concentration of < 10 mol%; whereas aggregates of tethered lipids may occur at lipopolymer concentrations >10 mol%. Polymer-tethered bilayers of TYPE I consisting of Pmox lipopolymers are interesting as artificial cell substrates because changes in lipopolymer concentration (substrate stiffness) are not associated with lipopolymer-induced bilayer compartmentalizations[216,217].

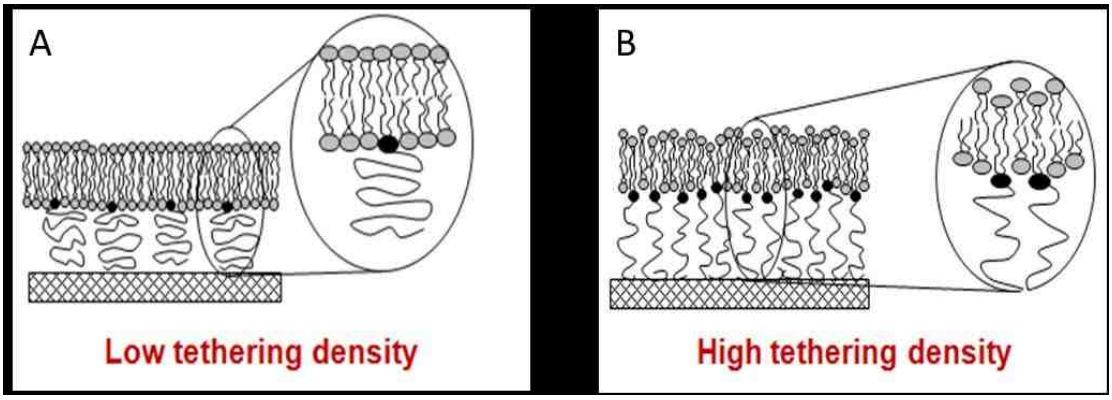

Figure 4.2. 3 the role of Poly(2-Methyl-2-Oxazoline) Lipopolymer within a polymer-tethered bilayer substrate[202].

4.2.2 Cellular Mechanoresponse of Fibroblasts on TYPE I Single Bilayer Substrates

As already mentioned, external mechanical cues may influence anchorage-dependent cells, thereby leading to changes in cell morphology and motility. Stimulation of signaling pathways and gene expression through mechanotransduction can alter cell spreading area, cell migration speed and direction, and cause the alternation of binding proteins in focal adhesion sites on TYPE I substrates of various lipopolymer concentrations (substrate stiffness). In the following, different aspects of cellular mechanosensitivity on TYPE I substrates are examined in more detail.

4.2.2.1 Cell Spreading on TYPE I Substrates

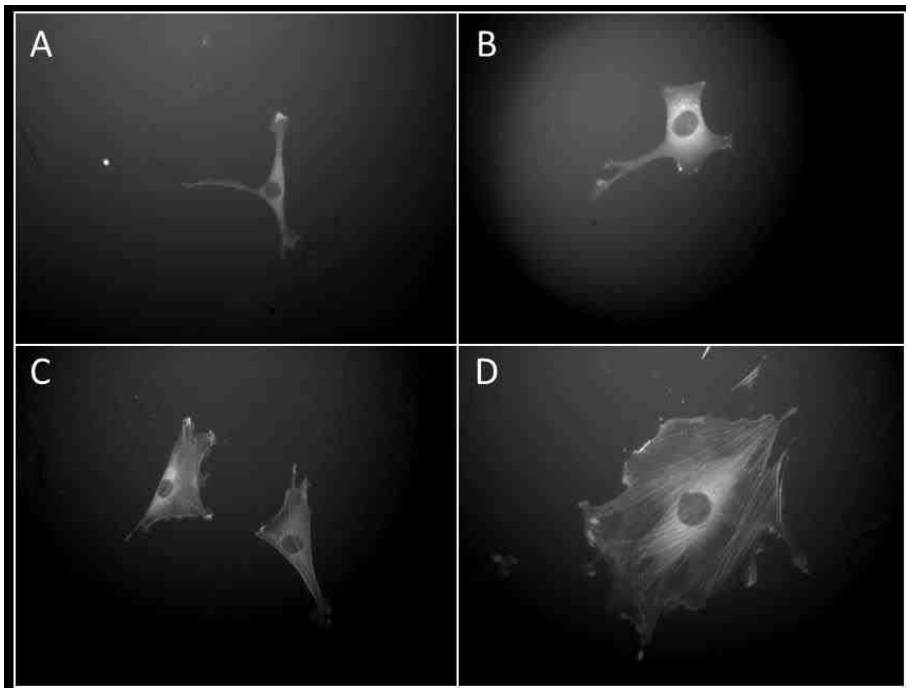

Figure 4.2. 4 GFP-Actin transfected MEF Fibroblast cells on TYPE I substrates comprised of low to high lipopolymer concentration (a) 5 mol% (b) 10 mol% (c) 15 mol% (d) 20 mol%.

The representative EPI micrographs in Figure 4.2.4 illustrate the influence of lipopolymer concentration, c_{tether}, in TYPE I bilayers on the spreading of GFP-Actin transfected MEF fibroblasts. Specifically, MEF Fibroblasts exhibit increased cell area and formation of more polygonic cells with increasing lipopolymer concentrations of c_{tether}= 5 (A), 10 (B), 15 (C), 20 mol% (D). Systematic analysis of cell spreading behavior on laminin-functionalized TYPE I bilayers demonstrate that there is a statistically significant correlation between cell area and c_{tether}.

As depicted in Figure 4.2.5, the average cell spreading area of MEF fibroblasts on TYPE I substrates with 2.5 mol% DSPE-PEG 5000 was found to be 550 μm^2. Furthermore, the average spreading area increased by 56% between 5 and 15 mol% DSPE-PEG 5000 on comparable substrates. As Fig. 4.2.5 also shows, the cell spreading areas on laminin-functionalized TYPE I substrates reach a plateau if lipopolymer concentrations in these membrane systems are larger than 20 mol% within TYPE I substrate. Notably, there is an interesting correlation between the influence of lipopolymer concentration on cell spreading area and the influence of lipopolymer content on the extent of membrane buckling formation (i.e., the percentage of the membrane occupied by buckling regions.)

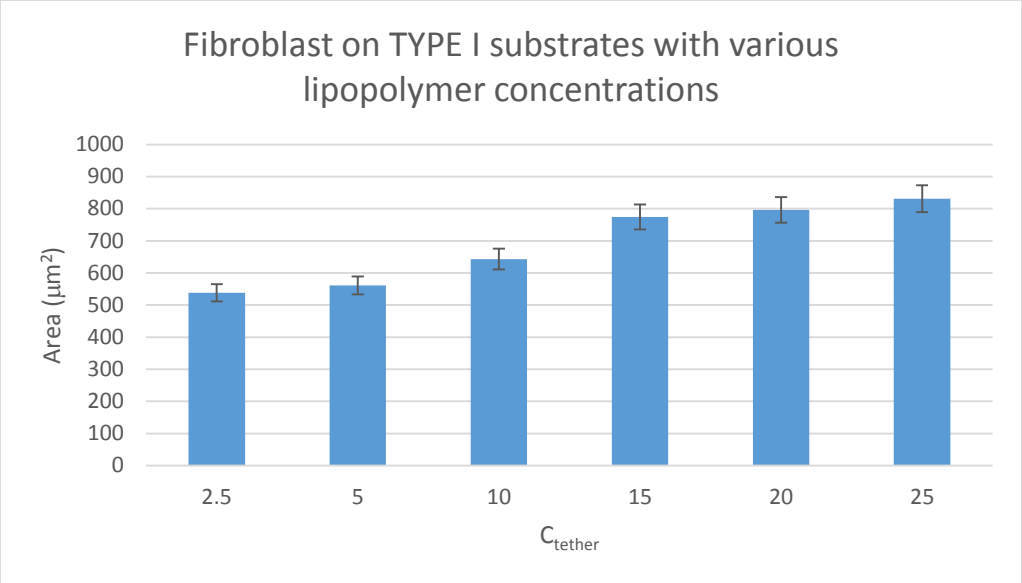

Figure 4.2. 5 MEF Fibroblast cell spreading Area on TYPE I substrates. Number of cells spreading analysis on each substrate ranging from 80 to 120 individual cells.

4.2.2.2 Cytoskeleton Organization of MEF Fibrooblast Cells on TYPE I Substrates

Cytoskeleton organization is another indicator of cellular mechanosensitivity. This behavior is already illustrated in Fig. 4.2.4, which shows the increased stress fiber formation of GFP-Actin transfected MEF Fibroblast on laminin-functionalized TYPE I substrates of increasing c_{tether}. Comparison of fibroblast data with the result of mean-field calculations of TYPE I substrates suggests that the extent of stress fiber formation is directly related to substrate stiffness. The influence of lipopolymer concentration on cytoskeletal organization is illustrated more quantitatively in Figure 4.2.6 where the percentage of cells forming ventral actin stress fibers is plotted as a function of increasing lipopolymer concentration. The tendency of cells to form stress fibers on TYPE I substrates is significantly increased from 0 to 20 mol% DSPE-PEG 5000; after 20 mol% c_{tether}, the

percentage of cells with stress fibers remains steady, in good agreement with the tendency of buckling structure formation in such membranes.

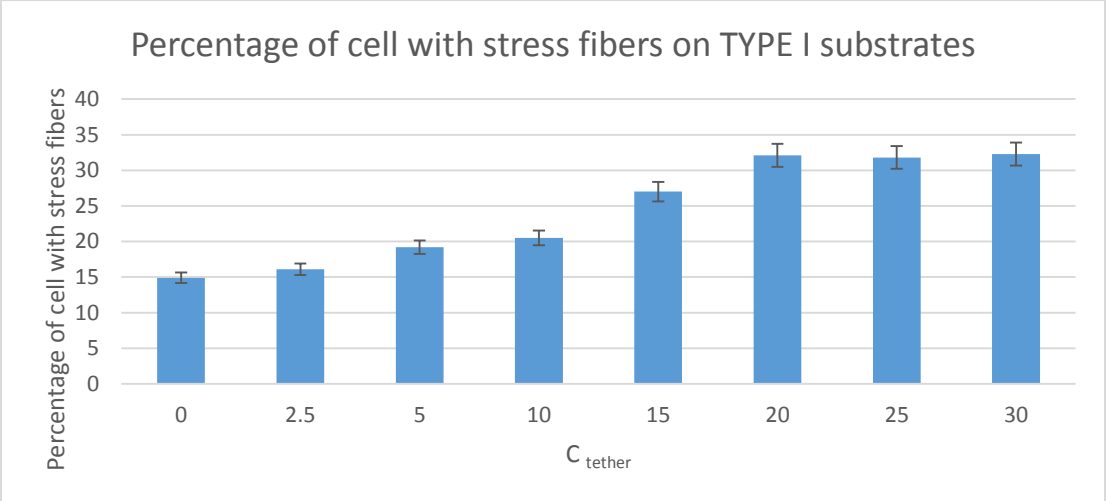

Figure 4.2. 6 Ratio of MEF Fibroblasts with stress ventral stress fiber on TYPE I substrate with increasing Ctether. Number of individual cells on substrates with different Ctether range from 80 to 120

4.2.2.3 Cell Migration on TYPE I Substrates

Cellular mechanosensitivity can also be examined in terms of cell migrations speed. Consequently, cell migration experiments were pursued on laminin-functionalized polymer-tethered membranes of TYPE I. The experiments showed that fibroblast migration speed increases with increasing concentration of lipopolymers between 5 and 30 mol%. As presented in Figure 4.2.7, the average cell migration speed on laminin-functionalized TYPE I substrates increases from 0.352 µm/min to 0.880 µm/min by altering lipopolymer concentration in such membranes from 5 to 20 mol% DSPE-PEG5000. Interestingly, 3T3 fibroblast migration speed on TYPE II substrates was reported to increase with increasing bilayer stacking, illustrating an opposite effect

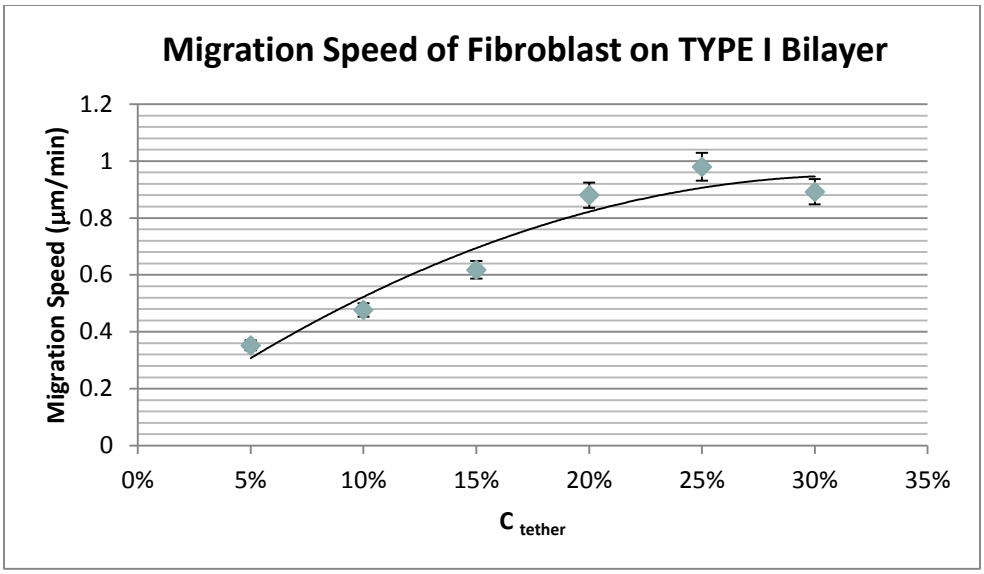

Figure 4.2. 7 MEF Fibroblast migration speed on TYPE I substrate with various lipopolymer concentrations.

4.3 Alternative Physisorbed Polymer-Tethered Lipid Single Bilayer with Lipopolymer Gradient TYPE I

In this work we report the fabrication of two types of physisorbed polymer-tethered lipid bilayers where the lateral distribution of lipopolymers can be regulated. In the case of TYPE Ia membrane systems, polymer-tethered membranes are characterized by a sharp boundary between regions of low (no buckling structures) and high (with buckling structures) lipopolymer concentrations. Importantly, the sharp boundary remains static after physisorption of the polymer-tethered membrane to the solid substrate. In contrast, TYPE Ib membranes exhibit a gradual concentration gradient in lipopolymer concentration achieved by adjusting the phospholipid-lipopolymer mixing ratio at the air-water interface prior to LB transfer. Again, this gradient can be maintained after the

transfer of the polymer-tethered membrane to the solid (glass) substrate. These membranes illustrate that TYPE I bilayers have exciting properties including the ability to fabricate substrates with well-defined elasticity patterns and gradients, representing an attractive tool in the analysis of cellular mechanosensitivity.

4.3.1 Design and Fabrication of Sharp Boundary (TYPE Ia) and Gradient Pattern (TYPE Ib) Polymer-Tethered Single Bilayer

4.3.1.1 Buckling Pattern and Structures with Various Polyethyleneglycol (PEG)-Based Lipopolymer Concentrations

Previously, we demonstrated that physisorbed polymer-tethered phospholipid bilayers with different concentrations of lipopolymers in their inner monolayer display distinct, lipopolymer concentration-dependent, buckling structures. The formation of these structures was confirmed by AFM and was explained in terms of a stress relaxation phenomenon caused by stress-inducing lipopolymers in the membrane system. In the case of lipopolymers with amphiphilic polymer moieties, such as poly(ethylene glycol) (PEG) and poly(2-ethyl-2-oxazoline), buckling structures were easily resolvable by optical microscopy, such as EPI microscopy. At low lipopolymer concentrations, buckling structures were found to exist as circular or straight-sided blisters. With increasing lipopolymer concentration, blisters were reported to become more elaborate and branched and to eventually develop into a compartmentalizing buckling pattern. Fig.4.3.1 [A] and [B] illustrate typical EPI micrographs of buckling structures in polymer-tethered lipid bilayers containing different amounts of DSPE-PEG 5000. At 5 mol%, lateral stress is

comparably low and membrane buckling regions exist as straight-sided blisters (Fig. 4.3.1[A]). In contrast, at 40 mol%, lateral stress is high resulting in the formation of membrane-compartmentalizing buckling regions (Fig. 4.3.1[B]).

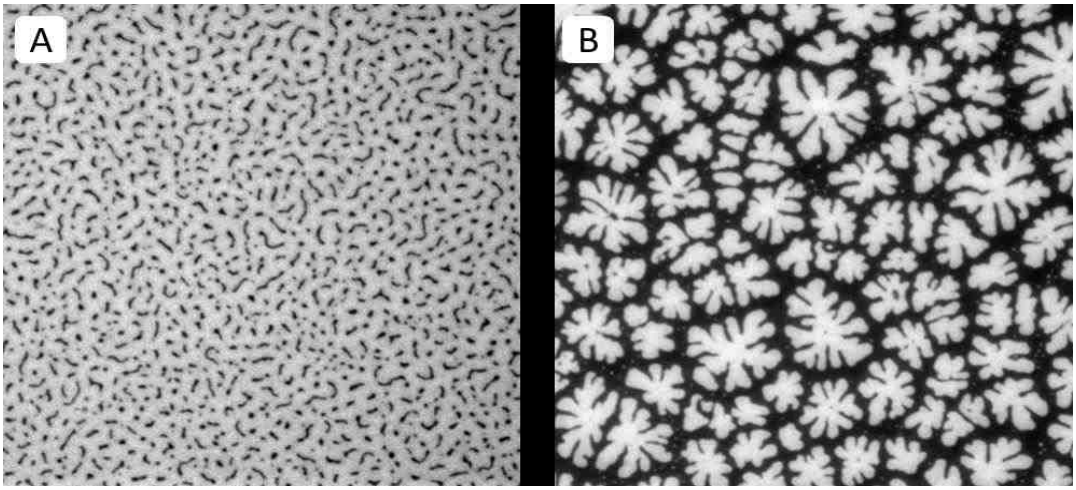

Figure 4.3. 1 EPI micrographs of physisorbed polymer-tethered lipid bilayers of 5 mol% (A) and 40 mol% DSPE-PEG 5000 (B)[226]. All pictures were taken with 40x objective and 1.6x Optovar magnification. The size of the micrographs is 100 µm x 100 µm.

4.3.1.2 Impact of Lipopolymer Density on Stiffness of TYPE Ia and Ib Lipid Bilayer Substrates

Fig. 4.3.2 [A]-[D] displays corresponding AFM micrographs of different regions of a typical TYPE I monolayer containing DSPE-PEG5000 (length scale 20 µm x 20 µm). While Fig. 4.3.2 [A] shows a monolayer region, which is characterized by straight-sided blisters, Fig. 4.3.2 [B]-[D] depict a compartmentalizing buckling pattern of decreasing compartment size. Using previously applied protocols, analysis of buckling width, 2b (Fig. 4.3.2 [A]), and compartment density, N_{corr} (Figs. 4.3.2 [B]-[D]), suggests lipopolymer molar concentrations of 4 mol% (Fig. 4.3.2 [A]), 16 mol% (Fig. 4.3.2 [B]), 31 mol% (Fig. 4.3.2 [C]),

and 36 mol% (Fig. 4.3.2 [D]), are associated with a change in the plane strain modulus, E_f^*, of the membrane from 1.9-7.3 MPa.

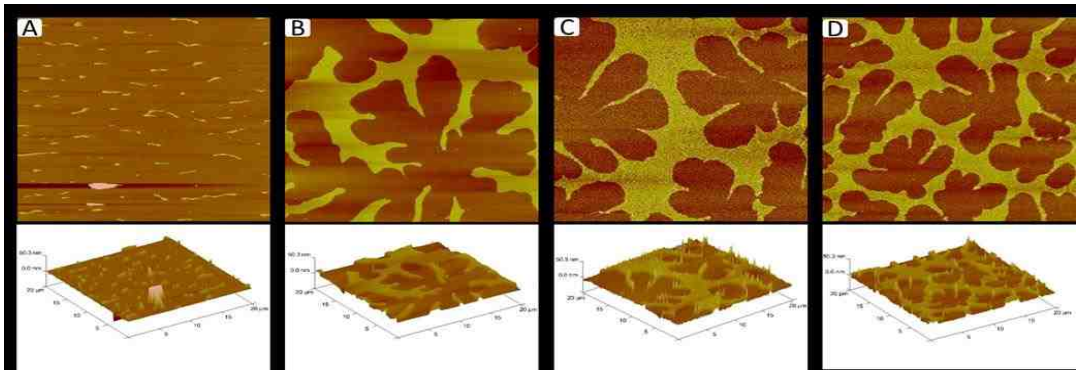

Figure 4.3. 2 AFM micrographs of different regions of a TYPE Ia physisorbed polymer-tethered monolayers exhibiting distinct degrees of membrane buckling[226]: straight-sided blisters [A], and compartmentalizing buckles of decreasing compartment size [C-D]. The decreasing compartment size indicates increasing lipopolymer molar concentrations. Image size: 20µm x 20µm.

4.3.1.3 Key Characteristics of TYPE Ia and Ib Single Lipid Bilayer Substrates

Fig. 4.3.3 shows representative EPI micrographs obtained from a TYPE I polymer-tethered lipid bilayer system. As outlined in the Experimental Section, the lipopolymer gradient in TYPE Ia membranes was allowed to build up at the air-water interface prior to film transfer to the solid substrate. Fig. 4.3.3 [A] presents a lower magnification micrograph captured using a 20x objective, which clearly illustrates the gradual transition from a region without optically resolvable buckling structures to one with well-developed, bilayer-compartmentalizing buckling patterns.

Fig. 4.3.3 [B]-[D] depict higher magnification micrographs using a 40x objective of different regions of a TYPE I bilayer sample, which are distinct in terms of buckling

formation. Fig.4.3.3 B exemplifies the region without optically resolvable buckling structures, which suggests a polymer-tethered lipid bilayer with less than 5 mol% DSPE-PEG 5000. The bilayer area in Fig. 4.3.3 [C] is characterized by straight-sided, partially branched blisters, indicative of a local DSPE-PEG 5000 molar concentration of 5-10 mol%. Also illustrated by Fig. 4.3.3 [C] is the tendency of sufficiently long buckling ridges to compartmentalize the lipid bilayer. Fig. 4.3.3 [D] shows a region of well developed, bilayer-compartmentalizing buckling structures indicating a local DSPE-PEG 5000 molar concentration of 15-20 mol%.

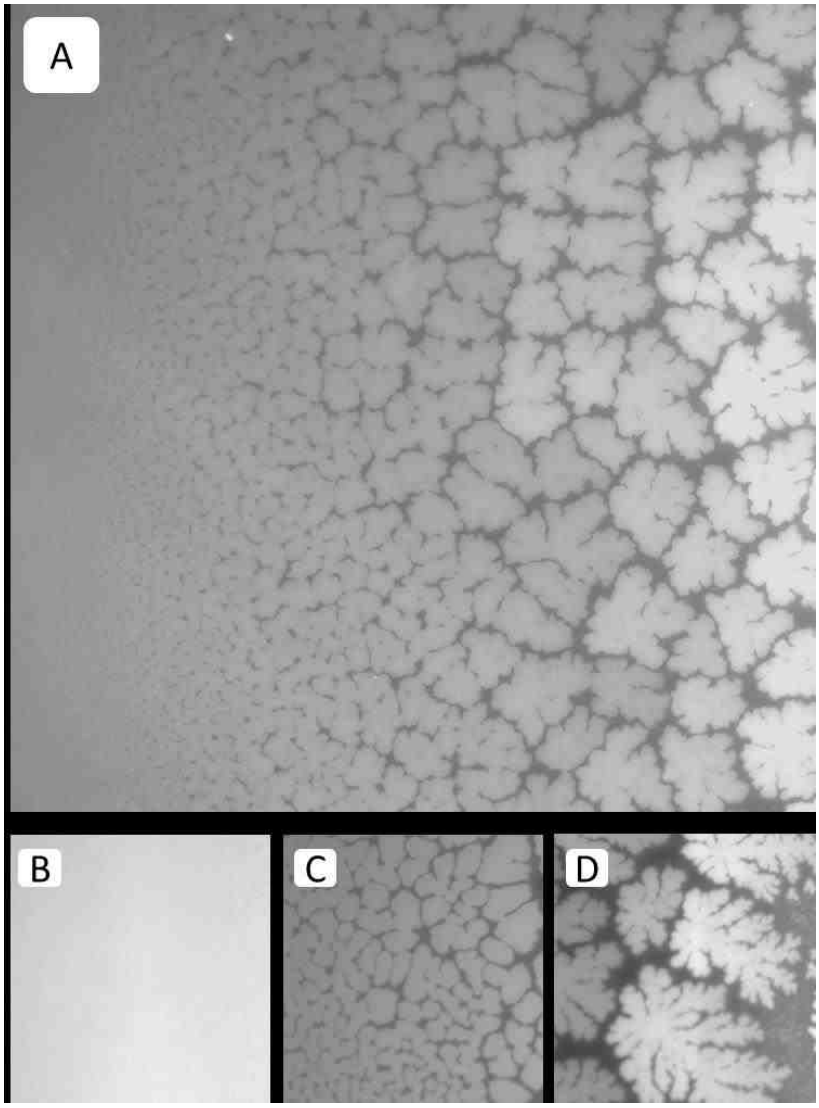

Figure 4.3. 3 Representative EPI micrographs of a TYPE Ia physisorbed polymer-tethered lipid bilayer. The gradual change of buckling structures in Fig. 4.3.3 A indicates the existence of a lateral lipopolymer gradient in the membrane system[226] (20x magnification). Figs. 4.3.3 B-D show magnified micrographs (40x magnification) of bilayer regions characterized by differences in buckling formation: no buckling (B), partially branched blisters (C), and well developed, bilayer-compartmentalizing buckles (D). The image size of A is 320 µm x 320 µm, whereas that of B, C and D is 160 µm x 160 µm

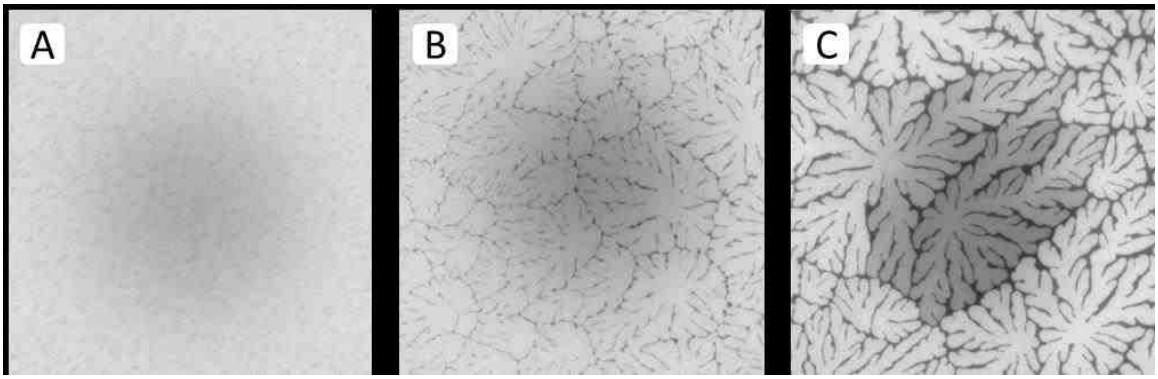

Figure 4.3. 4 Fluorescence recovery after photobleaching of dye-labeled lipids in different regions of a TYPE Ia bilayer sample (images taken 1.5 min after spot photobleaching) exhibiting a buckling-free region (A), a region with branched buckling structures (B), and a region with bilayer-compartmentalizing buckles (C). The micrographs illustrate the fluidity of lipids in the bright (buckle-free) regions of the bilayer and confirm the ability of buckling structures to act as efficient lipid diffusion barriers, as reported previously[226].

Results from spot bleaching experiments in Figs. 4.3.4 [A]-[C] illustrate the influence of buckling structures on lipid lateral fluidity in different regions of a TYPE 1 bilayer. In the region without optically resolvable buckling structures (Fig. 4.3.4 [A]), the circular bleaching spot exhibits a gradual transition of the bleaching intensity indicating good fluidity within the bilayer (images taken 1.5 min after spot photobleaching). In the region of straight-sided, partially branched blisters (Fig. 4.3.4 [B]), qualitatively similar fluorescence recovery can be observed, which displays lateral fluidity outside buckling areas. Fig.4.3.4 [C] best demonstrates that buckling areas act as efficient lipid diffusion barriers, as reported previously for physisorbed polymer-tethered lipid bilayers containing poly(2-ethyl-oxazoline) or PEG lipopolymers. Combined AFM and spot photobleaching experiments revealed that in such cases no lipid bilayer can form on top of buckling regions. Consequently, in TYPE Ia bilayers, these regions of “buckling-induced

dewetting" cause the formation of diffusion obstacles at low to medium lipopolymer concentrations and the compartmentalization of the lipid bilayer system at high lipopolymer concentrations. Notably, the available diffusion data reveal a complex length scale-dependent lipid diffusion behavior in physisorbed polymer-tethered lipid bilayers, which exhibits remarkable parallels to those observed in plasma membranes. At sub-optical resolution length scale (~100nm), wide-field single molecule fluorescence microscopy experiments show that lipid diffusion is well described by a model of obstacle-induced obstructed diffusion. Here the degree of obstruction is determined by the density of lipopolymers in the membrane system. Interestingly, the observed obstruction of lipid diffusion at this length scale seems to be, in part, associated with a lipopolymer-induced roughening of the bilayer, which alters membrane tension. At micron-size length scale, the formation of diffusion barriers in buckled regions reveal a second type of obstructed lipid diffusion. In this case, the degree of obstruction is determined by the length and connectivity of buckles. The complex lipid diffusion behavior in physisorbed polymer-tethered membranes was recently demonstrated through long-term tracking of photostable quantum dot-conjugated lipids[218] . These experiments not only showed a lipopolymer density-dependent obstruction of lipid diffusion over the entire detected length scale range, but also exhibited the feature of hop diffusion at a particular length scale (qualitatively similar to plasma membranes). It should be noted that the described lipid diffusion properties are distinct from those reported on chemisorbed polymer-tethered lipid bilayers.

As described before, physisorbed polymer-tethered lipid bilayers not only show fascinating diffusion behavior, but are also characterized by interesting mechanical properties. Previously, mean-field calculations have shown that the mechanical properties of polymer-tethered membranes depend on lipopolymer density. Interestingly, the bending elasticity, K_c, of a typical red blood cell membrane of about 50 kBT corresponds to that of a polymer-tethered lipid bilayer of 5 mol% DSPE-PEG 5000 and K_c = 400 kBT of a typical membrane of Dictyostelium discoideum (wild type) is comparable to Kc values in polymer-tethered membranes of 20 mol% DSPE-PEG 5000. In contrast, a fluid lipid bilayer without lipopolymer is notably softer than typical cell membranes. Importantly, there is an empirical correlation between the extent of buckling formation and membrane elastic properties. We already described that a more quantitative relationship between buckle formation and membrane elasticity can be developed by linking experimentally determined buckling parameters, such as the buckling width, 2b, or the maximum height of buckles, w_{max}, to mean-field calculations of polymer-lipopolymer mixtures and buckling theory of an Euler column. In this case, the Euler column approximation can be applied because the buckling width is notably larger than the overall membrane thickness, h, and because the Young's modulus of the glass substrate is much higher than that of the polymer-tethered membrane. In the case of compartment-forming buckling structures, information about the density of lipopolymers and the corresponding membrane elasticity can be also obtained by determining the compartment density, N_{corr}.[217] The buckling parameter information needed for quantitative correlation can be best acquired from the analysis of EPI and AFM

micrographs of polymer-tethered lipid monolayers. Fig. 4.3.5 [A]-[E] illustrates representative EPI micrographs of different regions within a TYPE Ia polymer-tethered monolayer sample. The micrographs depict the gradual transition from regions of low lipopolymer concentration (≤5 mol% DSPE-PEG 5000) (Fig. 4.3.5 [A]) to those of elevated lipopolymer concentration (~30 mol% DSPE-PEG 5000) (Fig. 4.3.5 [E]). Monolayer micrographs show typical phase inversion (relative to corresponding bilayer system) observed on polymer-tethered membranes with PEG lipopolymers (i.e., bright phase represents buckling regions in monolayer, while dark phase represents buckling regions in bilayer).

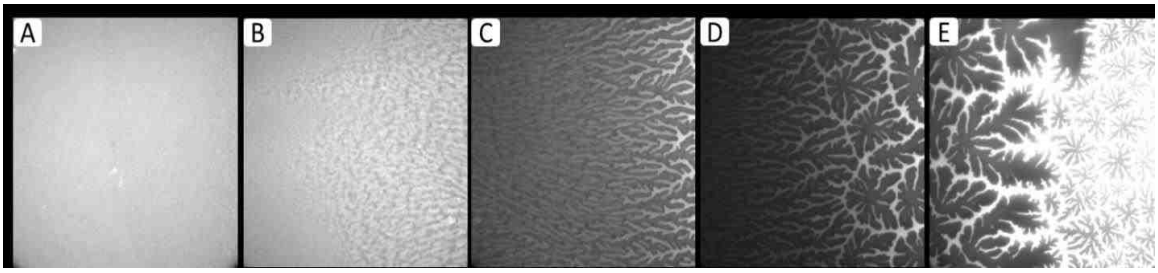

Figure 4.3. 5 EPI fluorescence micrographs of different regions of a TYPE Ia physisorbed polymer-tethered monolayer illustrating the gradient in terms of buckling structures representative of changes in lipopolymer density[226]: no optically resolvable buckles (A),straight-sided blisters (B), increasingly branched blisters (C), branched blisters and compartmentalizing buckles (D), and compartmentalizing buckles (E). Image size: 160 µm x 160 µm.

The data presented for TYPE Ia membranes in Figs. 4.3.2-5 bring to light a fascinating model membrane system with gradually changing properties of membrane organization, dynamics, and elasticity. The significance of the TYPE Ia architecture is that gradients are static and do not change over time. This static behavior is caused by the

physisorption of lipopolymers onto the glass substrate preventing the gradual relaxation of the lipopolymer gradient. Resulting differences in lipopolymer density in TYPE Ia systems demonstrate the ability to maintain regions of different lateral stress within one membrane sample. These regions manifest themselves in terms of clearly distinguishable buckling structures. Furthermore, the lateral lipopolymer gradient leads to remarkable length scale-dependent lipid fluidity gradient in TYPE Ia bilayer systems ranging from regions of low obstruction of lipid diffusion to those characterized by significant lipopolymer-induced obstructed and hop diffusion processes. Here it is important to recognize that the physisorption of lipopolymers on the glass substrate does cause the obstruction of lipid diffusion, but typically not to the degree of complete membrane immobilization. A simple fluid lipid bilayer system with a comparable static gradient does not appear to be feasible as the lateral mobility of lipids will decrease any previously formed gradient over time. This is beautifully illustrated by the analysis of transient gradients of charged lipids in micro-patterned solid-supported lipid bilayers[240] . In this case, the gradient of charged, dye-labeled lipids was created by applying an electric field and the time evolution of the gradient was analyzed after turning off the applied electric field, thus providing information about lipid diffusivity. However, in the case of engineered solid substrates with specific gradient properties (e. g., surface charge or curvature), lipid bilayer structures with membrane constituent gradients seem possible. An alternative gradient strategy could be achieved by the use of polymerizable lipids to build a lipid bilayer system with a lateral gradient in lipid crosslinking density[240].

Physisorbed polymer-tethered phospholipid bilayers with sharp a boundary between regions of low and high lipopolymer concentrations (TYPE Ib):

The immobilization of physisorbed lipopolymers on the glass surface not only offers the possibility to fabricate membrane systems with lateral lipopolymer density gradients, but also those with a sharp boundary between regions of low and high lipopolymer molar concentrations. As described in the Experimental Section, TYPE Ib membranes were built by regulating the phospholipid-lipopolymer mixing ratio at the air-water interface and by conducting partial LB transfers at altered lipopolymer concentrations.

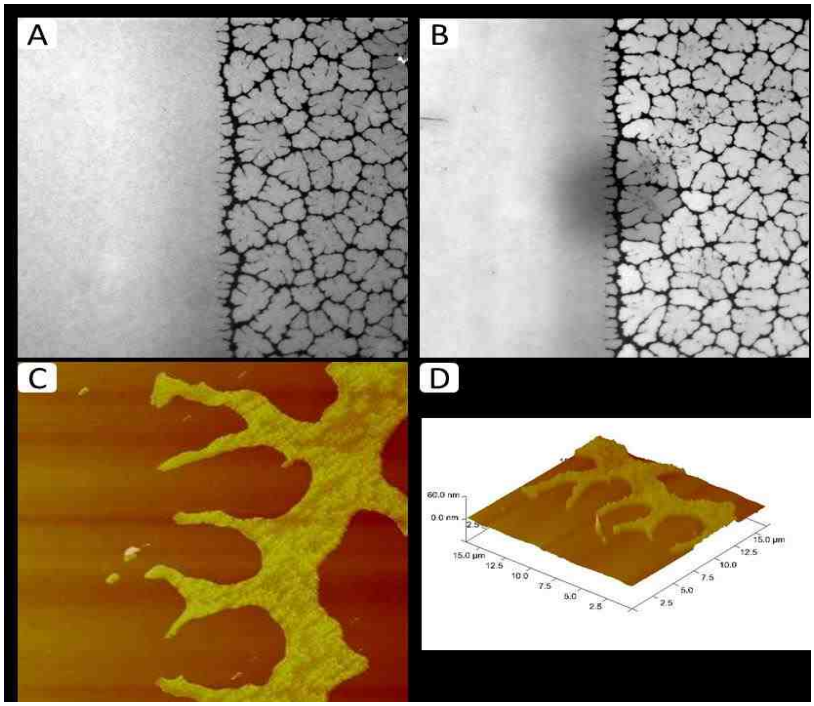

Figure 4.3. 6 : EPI (A, B) and AFM micrographs (C, D) of TYPE Ib physisorbed polymer-tethered lipid bilayer and monolayer[226], respectively. Micrographs confirm the existence of a sharp boundary between regions of low and high lipopolymer densities with distinct properties of membrane dynamics and elasticity. (EPI micrograph image size: 160 µm x 160 µm; AFM micrograph image size: 20 µm x 20 µm

Fig. 4.3.6 [A]-[D] shows representative EPI and AFM micrographs of such a physisorbed polymer-tethered lipid membrane. The EPI micrograph in Fig. 4.3.6[A] illustrates two sharply separated membrane regions, a homogeneous region and a region characterized by compartmentalizing buckling structures. As outlined in the Materials and Methods section, the homogeneous and non-homogeneous buckled regions contain approximately 5 and 30 mol% DSPE-PEG5000, respectively. The shape of the bleaching spot in Fig. 4.3.6 [B] demonstrates good bilayer fluidity in the homogeneous region of the membrane with the low lipopolymer density. In contrast, the partially recovered bleaching spot in the non-homogeneous region shows that the "dark phase" acts as a lipid diffusion barrier. This behavior suggests that the non-homogeneous region is not caused by phospholipid-lipopolymer phase separation, but instead is a typical fingerprint of membrane buckling and buckling-induced "dewetting". Indeed, the presence of buckling structures is confirmed by AFM micrographs in Figs.4.3.6 [C] and [D] that show representative AFM data from the boundary region of a typical TYPE Ib polymer-tethered monolayer. Again it should be emphasized that the sharp boundary between regions of low and high lipopolymer densities, which exhibit distinctly different dynamic end elastic properties, remains unchanged over an extended period of time. Of course, the concept of TYPE Ib membranes should not remain limited to those with one sharp boundary. Modifications to the membrane fabrication process can be envisioned, which lead to well-defined patterned polymer-tethered bilayer systems. Previously, several successful strategies have been pursued to build patterned solid-supported lipid bilayers. For example, Groves et al. used patterned grids of photoresist, aluminum oxide, or gold on

oxidized silicon substrates to form patterned solid-supported lipid bilayers[241] . Other patterning strategies include the photochemical patterning and patterning via the controlled crosslinking of polymerizable lipids[242]. An interesting example of patterning in polymer-supported membranes represents the controlled formation of stripe phases in polymer-tethered lipid bilayers comprised of lipids and lipopolymers, in which stripe formation was controlled through changing LB transfer conditions[243].

4.3.2 Cellular Mechanoresponse of Fibroblasts on TYPE I Alternative Single Lipid Bilayer Substrates

4.3.2.1 Cellular Mechanosensitivity

As shown in Figure 4.3.7, confocal microscopy analysis demonstrates that MEF fibroblasts display notably different cell spreading behavior and morphologies in low c_{tether} and high c_{tether} regions of a TYPE Ib bilayer system. As regions of low and high c_{tether} are associated with distinct substrate stiffness, linker-functionalized TYPE Ib systems are suitable as artificial substrates to probe cellular mechanosensitivity. Similar to patterened polymeric substrates with different elasticities[240,243] , TYPE Ib biomembrane-mimicking substrates are attractive tools in cell affinity assays. To test the functionality of laminin-functionalized TYPE Ib bilayers, cellular mechanoresponse was investigated in terms of phenotypical change of fibroblasts using DIC and epifluorescence analysis.

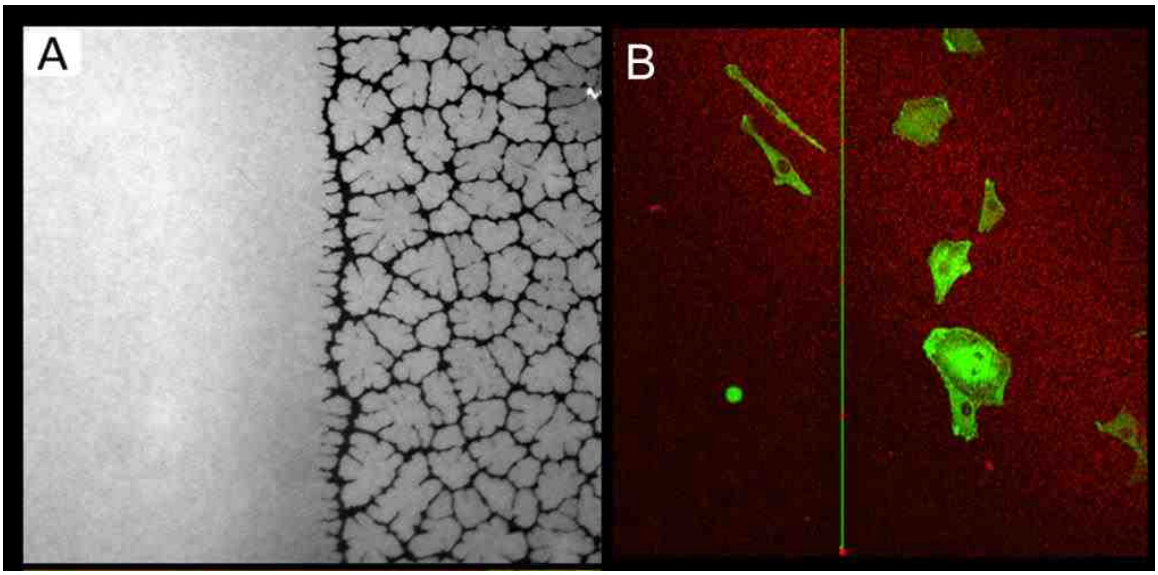

Figure 4.3. 7 Representative micrograph [B] of fibroblasts plated on TYPE Ib patterned polymer-tethered lipid bilayer substrates [left half: ctether = 5%mol, right half: ctether = 30%mol]; EPI micrographs of patterned polymer-tethered lipid bilayers show sharply separated membrane regions, a homogeneous region, (ctether = 5 mol%) and compartmentalized region, (ctether = 30 mol%) [A].

Figure 4.3.8 shows results from a quantitative analysis of cell morphology populations on TYPE Ib single bilayer substrates with regions containing low and high lipopolymer concentrations (cell morphology analysis was preformed 24 hours after plating.). As Fig. 4.3.8 illustrates, cells in the region of elevated lipopolymer concentration (higher substrate stiffness) predominently display polygonic and triangle morphologies, whereas those in the low lipopolymer region (lower substrate stiffness) mainly show spindle and amoeboid cell shapes. Interestingly, it is worth noticing that the spindle cell shape is similar to cellular morphologies observed in 3D matrices models[119,201,244] . Thus, the TYPE Ib single bilayer substrates can represent a model for cell behavior in the twilight zone of different tissue organization such as muscle and neuron cells.

The relative abundance of different shapes of cell phenotype was correlated to substrate mechanical properties. The morphology histogram in Figure 4.3.8 shows that varying populations of cell shapes with respect to region of TYPE Ib single bilayer substrates with high lipopolymer and low lipopolymer concentrations (Shape analysis preformed 24 hours following plating). In previous studies, the cell phenotypes were significant in that they show intriguing parallels and remarkable differences compared to mechanoresponse observed on traditional culturing surface and on 2D PAA gels of adjustable viscoelasticity. With larger polygonic and triangle shapes being typical on the stiffer substrate surfaces and smaller shapes such as spindle and amoeboid are representative for softer PAA substrates. As reported in Figure 4.3.8, the phenotype of cellular shape match to the general trend as described above. On stiffer region, the predominant morphology of fibroblast on glass is polygonic, crescent and triangle; on the softer region with lower lipopolymer concentration, the major populations of cell phenotypes are spindle and amoeboid respectively.

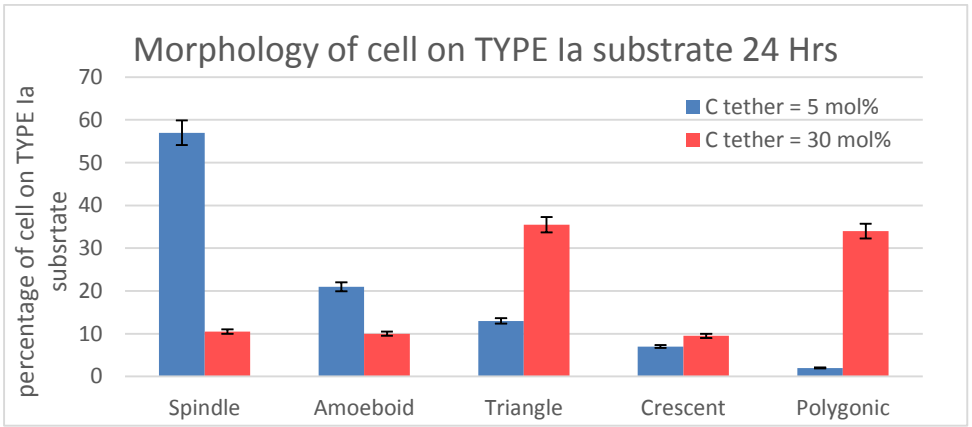

Figure 4.3. 8 Cellular phenotype histograms for fibroblast plated on TYPE Ib substrate after plating 24 hours

The other important indicator of cellular mechanoresponse to artificial substrates is cell spreading area. As reported in Figure 4.3.9, cell spreading area 24 hours after plating on TYPE Ib single bilayer substrates was analyzed using EPI and bright-field microscopy. Here a notable difference of cell spreading area was observed between regions of low and high lipopolymer concentrations. Specifically, the region of low lipopolymer concentration is characterized by smaller cell spreading areas compared to the region of high lipoplymer content, which shows larger cell spreading areas.

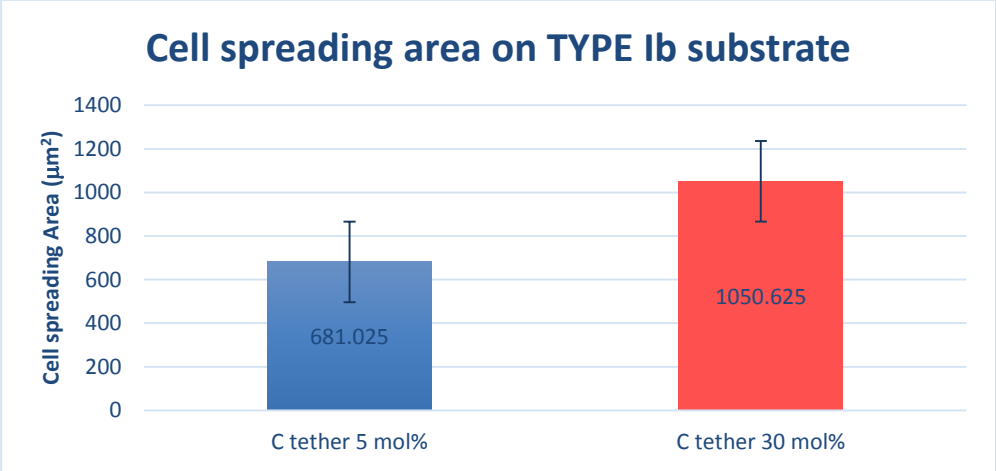

Figure 4.3. 9 MEF fibroblast cell spreading area on TYPE Ib substrate after 24 hours.

4.3.2.2 Cytoskeletal Organization of Fibroblast on TYPE Ib Substrate

The cytoskeleton structure plays an important role in different cellular properties, including cell shape, growth and migration. It is also an indicator of a cell's mechanical interaction with the environment. Actin filaments, as one of the three main constituents of cytoskeletal organization, are believed to act not only as mediators during cellular mechanotransduction, but also as important components of cellular mechanoresponse

by transmitting myosin-generated forces to cellular adhesions and by regulating cell protrusion at the leading edge of migrating cells. To test the functionality of linker-functionalized TYPE Ib bilayers as biomembrane-mimcking cell substrates of cellular mechanosensitivity analysis, we therefore also analyzed the percentage of cells with visible ventral stress fibers in low and high lipopolymer regions of TYPE Ib bilayers at 24 and 48h after plating. In this case, experiments were conducted using GFP-Actin transfected MEF fibroblasts. Figure 4.3.10 demonstrates the significant difference of ventral stress fiber formation in TYPE Ib regions of low and high lipopolymer concentrations. Figure 4.3.10 shows that the percentage of cells with visible stress fibers is substantially higher in the region of high lipopolymer concentration (high substrate stiffness) compared to the region of low lipopolymer concentration (low substrate stiffness). Here stress fiber structures of the actin cytoskeleton typically represent bundles of actin filaments. These structures can be divided into three major groups based on subcellular location and interaction with focal adhesions, which include ventral stress fibers, transverse arcs and dorsal stress fibers. Another significant finding from Fig. 4.3.10 is that the percentage of cells with ventral stress fibers is slightly smaller at 48 hours after plating compared to 24 hours after plating. This result illustrates the integrity of the linker-functionalized TYPE I bilayer architecture in the presence of plated cells. In case, the bilayer structures would not withstand cellular pulling forces, an increase of the stress fiber-forming cell population would be expected over time. Note cells show substantial stress fiber formation on glass substrates.

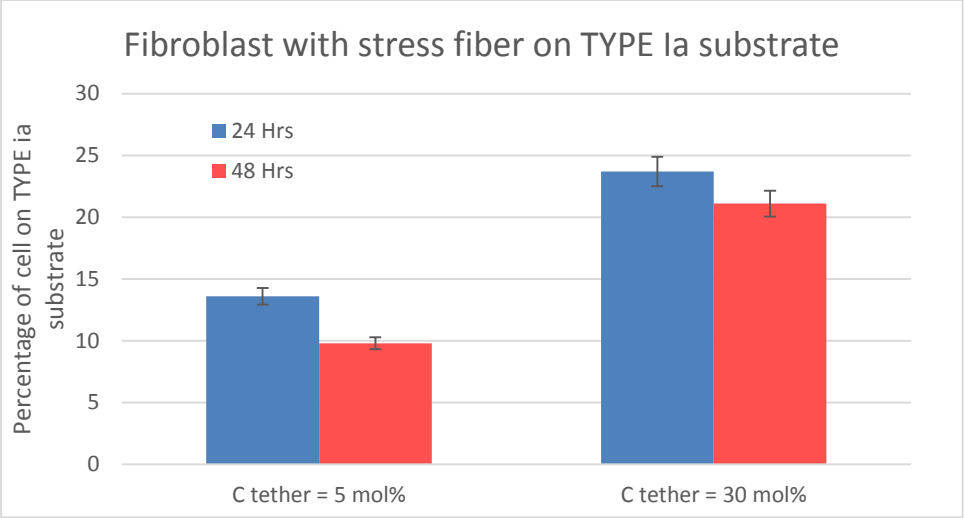

Figure 4.3. 10 Ration of MEF Fibroblast with ventral stress fiber on TYPE Ib single bilayer substrates after plating 24 hours and 48 hours.

4.3.2.3 Cell Migration and Tortuosity

Cell migration represents another property of cellular mechanoresponse. Analysis of cell migration on patterned substrates are particularly interesting because it provides insight into the substrate stiffness affinity of migrating cells[57] Previous experiments on biomembrane-mimicking bilayer substrates of TYPEs I and II have demonstrated the influence of substrate stiffness on cell migration, similar to comparable findings of migrating cells on polymeric substrates of adjustable stiffness[55] As described before, cell migration on a TYPE II substrate bilayer has been monitored by altering the degree of bilayer stacking, whereas cell motility on TYPE I systems was accomplished by changing the concentration of lipopolymers. In Figure 4.3.11 shown below, cell migration speed is faster in the area comprised of lower lipopolymer concentration compared to higher tethering region on TYPE II alternative substrate with sharp boundary pattern.

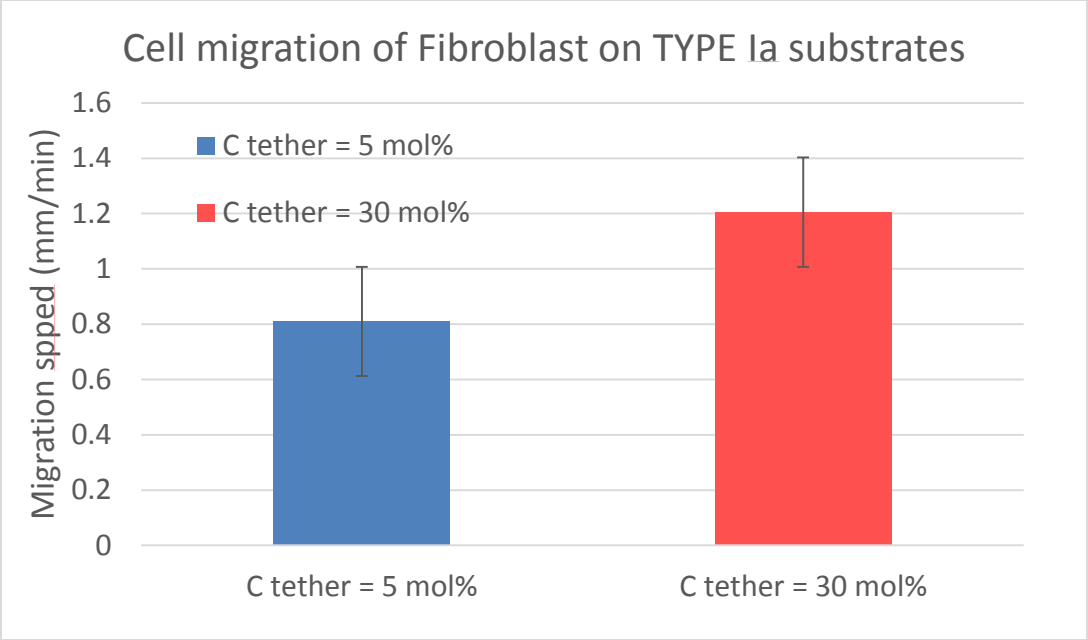

Figure 4.3. 11 : Comparison of fibroblast migration shows higher migration speed at the region of ctether = 5 mol% relative to region of ctether = 30 mol%.

On the other hand, the cell migration direction on TYPE II alternative substrate is significant influenced by the pattern of the bilayer structures. On sharp boundary between -high and low DSPE-PEG5000 concentration single bilayer, cell are freely moving on region with the same c_{tether}. However, as Figure 4.3.12 shows, the movement of cells from low to high concentrations of c_{tether} is inhibited (i.e., cells turn around to stay in the area of low c_{tether}). In contrast, cells can move freely from the area of high to low c_{tether}. In previous experiments, fibroblast cell on the immobilized artificial substrates are intent to move from softer to stiffer regions.

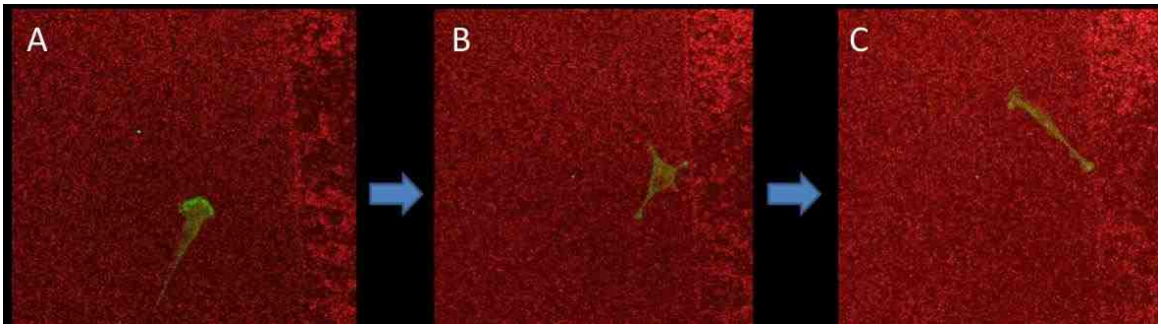

Figure 4.3. 12 Fibroblast cells on TYPE Ib sharp boundary bilayer system display migration directionality towards low ctether.

Interestingly on TYPE Ia substrates with a gradual gradient in lipopolymer concentration, cells appear to be able to move freely between different regions of different lipopolymer concentrations (Figure 4.3.13). However, these experiments also show that cell migration is in part influenced by the presence of bilayer-compartmentalizing buckling structures. Specifically, these experiments reveal that such lipid diffusion barriers are able to hinder, at least for some time, the free migration of cells. However, the specific processes associated with this hindered cell migration by membrane buckling structures are currently not well understood.

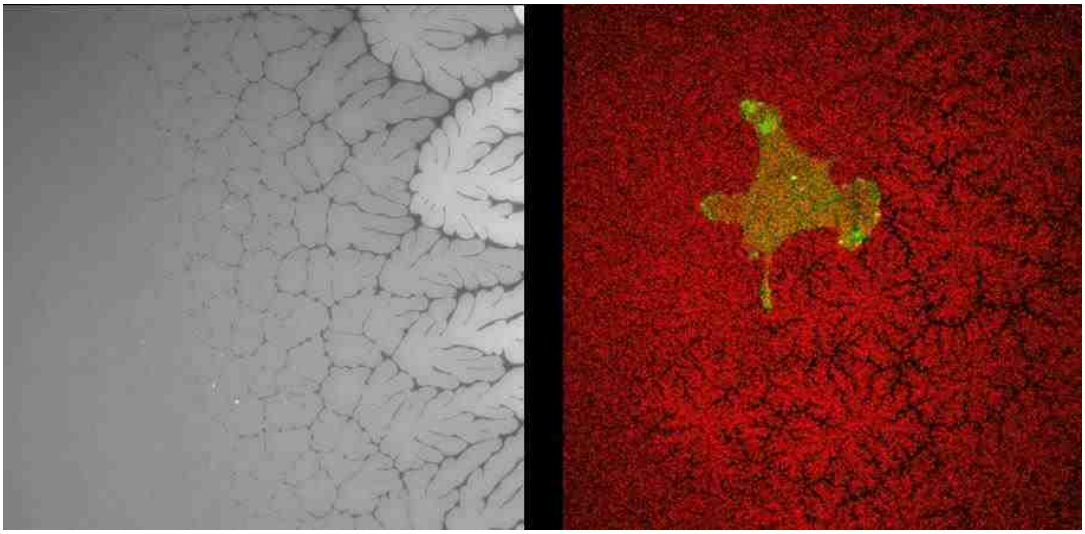

Figure 4.3. 13 : EPI micrographs of TYPE Ia with gradual lipopolymer gradient from low ctether (5mol%) to high ctether (30mol%) (left). The low tethering density region corresponds to a softer substrate (~2MPa), whereas the high tethering region represents a stiffer substrate (~ 7MPa). Fibroblasts are able to migrate on laminin-functionalized TYPE Ia substrates, albeit buckling structures may cause the temporary hindrance of cell movement

CONCLUSION AND OUTLOOKS

5.1 Conclusion

Mechanical cues are increasingly recognized to play a crucial role in the regulation of cellular fate and function. However, the underlying mechanisms of cellular mechanotransduction still remain a topic of open debate. Traditionally, advancements in this field have been made using polymeric substrates of adjustable stiffness with immobilized linkers. Recently, we introduced an alternative strategy, in which cells are plated on a laminin-functionalized, polymer-tethered multi-bilayer stack of adjustable substrate stiffness.

First, a cell surface-mimicking polymer-tethered multi-bilayer system with N-cadherin linkers (TYPE II) has been designed and employed for the investigation of the mechanosensitivity of C2C12 myoblasts. Experiments are presented, which demonstrate that properties of plated cells such as morphology, cytoskeletal organization, cellular traction forces, and migration speed, can be changed by altering the number of bilayers in the stack. Furthermore, application of sensitive fluorescence detection techniques confirms the dynamic assembly of bilayer-bound N-cadherin linkers underneath plated cells without impairing cell spreading and migration. This remarkable behavior can be attributed to the distinct properties of individual and clustered N-cadherins in polymer-tethered membrane systems. Together our data

illustrate that these biomembrane-mimicking cell substrates better replicate the dynamics and plasticity found at cell-cell interfaces than traditional polymeric cell substrates with polymer-conjugated linkers.

To expand the range of accessible substrate stiffnesses, cellular properties were also investigated on a linker-functionalized polymer-tethered single bilayer, in which substrate stiffness is altered by lipopolymer concentration (TYPE I substrate). Experimental results are presented, which show that lipopolymer concentration in TYPE I bilayers has a profound influence on cellular properties, including cell spreading, morphology, cytoskeletal organization, and motility. Importantly, depending on lipopolymer type, these membrane systems allow formation of homogeneous and compartmentalized bilayers, influencing cell behavior differently.

Third, the LB/LS deposition approach for the fabrication of TYPE I bilayers enables the design of single polymer-tethered lipid bilayers systems with a lateral gradient in lipopolymer concentration (TYPE Ia), as well as a sharp boundary between regions of low and high lipopolymer concentrations (TYPE Ib). Specifically, we show that the lipopolymer gradient has a notable impact on spreading, cytoskeletal organization, and motility of 3T3 fibroblasts. Taken together, the presented experiments support the central hypothesis that cellular mechanoresponse can be tuned through substrate stiffness on linker-functionalized polymer-tethered membrane architectures.

5.2 Outlooks

This research contained within this thesis focused on the cellular mechanoresponse induced by changes in substrate mechanical properties, linker type, and surface

topography of complementary biomembrane-mimicking cell substrates based on polymer-tethered single- and multi-bilayers. As described within this work, adherent cells attach to bilayer-bound ECM-mimicking laminin linkers or cell-cell-mimicking cadherin linkers. In particular, the following three different future research directions are envisioned:

1. Design/characterization of TYPE II substrates with alternative surface topography.
2. Experiments on TYPE II substrates with different linkers.
3. Examination of dynamic linker assembly and disassembly mechanisms.

These different directions are discussed in more detail below.

1. By designing polymer-tethered double bilayers, in which substrate stiffness can be adjusted by lipopolymer concentration, it will be possible conduct experiments on plated cells in the presence of compartmentalized bilayers. Furthermore, double bilayer systems can be built, which have either a lateral gradient in substrate elasticity (lipopolymer content) or a sharp boundary between regions of low and high lipopolymer densities. Such systems would expand the range of artificial cell substrates with gradients or patterns in substrate elasticity, such as PDMS gels with a microtopographical surface to guide cellular fate and function[174,176,245]. Polymer-tethered multi-bilayers with patterns or gradients in substrate elasticity will be particularly beneficial to obtain more insight into the influence of mechanical signals across cell-cell interfaces.
2. Diffusion mediated assembly and disassembly processes of linkers on biomemebrane-mimicking substrate are not only important in the formation of FAs, but also in the formation of adherent junctions. Through, the analysis of linker

assembly and disassembly mechanisms a deeper understanding about the role of linker dynamics and plasticity in cell spreading and migration can be provided, as well as insight into cellular mechanosensing.

3. Diffusion mediated assembly and disassembly processes of linkers on biomemebrane-mimicking substrate are not only important in the formation of FAs, but also in the formation of adherent junctions. Through the analysis of linker assembly and disassembly mechanisms, a deeper understanding about the role of linker dynamics and plasticity during cell spreading/migration and cellular mechanosensing can be obtained.

The biomembrane-mimicking cell substrate could also be potentially significant in a variety of different practical applications. For example, the very low cytotoxicity of these artificial substrates makes them attractive candidates for culturing primary cells. Such an application could be useful in future cell-based drug screening assays. Polymer-tethered single- and multi-bilayers with cadherin linkers could also be employed in research related to the epithelial-to-mesenchymal transition of cancer cells[57,75,246] . Also the mechanical and topographical properties of substrates affecting matrix resistance to cell tension forces have been shown to influence mutagenesis in cell development. Studies with different linker-functionalized cell substrates of tunable mechanical properties provide a tool of controlling mechanoresponse physically, physiologically and biochemically, resulting in a better understanding of processes associated with cellular mechanotransduction.

LIST OF REFERENCES

LIST OF REFERENCES

(1) Farquhar, M. G.; Palade, G. E. Junctional complexes in various epithelia. *J Cell Biol* **1963**, *17*, 375-412.

(2) Volk, T.; Geiger, B. A 135-kd membrane protein of intercellular adherens junctions. *EMBO J* **1984**, *3*, 2249-2260.

(3) Solon, J.; Levental, I.; Sengupta, K.; Georges, P. C.; Janmey, P. A. Fibroblast adaptation and stiffness matching to soft elastic substrates. *Biophysical journal* **2007**, *93*, 4453-4461.

(4) Georges, P. C.; Hui, J. J.; Gombos, Z.; McCormick, M. E.; Wang, A. Y.; Uemura, M.; Mick, R.; Janmey, P. A.; Furth, E. E.; Wells, R. G. Increased stiffness of the rat liver precedes matrix deposition: implications for fibrosis. *Am J Physiol Gastrointest Liver Physiol* **2007**, *293*, G1147-1154.

(5) Goldmann, W. H. Mechanotransduction in cells. *Cell Biol Int* **2012**, *36*, 567-570.

(6) Zaman, M. H.; Trapani, L. M.; Sieminski, A. L.; Mackellar, D.; Gong, H.; Kamm, R. D.; Wells, A.; Lauffenburger, D. A.; Matsudaira, P. Migration of tumor cells in 3D matrices is governed by matrix stiffness along with cell-matrix adhesion and proteolysis. *Proc Natl Acad Sci U S A* **2006**, *103*, 10889-10894.

(7) Engler, A. J.; Sen, S.; Sweeney, H. L.; Discher, D. E. Matrix elasticity directs stem cell lineage specification. *Cell* **2006**, *126*, 677-689.

(8) Ingber, D. E. Cellular mechanotransduction: putting all the pieces together again. *FASEB J* **2006**, *20*, 811-827.

(9) Bonakdar, N.; Luczak, J.; Lautscham, L.; Czonstke, M.; Koch, T. M.; Mainka, A.; Jungbauer, T.; Goldmann, W. H.; Schroder, R.; Fabry, B. Biomechanical characterization of a desminopathy in primary human myoblasts. *Biochem Biophys Res Commun* **2012**, *419*, 703-707.

(10) Chaudhuri, O.; Koshy, S. T.; Branco da Cunha, C.; Shin, J. W.; Verbeke, C. S.; Allison, K. H.; Mooney, D. J. Extracellular matrix stiffness and composition jointly regulate the induction of malignant phenotypes in mammary epithelium. *Nat Mater* **2014**, *13*, 970-978.

(11) Friedl, P.; Gilmour, D. Collective cell migration in morphogenesis, regeneration and cancer. *Nat Rev Mol Cell Biol* **2009**, *10*, 445-457.

(12) Kim, T. H.; An, D. B.; Oh, S. H.; Kang, M. K.; Song, H. H.; Lee, J. H. Creating stiffness gradient polyvinyl alcohol hydrogel using a simple gradual freezing-thawing method to investigate stem cell differentiation behaviors. *Biomaterials* **2015**, *40*, 51-60.

(13) Kim, T. J.; Seong, J.; Ouyang, M.; Sun, J.; Lu, S.; Hong, J. P.; Wang, N.; Wang, Y. Substrate rigidity regulates Ca2+ oscillation via RhoA pathway in stem cells. *J Cell Physiol* **2009**, *218*, 285-293.

(14) Kloboucek, A.; Behrisch, A.; Faix, J.; Sackmann, E. Adhesion-induced receptor segregation and adhesion plaque formation: A model membrane study. *Biophysical journal* **1999**, *77*, 2311-2328.

(15) Friedl, P.; Wolf, K. Plasticity of cell migration: a multiscale tuning model. *J Cell Biol* **2010**, *188*, 11-19.

(16) Janmey, P. A.; McCormick, M. E.; Rammensee, S.; Leight, J. L.; Georges, P. C.; MacKintosh, F. C. Negative normal stress in semiflexible biopolymer gels. *Nat Mater* **2007**, *6*, 48-51.

(17) Biswas, K. H.; Hartman, K. L.; Yu, C. H.; Harrison, O. J.; Song, H.; Smith, A. W.; Huang, W. Y.; Lin, W. C.; Guo, Z.; Padmanabhan, A.; Troyanovsky, S. M.; Dustin, M. L.; Shapiro, L.; Honig, B.; Zaidel-Bar, R.; Groves, J. T. E-cadherin junction formation involves an active kinetic nucleation process. *Proc Natl Acad Sci U S A* **2015**, *112*, 10932-10937.

(18) Coughlin, M. F.; Bielenberg, D. R.; Lenormand, G.; Marinkovic, M.; Waghorne, C. G.; Zetter, B. R.; Fredberg, J. J. Cytoskeletal stiffness, friction, and fluidity of cancer cell lines with different metastatic potential. *Clin Exp Metastasis* **2013**, *30*, 237-250.

(19) Evans, N. D.; Minelli, C.; Gentleman, E.; LaPointe, V.; Patankar, S. N.; Kallivretaki, M.; Chen, X.; Roberts, C. J.; Stevens, M. M. Substrate stiffness affects early differentiation events in embryonic stem cells. *Eur Cell Mater* **2009**, *18*, 1-13; discussion 13-14.

(20) Kametani, Y.; Takeichi, M. Basal-to-apical cadherin flow at cell junctions. *Nat Cell Biol* **2007**, *9*, 92-98.

(21) Peglion, F.; Llense, F.; Etienne-Manneville, S. Adherens junction treadmilling during collective migration. *Nat Cell Biol* **2014**, *16*, 639-651.

(22) Grakoui, A.; Bromley, S. K.; Sumen, C.; Davis, M. M.; Shaw, A. S.; Allen, P. M.; Dustin, M. L. The immunological synapse: a molecular machine controlling T cell activation. *Science* **1999**, *285*, 221-227.

(23) Mossman, K. D.; Campi, G.; Groves, J. T.; Dustin, M. L. Altered TCR signaling from geometrically repatterned immunological synapses. *Science* **2005**, *310*, 1191-1193.

(24) Minner, D. E.; Herring, V. L.; Siegel, A. P.; Kimble-Hill, A.; Johnson, M. A.; Naumann, C. A. Iterative layer-by-layer assembly of polymer-tethered multi-bilayers using maleimide-thiol coupling chemistry. *Soft Matter* **2013**, *9*, 9643-9650.

(25) Kaizuka, Y.; Groves, J. T. Structure and dynamics of supported intermembrane junctions. *Biophysical journal* **2004**, *86*, 905-912.

(26) Murray, D. H.; Tamm, L. K.; Kiessling, V. Supported double membranes. *J Struct Biol* **2009**, *168*, 183-189.

(27) Tabaei, S. R.; Jonsson, P.; Branden, M.; Hook, F. Self-assembly formation of multiple DNA-tethered lipid bilayers. *J Struct Biol* **2009**, *168*, 200-206.

(28) Chung, M.; Lowe, R. D.; Chan, Y. H.; Ganesan, P. V.; Boxer, S. G. DNA-tethered membranes formed by giant vesicle rupture. *J Struct Biol* **2009**, *168*, 190-199.

(29) Han, X.; Achalkumar, A. S.; Cheetham, M. R.; Connell, S. D.; Johnson, B. R.; Bushby, R. J.; Evans, S. D. A self-assembly route for double bilayer lipid membrane formation. *Chemphyschem : a European journal of chemical physics and physical chemistry* **2010**, *11*, 569-574.

(30) Barenholz, Y.; Gibbes, D.; Litman, B. J.; Goll, J.; Thompson, T. E.; Carlson, R. D. A simple method for the preparation of homogeneous phospholipid vesicles. *Biochemistry* **1977**, *16*, 2806-2810.

(31) Castellana, E. T.; Kataoka, S.; Albertorio, F.; Cremer, P. S. Direct writing of metal nanoparticle films inside sealed microfluidic channels. *Anal Chem* **2006**, *78*, 107-112.

(32) Akashi, K.; Miyata, H.; Itoh, H.; Kinosita, K., Jr. Preparation of giant liposomes in physiological conditions and their characterization under an optical microscope. *Biophysical journal* **1996**, *71*, 3242-3250.

(33) Rozovsky, S.; Kaizuka, Y.; Groves, J. T. Formation and spatio-temporal evolution of periodic structures in lipid bilayers. *J Am Chem Soc* **2005**, *127*, 36-37.

(34) Tamm, L. K.; McConnell, H. M. Supported phospholipid bilayers. *Biophys J* **1985**, *47*, 105-113.

(35) Voskuhl, J.; Ravoo, B. J. Molecular recognition of bilayer vesicles. *Chemical Society reviews* **2009**, *38*, 495-505.

(36) Carman, C. V. Overview: imaging in the study of integrins. *Methods Mol Biol* **2012**, *757*, 159-189.

(37) Digman, M. A.; Gratton, E. Scanning image correlation spectroscopy. *Bioessays* **2012**, *34*, 377-385.

(38) Carisey, A.; Stroud, M.; Tsang, R.; Ballestrem, C. Fluorescence recovery after photobleaching. *Methods Mol Biol* **2011**, *769*, 387-402.

(39) Day, C. A.; Kraft, L. J.; Kang, M.; Kenworthy, A. K. Analysis of protein and lipid dynamics using confocal fluorescence recovery after photobleaching (FRAP). *Curr Protoc Cytom* **2012**, *Chapter 2*, Unit2 19.

(40) Kang, M.; Day, C. A.; Kenworthy, A. K.; DiBenedetto, E. Simplified equation to extract diffusion coefficients from confocal FRAP data. *Traffic* **2012**, *13*, 1589-1600.

(41) Axelrod, D.; Koppel, D. E.; Schlessinger, J.; Elson, E.; Webb, W. W. Mobility measurement by analysis of fluorescence photobleaching recovery kinetics. *Biophys J* **1976**, *16*, 1055-1069.

(42) Soumpasis, D. M. Theoretical analysis of fluorescence photobleaching recovery experiments. *Biophys J* **1983**, *41*, 95-97.

(43) Carvalho, F. A.; Santos, N. C. Atomic force microscopy-based force spectroscopy--biological and biomedical applications. *IUBMB Life* **2012**, *64*, 465-472.

(44) Carvalho, F. A.; Martins, I. C.; Santos, N. C. Atomic force microscopy and force spectroscopy on the assessment of protein folding and functionality. *Arch Biochem Biophys* **2013**, *531*, 116-127.

(45) Singh, S.; Keller, D. J. Atomic force microscopy of supported planar membrane bilayers. *Biophys J* **1991**, *60*, 1401-1410.

(46) Fischer, C. L.; Blanchette, D. R.; Brogden, K. A.; Dawson, D. V.; Drake, D. R.; Hill, J. R.; Wertz, P. W. The roles of cutaneous lipids in host defense. *Biochimica et biophysica acta* **2014**, *1841*, 319-322.

(47) Longo, M. L.; Blanchette, C. D. Imaging cerebroside-rich domains for phase and shape characterization in binary and ternary mixtures. *Biochimica et biophysica acta* **2010**, *1798*, 1357-1367.

(48) Chiantia, S.; Ries, J.; Kahya, N.; Schwille, P. Combined AFM and two-focus SFCS study of raft-exhibiting model membranes. *Chemphyschem : a European journal of chemical physics and physical chemistry* **2006**, *7*, 2409-2418.

(49) Butler, J. P.; Tolic-Norrelykke, I. M.; Fabry, B.; Fredberg, J. J. Traction fields, moments, and strain energy that cells exert on their surroundings. *Am J Physiol Cell Physiol* **2002**, *282*, C595-605.

(50) Barocas, V. H.; Tranquillo, R. T. An anisotropic biphasic theory of tissue-equivalent mechanics: the interplay among cell traction, fibrillar network deformation, fibril alignment, and cell contact guidance. *J Biomech Eng* **1997**, *119*, 137-145.

(51) Dembo, M.; Oliver, T.; Ishihara, A.; Jacobson, K. Imaging the traction stresses exerted by locomoting cells with the elastic substratum method. *Biophysical journal* **1996**, *70*, 2008-2022.

(52) Wang, N.; Tolic-Norrelykke, I. M.; Chen, J.; Mijailovich, S. M.; Butler, J. P.; Fredberg, J. J.; Stamenovic, D. Cell prestress. I. Stiffness and prestress are closely associated in adherent contractile cells. *Am J Physiol Cell Physiol* **2002**, *282*, C606-616.

(53) Yang, Z.; Lin, J. S.; Chen, J.; Wang, J. H. Determining substrate displacement and cell traction fields--a new approach. *J Theor Biol* **2006**, *242*, 607-616.

(54) Schwarz, U. S.; Gardel, M. L. United we stand: integrating the actin cytoskeleton and cell-matrix adhesions in cellular mechanotransduction. *Journal of cell science* **2012**, *125*, 3051-3060.

(55) Muller, M.: *Introduction to confocal fluorescence microscopy 2nd Edition*; SPIE Press, 2006.

(56) Koch, T. M.; Munster, S.; Bonakdar, N.; Butler, J. P.; Fabry, B. 3D Traction forces in cancer cell invasion. *PLoS One* **2012**, *7*, e33476.

(57) Discher, D. E.; Janmey, P.; Wang, Y. L. Tissue cells feel and respond to the stiffness of their substrate. *Science* **2005**, *310*, 1139-1143.

(58) Zaidel-Bar, R.; Kam, Z.; Geiger, B. Polarized downregulation of the paxillin-p130CAS-Rac1 pathway induced by shear flow. *Journal of cell science* **2005**, *118*, 3997-4007.

(59) Nam, J.; Johnson, J.; Lannutti, J. J.; Agarwal, S. Modulation of embryonic mesenchymal progenitor cell differentiation via control over pure mechanical modulus in electrospun nanofibers. *Acta Biomater* **2011**, *7*, 1516-1524.

(60) Engler, A. J.; Griffin, M. A.; Sen, S.; Bonnemann, C. G.; Sweeney, H. L.; Discher, D. E. Myotubes differentiate optimally on substrates with tissue-like stiffness: pathological implications for soft or stiff microenvironments. *J Cell Biol* **2004**, *166*, 877-887.

(61) Ghosh, K.; Pan, Z.; Guan, E.; Ge, S.; Liu, Y.; Nakamura, T.; Ren, X. D.; Rafailovich, M.; Clark, R. A. Cell adaptation to a physiologically relevant ECM mimic with different viscoelastic properties. *Biomaterials* **2007**, *28*, 671-679.

(62) Prager-Khoutorsky, M.; Lichtenstein, A.; Krishnan, R.; Rajendran, K.; Mayo, A.; Kam, Z.; Geiger, B.; Bershadsky, A. D. Fibroblast polarization is a matrix-rigidity-dependent process controlled by focal adhesion mechanosensing. *Nat Cell Biol* **2011**, *13*, 1457-1465.

(63) Vaughan, R. B.; Trinkaus, J. P. Movements of epithelial cell sheets in vitro. *Journal of cell science* **1966**, *1*, 407-413.

(64) Friedl, P.; Wolf, K. Proteolytic interstitial cell migration: a five-step process. *Cancer Metastasis Rev* **2009**, *28*, 129-135.

(65) Carmona-Fontaine, C.; Matthews, H. K.; Kuriyama, S.; Moreno, M.; Dunn, G. A.; Parsons, M.; Stern, C. D.; Mayor, R. Contact inhibition of locomotion in vivo controls neural crest directional migration. *Nature* **2008**, *456*, 957-961.

(66) Nobes, C. D.; Hall, A. Rho GTPases control polarity, protrusion, and adhesion during cell movement. *J Cell Biol* **1999**, *144*, 1235-1244.

(67) Wolf, K.; Wu, Y. I.; Liu, Y.; Geiger, J.; Tam, E.; Overall, C.; Stack, M. S.; Friedl, P. Multi-step pericellular proteolysis controls the transition from individual to collective cancer cell invasion. *Nat Cell Biol* **2007**, *9*, 893-904.

(68) Gaggioli, C.; Hooper, S.; Hidalgo-Carcedo, C.; Grosse, R.; Marshall, J. F.; Harrington, K.; Sahai, E. Fibroblast-led collective invasion of carcinoma cells with differing roles for RhoGTPases in leading and following cells. *Nat Cell Biol* **2007**, *9*, 1392-1400.

(69) Ewald, A. J.; Brenot, A.; Duong, M.; Chan, B. S.; Werb, Z. Collective epithelial migration and cell rearrangements drive mammary branching morphogenesis. *Dev Cell* **2008**, *14*, 570-581.

(70) Lee, G. Y.; Kenny, P. A.; Lee, E. H.; Bissell, M. J. Three-dimensional culture models of normal and malignant breast epithelial cells. *Nat Methods* **2007**, *4*, 359-365.

(71) Friedl, P.; Noble, P. B.; Walton, P. A.; Laird, D. W.; Chauvin, P. J.; Tabah, R. J.; Black, M.; Zanker, K. S. Migration of coordinated cell clusters in mesenchymal and epithelial cancer explants in vitro. *Cancer Res* **1995**, *55*, 4557-4560.

(72) Farooqui, R.; Fenteany, G. Multiple rows of cells behind an epithelial wound edge extend cryptic lamellipodia to collectively drive cell-sheet movement. *Journal of cell science* **2005**, *118*, 51-63.

(73) Affolter, M.; Bellusci, S.; Itoh, N.; Shilo, B.; Thiery, J. P.; Werb, Z. Tube or not tube: remodeling epithelial tissues by branching morphogenesis. *Dev Cell* **2003**, *4*, 11-18.

(74) Affolter, M.; Caussinus, E. Tracheal branching morphogenesis in Drosophila: new insights into cell behaviour and organ architecture. *Development* **2008**, *135*, 2055-2064.

(75) Ridley, A. J.; Schwartz, M. A.; Burridge, K.; Firtel, R. A.; Ginsberg, M. H.; Borisy, G.; Parsons, J. T.; Horwitz, A. R. Cell migration: integrating signals from front to back. *Science* **2003**, *302*, 1704-1709.

(76) Friedl, P.; Brocker, E. B. The biology of cell locomotion within three-dimensional extracellular matrix. *Cell Mol Life Sci* **2000**, *57*, 41-64.

(77) Mierke, C. T.; Rosel, D.; Fabry, B.; Brabek, J. Contractile forces in tumor cell migration. *Eur J Cell Biol* **2008**, *87*, 669-676.

(78) Ladoux, B.; Nicolas, A. Physically based principles of cell adhesion mechanosensitivity in tissues. *Reports on progress in physics. Physical Society* **2012**, *75*, 116601.

(79) Fraley, S. I.; Feng, Y.; Krishnamurthy, R.; Kim, D. H.; Celedon, A.; Longmore, G. D.; Wirtz, D. A distinctive role for focal adhesion proteins in three-dimensional cell motility. *Nat Cell Biol* **2010**, *12*, 598-604.

(80) Petrie, R. J.; Gavara, N.; Chadwick, R. S.; Yamada, K. M. Nonpolarized signaling reveals two distinct modes of 3D cell migration. *J Cell Biol* **2012**, *197*, 439-455.

(81) Wolf, K.; Muller, R.; Borgmann, S.; Brocker, E. B.; Friedl, P. Amoeboid shape change and contact guidance: T-lymphocyte crawling through fibrillar collagen is independent of matrix remodeling by MMPs and other proteases. *Blood* **2003**, *102*, 3262-3269.

(82) Bao, G.; Kamm, R. D.; Thomas, W.; Hwang, W.; Fletcher, D. A.; Grodzinsky, A. J.; Zhu, C.; Mofrad, M. R. Molecular Biomechanics: The Molecular Basis of How Forces Regulate Cellular Function. *Mol Cell Biomech* **2010**, *3*, 91-105.

(83) Li, Y.; Chu, J. S.; Kurpinski, K.; Li, X.; Bautista, D. M.; Yang, L.; Sung, K. L.; Li, S. Biophysical regulation of histone acetylation in mesenchymal stem cells. *Biophysical journal* **2011**, *100*, 1902-1909.

(84) Ogawa, H.; Baba, Y.; Oka, K. Directional sensitivity of dendritic calcium responses to wind stimuli in the cricket giant interneuron. *Neurosci Lett* **2004**, *358*, 185-188.

(85) Bovendeerd, P. H. Modeling of cardiac growth and remodeling of myofiber orientation. *J Biomech* **2012**, *45*, 872-881.

(86) Wu, F.; Lin, D. D.; Chang, J. H.; Fischbach, C.; Estroff, L. A.; Gourdon, D. Effect of the Materials Properties of Hydroxyapatite Nanoparticles on Fibronectin Deposition and Conformation. *Cryst Growth Des* **2015**, *15*, 2452-2460.

(87) Desmond, M. E.; Knepper, J. E.; DiBenedetto, A. J.; Malaugh, E.; Callejo, S.; Carretero, R.; Alonso, M. I.; Gato, A. Focal adhesion kinase as a mechanotransducer during rapid brain growth of the chick embryo. *Int J Dev Biol* **2014**, *58*, 35-43.

(88) Delmas, P.; Hao, J.; Rodat-Despoix, L. Molecular mechanisms of mechanotransduction in mammalian sensory neurons. *Nat Rev Neurosci* **2011**, *12*, 139-153.

(89) Ingber, D. E. Tensegrity-based mechanosensing from macro to micro. *Prog Biophys Mol Biol* **2008**, *97*, 163-179.

(90) Cameron, A. R.; Frith, J. E.; Cooper-White, J. J. The influence of substrate creep on mesenchymal stem cell behaviour and phenotype. *Biomaterials* **2011**, *32*, 5979-5993.

(91) Lo, C. M.; Wang, H. B.; Dembo, M.; Wang, Y. L. Cell movement is guided by the rigidity of the substrate. *Biophysical journal* **2000**, *79*, 144-152.

(92) Pelham, R. J., Jr.; Wang, Y. Cell locomotion and focal adhesions are regulated by substrate flexibility. *Proc Natl Acad Sci U S A* **1997**, *94*, 13661-13665.

(93) Shiu, Y. T.; Li, S.; Marganski, W. A.; Usami, S.; Schwartz, M. A.; Wang, Y. L.; Dembo, M.; Chien, S. Rho mediates the shear-enhancement of endothelial cell migration and traction force generation. *Biophysical journal* **2004**, *86*, 2558-2565.

(94) Simmons, C. A.; Matlis, S.; Thornton, A. J.; Chen, S.; Wang, C. Y.; Mooney, D. J. Cyclic strain enhances matrix mineralization by adult human mesenchymal stem cells via the extracellular signal-regulated kinase (ERK1/2) signaling pathway. *J Biomech* **2003**, *36*, 1087-1096.

(95) Wang, J. H. Mechanobiology of tendon. *J Biomech* **2006**, *39*, 1563-1582.

(96) Mack, P. J.; Kaazempur-Mofrad, M. R.; Karcher, H.; Lee, R. T.; Kamm, R. D. Force-induced focal adhesion translocation: effects of force amplitude and frequency. *Am J Physiol Cell Physiol* **2004**, *287*, C954-962.

(97) Sreenivasappa, H.; Chaki, S. P.; Lim, S. M.; Trzeciakowski, J. P.; Davidson, M. W.; Rivera, G. M.; Trache, A. Selective regulation of cytoskeletal tension and cell-matrix adhesion by RhoA and Src. *Integr Biol (Camb)* **2014**, *6*, 743-754.

(98) Byfield, F. J.; Reen, R. K.; Shentu, T. P.; Levitan, I.; Gooch, K. J. Endothelial actin and cell stiffness is modulated by substrate stiffness in 2D and 3D. *J Biomech* **2009**, *42*, 1114-1119.

(99) Hoyer, J.; Distler, A.; Haase, W.; Gogelein, H. Ca2+ influx through stretch-activated cation channels activates maxi K+ channels in porcine endocardial endothelium. *Proc Natl Acad Sci U S A* **1994**, *91*, 2367-2371.

(100) Hoyer, J.; Kohler, R.; Haase, W.; Distler, A. Up-regulation of pressure-activated Ca(2+)-permeable cation channel in intact vascular endothelium of hypertensive rats. *Proc Natl Acad Sci U S A* **1996**, *93*, 11253-11258.

(101) Kraichely, R. E.; Farrugia, G. Mechanosensitive ion channels in interstitial cells of Cajal and smooth muscle of the gastrointestinal tract. *Neurogastroenterol Motil* **2007**, *19*, 245-252.

(102) Suchyna, T. M.; Sachs, F. Mechanosensitive channel properties and membrane mechanics in mouse dystrophic myotubes. *J Physiol* **2007**, *581*, 369-387.

(103) Gether, U. Uncovering molecular mechanisms involved in activation of G protein-coupled receptors. *Endocr Rev* **2000**, *21*, 90-113.

(104) Gudi, S. R.; Clark, C. B.; Frangos, J. A. Fluid flow rapidly activates G proteins in human endothelial cells. Involvement of G proteins in mechanochemical signal transduction. *Circ Res* **1996**, *79*, 834-839.

(105) Zou, Y.; Akazawa, H.; Qin, Y.; Sano, M.; Takano, H.; Minamino, T.; Makita, N.; Iwanaga, K.; Zhu, W.; Kudoh, S.; Toko, H.; Tamura, K.; Kihara, M.; Nagai, T.; Fukamizu, A.; Umemura, S.; Iiri, T.; Fujita, T.; Komuro, I. Mechanical stress activates angiotensin II type 1 receptor without the involvement of angiotensin II. *Nat Cell Biol* **2004**, *6*, 499-506.

(106) Jaalouk, D. E.; Lammerding, J. Mechanotransduction gone awry. *Nat Rev Mol Cell Biol* **2009**, *10*, 63-73.

(107) Guilak, F.; Tedrow, J. R.; Burgkart, R. Viscoelastic properties of the cell nucleus. *Biochem Biophys Res Commun* **2000**, *269*, 781-786.

(108) Vaziri, A.; Mofrad, M. R. Mechanics and deformation of the nucleus in micropipette aspiration experiment. *J Biomech* **2007**, *40*, 2053-2062.

(109) Jiang, H.; Sun, S. X. Cellular pressure and volume regulation and implications for cell mechanics. *Biophys J* **2013**, *105*, 609-619.

(110) Deguchi, S.; Maeda, K.; Ohashi, T.; Sato, M. Flow-induced hardening of endothelial nucleus as an intracellular stress-bearing organelle. *J Biomech* **2005**, *38*, 1751-1759.

(111) Mathur, A. B.; Reichert, W. M.; Truskey, G. A. Flow and high affinity binding affect the elastic modulus of the nucleus, cell body and the stress fibers of endothelial cells. *Ann Biomed Eng* **2007**, *35*, 1120-1130.

(112) Lee, J. S.; Chang, M. I.; Tseng, Y.; Wirtz, D. Cdc42 mediates nucleus movement and MTOC polarization in Swiss 3T3 fibroblasts under mechanical shear stress. *Mol Biol Cell* **2005**, *16*, 871-880.

(113) Webb, D. J.; Donais, K.; Whitmore, L. A.; Thomas, S. M.; Turner, C. E.; Parsons, J. T.; Horwitz, A. F. FAK-Src signalling through paxillin, ERK and MLCK regulates adhesion disassembly. *Nat Cell Biol* **2004**, *6*, 154-161.

(114) Riveline, D.; Zamir, E.; Balaban, N. Q.; Schwarz, U. S.; Ishizaki, T.; Narumiya, S.; Kam, Z.; Geiger, B.; Bershadsky, A. D. Focal contacts as mechanosensors: externally applied local mechanical force induces growth of focal contacts by an mDia1-dependent and ROCK-independent mechanism. *J Cell Biol* **2001**, *153*, 1175-1186.

(115) Fukata, M.; Watanabe, T.; Noritake, J.; Nakagawa, M.; Yamaga, M.; Kuroda, S.; Matsuura, Y.; Iwamatsu, A.; Perez, F.; Kaibuchi, K. Rac1 and Cdc42 capture microtubules through IQGAP1 and CLIP-170. *Cell* **2002**, *109*, 873-885.

(116) Siegrist, S. E.; Doe, C. Q. Microtubule-induced cortical cell polarity. *Genes Dev* **2007**, *21*, 483-496.

(117) Vincent, L. G.; Choi, Y. S.; Alonso-Latorre, B.; del Alamo, J. C.; Engler, A. J. Mesenchymal stem cell durotaxis depends on substrate stiffness gradient strength. *Biotechnol J* **2013**, *8*, 472-484.

(118) Tse, J. R.; Engler, A. J. Stiffness gradients mimicking in vivo tissue variation regulate mesenchymal stem cell fate. *PLoS One* **2011**, *6*, e15978.

(119) Scott, C. M.; Forster, C. L.; Kokkoli, E. Three-Dimensional Cell Entrapment as a Function of the Weight Percent of Peptide-Amphiphile Hydrogels. *Langmuir : the ACS journal of surfaces and colloids* **2015**, *31*, 6122-6129.

(120) Coughlin, M. F.; Fredberg, J. J. Changes in cytoskeletal dynamics and nonlinear rheology with metastatic ability in cancer cell lines. *Phys Biol* **2013**, *10*, 065001.

(121) Miron-Mendoza, M.; Seemann, J.; Grinnell, F. The differential regulation of cell motile activity through matrix stiffness and porosity in three dimensional collagen matrices. *Biomaterials* **2010**, *31*, 6425-6435.

(122) Elias, D. R.; Poloukhtine, A.; Popik, V.; Tsourkas, A. Effect of ligand density, receptor density, and nanoparticle size on cell targeting. *Nanomedicine* **2013**, *9*, 194-201.

(123) Slater, J. H.; Frey, W. Nanopatterning of fibronectin and the influence of integrin clustering on endothelial cell spreading and proliferation. *J Biomed Mater Res A* **2008**, *87*, 176-195.

(124) Anselme, K.; Davidson, P.; Popa, A. M.; Giazzon, M.; Liley, M.; Ploux, L. The interaction of cells and bacteria with surfaces structured at the nanometre scale. *Acta Biomater* **2010**, *6*, 3824-3846.

(125) Gines, A.; Cassivi, S. D.; Martenson, J. A., Jr.; Schleck, C.; Deschamps, C.; Sinicrope, F. A.; Alberts, S. R.; Murray, J. A.; Zinsmeister, A. R.; Vazquez-Sequeiros, E.; Nichols, F. C., 3rd; Miller, R. C.; Quevedo, J. F.; Allen, M. S.; Alexander, J. A.; Zais, T.; Haddock, M. G.; Romero, Y. Impact of endoscopic ultrasonography and physician specialty on the management of patients with esophagus cancer. *Dis Esophagus* **2008**, *21*, 241-250.

(126) Abercrombie, M.; Heaysman, J. E.; Pegrum, S. M. The locomotion of fibroblasts in culture. IV. Electron microscopy of the leading lamella. *Exp Cell Res* **1971**, *67*, 359-367.

(127) Geiger, B.; Spatz, J. P.; Bershadsky, A. D. Environmental sensing through focal adhesions. *Nat Rev Mol Cell Biol* **2009**, *10*, 21-33.

(128) Campbell, I. D.; Humphries, M. J. Integrin structure, activation, and interactions. *Cold Spring Harb Perspect Biol* **2011**, *3*.

(129) Arnaout, M. A.; Mahalingam, B.; Xiong, J. P. Integrin structure, allostery, and bidirectional signaling. *Annu Rev Cell Dev Biol* **2005**, *21*, 381-410.

(130) Xiong, J. P.; Stehle, T.; Zhang, R.; Joachimiak, A.; Frech, M.; Goodman, S. L.; Arnaout, M. A. Crystal structure of the extracellular segment of integrin alpha Vbeta3 in complex with an Arg-Gly-Asp ligand. *Science* **2002**, *296*, 151-155.

(131) Prevarskaya, N.; Skryma, R.; Shuba, Y. Calcium in tumour metastasis: new roles for known actors. *Nature reviews. Cancer* **2011**, *11*, 609-618.

(132) Chiquet, M. Regulation of extracellular matrix gene expression by mechanical stress. *Matrix Biol* **1999**, *18*, 417-426.

(133) Zimerman, B.; Volberg, T.; Geiger, B. Early molecular events in the assembly of the focal adhesion-stress fiber complex during fibroblast spreading. *Cell Motil Cytoskeleton* **2004**, *58*, 143-159.

(134) Alexandrova, A. Y.; Arnold, K.; Schaub, S.; Vasiliev, J. M.; Meister, J. J.; Bershadsky, A. D.; Verkhovsky, A. B. Comparative dynamics of retrograde actin flow and focal adhesions: formation of nascent adhesions triggers transition from fast to slow flow. *PLoS One* **2008**, *3*, e3234.

(135) Twiss, F.; de Rooij, J. Cadherin mechanotransduction in tissue remodeling. *Cell Mol Life Sci* **2013**, *70*, 4101-4116.

(136) Hulpiau, P.; van Roy, F. Molecular evolution of the cadherin superfamily. *Int J Biochem Cell Biol* **2009**, *41*, 349-369.

(137) Ozawa, M.; Baribault, H.; Kemler, R. The cytoplasmic domain of the cell adhesion molecule uvomorulin associates with three independent proteins structurally related in different species. *EMBO J* **1989**, *8*, 1711-1717.

(138) Davis, M. A.; Ireton, R. C.; Reynolds, A. B. A core function for p120-catenin in cadherin turnover. *J Cell Biol* **2003**, *163*, 525-534.

(139) Hinck, L.; Nathke, I. S.; Papkoff, J.; Nelson, W. J. Dynamics of cadherin/catenin complex formation: novel protein interactions and pathways of complex assembly. *J Cell Biol* **1994**, *125*, 1327-1340.

(140) Adams, C. L.; Nelson, W. J. Cytomechanics of cadherin-mediated cell-cell adhesion. *Curr Opin Cell Biol* **1998**, *10*, 572-577.

(141) Vasioukhin, V.; Bauer, C.; Yin, M.; Fuchs, E. Directed actin polymerization is the driving force for epithelial cell-cell adhesion. *Cell* **2000**, *100*, 209-219.

(142) Huveneers, S.; Oldenburg, J.; Spanjaard, E.; van der Krogt, G.; Grigoriev, I.; Akhmanova, A.; Rehmann, H.; de Rooij, J. Vinculin associates with endothelial VE-cadherin junctions to control force-dependent remodeling. *J Cell Biol* **2012**, *196*, 641-652.

(143) Niessen, C. M. Tight junctions/adherens junctions: basic structure and function. *J Invest Dermatol* **2007**, *127*, 2525-2532.

(144) Watabe-Uchida, M.; Uchida, N.; Imamura, Y.; Nagafuchi, A.; Fujimoto, K.; Uemura, T.; Vermeulen, S.; van Roy, F.; Adamson, E. D.; Takeichi, M. alpha-Catenin-vinculin interaction functions to organize the apical junctional complex in epithelial cells. *J Cell Biol* **1998**, *142*, 847-857.

(145) Aberle, H.; Schwartz, H.; Kemler, R. Cadherin-catenin complex: protein interactions and their implications for cadherin function. *J Cell Biochem* **1996**, *61*, 514-523.

(146) Tornavaca, O.; Chia, M.; Dufton, N.; Almagro, L. O.; Conway, D. E.; Randi, A. M.; Schwartz, M. A.; Matter, K.; Balda, M. S. ZO-1 controls endothelial adherens junctions, cell-cell tension, angiogenesis, and barrier formation. *J Cell Biol* **2015**, *208*, 821-838.

(147) de Rooij, J.; Kerstens, A.; Danuser, G.; Schwartz, M. A.; Waterman-Storer, C. M. Integrin-dependent actomyosin contraction regulates epithelial cell scattering. *J Cell Biol* **2005**, *171*, 153-164.

(148) Loerke, D.; le Duc, Q.; Blonk, I.; Kerstens, A.; Spanjaard, E.; Machacek, M.; Danuser, G.; de Rooij, J. Quantitative imaging of epithelial cell scattering identifies specific inhibitors of cell motility and cell-cell dissociation. *Sci Signal* **2012**, *5*, rs5.

(149) Desai, R. A.; Gao, L.; Raghavan, S.; Liu, W. F.; Chen, C. S. Cell polarity triggered by cell-cell adhesion via E-cadherin. *J Cell Sci* **2009**, *122*, 905-911.

(150) Krens, S. F.; Heisenberg, C. P. Cell sorting in development. *Curr Top Dev Biol* **2011**, *95*, 189-213.

(151) Maitre, J. L.; Berthoumieux, H.; Krens, S. F.; Salbreux, G.; Julicher, F.; Paluch, E.; Heisenberg, C. P. Adhesion functions in cell sorting by mechanically coupling the cortices of adhering cells. *Science* **2012**, *338*, 253-256.

(152) Jin, H.; Pi, J.; Huang, X.; Huang, F.; Shao, W.; Li, S.; Chen, Y.; Cai, J. BMP2 promotes migration and invasion of breast cancer cells via cytoskeletal reorganization and adhesion decrease: an AFM investigation. *Appl Microbiol Biotechnol* **2012**, *93*, 1715-1723.

(153) Martin, A. C.; Kaschube, M.; Wieschaus, E. F. Pulsed contractions of an actin-myosin network drive apical constriction. *Nature* **2009**, *457*, 495-499.

(154) Miller, C. J.; Davidson, L. A. The interplay between cell signalling and mechanics in developmental processes. *Nat Rev Genet* **2013**, *14*, 733-744.

(155) Dufour, S.; Mege, R. M.; Thiery, J. P. alpha-catenin, vinculin, and F-actin in strengthening E-cadherin cell-cell adhesions and mechanosensing. *Cell Adh Migr* **2013**, *7*, 345-350.

(156) Thomas, W. A.; Boscher, C.; Chu, Y. S.; Cuvelier, D.; Martinez-Rico, C.; Seddiki, R.; Heysch, J.; Ladoux, B.; Thiery, J. P.; Mege, R. M.; Dufour, S. alpha-Catenin and vinculin cooperate to promote high E-cadherin-based adhesion strength. *J Biol Chem* **2013**, *288*, 4957-4969.

(157) Benson, D. L.; Tanaka, H. N-cadherin redistribution during synaptogenesis in hippocampal neurons. *J Neurosci* **1998**, *18*, 6892-6904.

(158) Gumbiner, B. M. Regulation of cadherin-mediated adhesion in morphogenesis. *Nat Rev Mol Cell Biol* **2005**, *6*, 622-634.

(159) Paszek, M. J.; Zahir, N.; Johnson, K. R.; Lakins, J. N.; Rozenberg, G. I.; Gefen, A.; Reinhart-King, C. A.; Margulies, S. S.; Dembo, M.; Boettiger, D.; Hammer, D. A.; Weaver, V. M. Tensional homeostasis and the malignant phenotype. *Cancer Cell* **2005**, *8*, 241-254.

(160) Kim, N. G.; Koh, E.; Chen, X.; Gumbiner, B. M. E-cadherin mediates contact inhibition of proliferation through Hippo signaling-pathway components. *Proc Natl Acad Sci U S A* **2011**, *108*, 11930-11935.

(161) Schlegelmilch, K.; Mohseni, M.; Kirak, O.; Pruszak, J.; Rodriguez, J. R.; Zhou, D.; Kreger, B. T.; Vasioukhin, V.; Avruch, J.; Brummelkamp, T. R.; Camargo, F. D. Yap1 acts downstream of alpha-catenin to control epidermal proliferation. *Cell* **2011**, *144*, 782-795.

(162) Qi, S. Y.; Groves, J. T.; Chakraborty, A. K. Synaptic pattern formation during cellular recognition. *Proc Natl Acad Sci U S A* **2001**, *98*, 6548-6553.

(163) Groves, J. T.; Dustin, M. L. Supported planar bilayers in studies on immune cell adhesion and communication. *J Immunol Methods* **2003**, *278*, 19-32.

(164) Sackmann, E. Supported membranes: scientific and practical applications. *Science* **1996**, *271*, 43-48.

(165) Mirzadeh, H.; Shokrolahi, F.; Daliri, M. Effect of silicon rubber crosslink density on fibroblast cell behavior in vitro. *J Biomed Mater Res A* **2003**, *67*, 727-732.

(166) Wang, Z.; Hu, H.; Wang, Y.; Wang, Y.; Wu, Q.; Liu, L.; Chen, G. Fabrication of poly(3-hydroxybutyrate-co-3-hydroxyhexanoate) (PHBHHx) microstructures using soft lithography for scaffold applications. *Biomaterials* **2006**, *27*, 2550-2557.

(167) Vozzi, G.; Morelli, I.; Vozzi, F.; Andreoni, C.; Salsedo, E.; Morachioli, A.; Giusti, P.; Ciardelli, G. SOFT-MI: a novel microfabrication technique integrating soft-lithography and molecular imprinting for tissue engineering applications. *Biotechnol Bioeng* **2010**, *106*, 804-817.

(168) Tanaka, N.; Ota, H.; Fukumori, K.; Miyake, J.; Yamato, M.; Okano, T. Micro-patterned cell-sheets fabricated with stamping-force-controlled micro-contact printing. *Biomaterials* **2014**, *35*, 9802-9810.

(169) Li, J. Y.; Ho, Y. C.; Chung, Y. C.; Lin, F. C.; Liao, W. L.; Tsai, W. B. Preparation of micron/submicron hybrid patterns via a two-stage UV-imprint technique and their dimensional effects on cell adhesion and alignment. *Biofabrication* **2013**, *5*, 035003.

(170) Cuchiara, M. P.; Allen, A. C.; Chen, T. M.; Miller, J. S.; West, J. L. Multilayer microfluidic PEGDA hydrogels. *Biomaterials* **2010**, *31*, 5491-5497.

(171) Folch, A.; Ayon, A.; Hurtado, O.; Schmidt, M. A.; Toner, M. Molding of deep polydimethylsiloxane microstructures for microfluidics and biological applications. *J Biomech Eng* **1999**, *121*, 28-34.

(172) Rossomando, E. F.; Maldonado, B.; Crean, E. V.; Kollar, E. J. Protease secretion during onset of development in Dictyostelium discoideum. *J Cell Sci* **1978**, *30*, 305-318.

(173) Minner, D. E.; Rauch, P.; Kas, J.; Naumann, C. A. Polymer-tethered lipid multi-bilayers: a biomembrane-mimicking cell substrate to probe cellular mechano-sensing. *Soft Matter* **2014**, *10*, 1189-1198.

(174) Lautscham, L. A.; Lin, C. Y.; Auernheimer, V.; Naumann, C. A.; Goldmann, W. H.; Fabry, B. Biomembrane-mimicking lipid bilayer system as a mechanically tunable cell substrate. *Biomaterials* **2014**, *35*, 3198-3207.

(175) Mata, A.; Kim, E. J.; Boehm, C. A.; Fleischman, A. J.; Muschler, G. F.; Roy, S. A three-dimensional scaffold with precise micro-architecture and surface micro-textures. *Biomaterials* **2009**, *30*, 4610-4617.

(176) Sodunke, T. R.; Turner, K. K.; Caldwell, S. A.; McBride, K. W.; Reginato, M. J.; Noh, H. M. Micropatterns of Matrigel for three-dimensional epithelial cultures. *Biomaterials* **2007**, *28*, 4006-4016.

(177) Perera-Nunez, J.; Mendez-Vilas, A.; Labajos-Broncano, L.; Gonzalez-Martin, M. L. Ionic liquid microdroplets as versatile lithographic molds for sculpting curved topographies on soft materials surfaces. *Langmuir* **2010**, *26*, 17712-17719.

(178) Curley, J. L.; Jennings, S. R.; Moore, M. J. Fabrication of micropatterned hydrogels for neural culture systems using dynamic mask projection photolithography. *J Vis Exp* **2011**.

(179) Papavasiliou, G.; Songprawat, P.; Perez-Luna, V.; Hammes, E.; Morris, M.; Chiu, Y. C.; Brey, E. Three-dimensional pattering of poly (ethylene Glycol) hydrogels through surface-initiated photopolymerization. *Tissue Eng Part C Methods* **2008**, *14*, 129-140.

(180) Wu, J.; Miao, J. Production of centimeter-scale gradient patterns by graded elastomeric tip array. *ACS Appl Mater Interfaces* **2015**, *7*, 6991-7000.

(181) Orsi, S.; De Capua, A.; Guarnieri, D.; Marasco, D.; Netti, P. A. Cell recruitment and transfection in gene activated collagen matrix. *Biomaterials* **2010**, *31*, 570-576.

(182) Caliari, S. R.; Gonnerman, E. A.; Grier, W. K.; Weisgerber, D. W.; Banks, J. M.; Alsop, A. J.; Lee, J. S.; Bailey, R. C.; Harley, B. A. Collagen scaffold arrays for combinatorial screening of biophysical and biochemical regulators of cell behavior. *Adv Healthc Mater* **2015**, *4*, 58-64.

(183) Charras, G.; Sahai, E. Physical influences of the extracellular environment on cell migration. *Nat Rev Mol Cell Biol* **2014**, *15*, 813-824.

(184) Wells, R. G. The role of matrix stiffness in regulating cell behavior. *Hepatology* **2008**, *47*, 1394-1400.

(185) Pelham, R. J., Jr.; Wang, Y. L. Cell locomotion and focal adhesions are regulated by the mechanical properties of the substrate. *Biol Bull* **1998**, *194*, 348-349; discussion 349-350.

(186) Wang, Y. L.; Pelham, R. J., Jr. Preparation of a flexible, porous polyacrylamide substrate for mechanical studies of cultured cells. *Methods Enzymol* **1998**, *298*, 489-496.

(187) Wang, J. H.; Lin, J. S. Cell traction force and measurement methods. *Biomech Model Mechanobiol* **2007**, *6*, 361-371.

(188) Toworfe, G. K.; Composto, R. J.; Adams, C. S.; Shapiro, I. M.; Ducheyne, P. Fibronectin adsorption on surface-activated poly(dimethylsiloxane) and its effect on cellular function. *J Biomed Mater Res A* **2004**, *71*, 449-461.

(189) Shadpour, H.; Allbritton, N. L. In situ roughening of polymeric microstructures. *ACS Appl Mater Interfaces* **2010**, *2*, 1086-1093.

(190) Ghibaudo, M.; Trichet, L.; Le Digabel, J.; Richert, A.; Hersen, P.; Ladoux, B. Substrate topography induces a crossover from 2D to 3D behavior in fibroblast migration. *Biophys J* **2009**, *97*, 357-368.

(191) le Digabel, J.; Ghibaudo, M.; Trichet, L.; Richert, A.; Ladoux, B. Microfabricated substrates as a tool to study cell mechanotransduction. *Med Biol Eng Comput* **2010**, *48*, 965-976.

(192) Kim, S. H.; Choi, Y. R.; Park, M. S.; Shin, J. W.; Park, K. D.; Kim, S. J.; Lee, J. W. ERK 1/2 activation in enhanced osteogenesis of human mesenchymal stem cells in poly(lactic-glycolic acid) by cyclic hydrostatic pressure. *J Biomed Mater Res A* **2007**, *80*, 826-836.

(193) Mitragotri, S.; Lahann, J. Physical approaches to biomaterial design. *Nat Mater* **2009**, *8*, 15-23.

(194) Shao, Y.; Fu, J. Integrated micro/nanoengineered functional biomaterials for cell mechanics and mechanobiology: a materials perspective. *Adv Mater* **2014**, *26*, 1494-1533.

(195) Baker, B. M.; Chen, C. S. Deconstructing the third dimension: how 3D culture microenvironments alter cellular cues. *Journal of cell science* **2012**, *125*, 3015-3024.

(196) Ulrich, T. A.; Jain, A.; Tanner, K.; MacKay, J. L.; Kumar, S. Probing cellular mechanobiology in three-dimensional culture with collagen-agarose matrices. *Biomaterials* **2010**, *31*, 1875-1884.

(197) Bian, W.; Liau, B.; Badie, N.; Bursac, N. Mesoscopic hydrogel molding to control the 3D geometry of bioartificial muscle tissues. *Nat Protoc* **2009**, *4*, 1522-1534.

(198) Hadjipanayi, E.; Mudera, V.; Brown, R. A. Guiding cell migration in 3D: a collagen matrix with graded directional stiffness. *Cell Motil Cytoskeleton* **2009**, *66*, 121-128.

(199) Kamei, K.; Mashimo, Y.; Koyama, Y.; Fockenberg, C.; Nakashima, M.; Nakajima, M.; Li, J.; Chen, Y. 3D printing of soft lithography mold for rapid production of polydimethylsiloxane-based microfluidic devices for cell stimulation with concentration gradients. *Biomed Microdevices* **2015**, *17*, 36.

(200) Lautscham, L. A.; Kammerer, C.; Lange, J. R.; Kolb, T.; Mark, C.; Schilling, A.; Strissel, P. L.; Strick, R.; Gluth, C.; Rowat, A. C.; Metzner, C.; Fabry, B. Migration in Confined 3D Environments Is Determined by a Combination of Adhesiveness, Nuclear Volume, Contractility, and Cell Stiffness. *Biophys J* **2015**, *109*, 900-913.

(201) Ng, C. P.; Pun, S. H. A perfusable 3D cell-matrix tissue culture chamber for in situ evaluation of nanoparticle vehicle penetration and transport. *Biotechnol Bioeng* **2008**, *99*, 1490-1501.

(202) Spivey, E. C.; Xhemalce, B.; Shear, J. B.; Finkelstein, I. J. 3D-printed microfluidic microdissector for high-throughput studies of cellular aging. *Anal Chem* **2014**, *86*, 7406-7412.

(203) Gil, V.; del Rio, J. A. Analysis of axonal growth and cell migration in 3D hydrogel cultures of embryonic mouse CNS tissue. *Nat Protoc* **2012**, *7*, 268-280.

(204) Kievit, F. M.; Florczyk, S. J.; Leung, M. C.; Veiseh, O.; Park, J. O.; Disis, M. L.; Zhang, M. Chitosan-alginate 3D scaffolds as a mimic of the glioma tumor microenvironment. *Biomaterials* **2010**, *31*, 5903-5910.

(205) Ozdil, B.; Onal, S.; Oruc, T.; Pesen Okvur, D. Fabrication of 3D Controlled in vitro Microenvironments. *MethodsX* **2014**, *1*, 60-66.

(206) Yu, Q.; Braswell, S.; Christin, B.; Xu, J.; Wallace, P. M.; Gong, H.; Kaminsky, D. Surface-enhanced Raman scattering on gold quasi-3D nanostructure and 2D nanohole arrays. *Nanotechnology* **2010**, *21*, 355301.

(207) Singh, M.; Berkland, C.; Detamore, M. S. Strategies and applications for incorporating physical and chemical signal gradients in tissue engineering. *Tissue Eng Part B Rev* **2008**, *14*, 341-366.

(208) Lee, K. Y.; Mooney, D. J. Alginate: properties and biomedical applications. *Prog Polym Sci* **2012**, *37*, 106-126.

(209) Crowe-Willoughby, J. A.; Weiger, K. L.; Özçam, A. E.; Genzer, J. Formation of silicone elastomer networks films with gradients in modulus. *Polymer* **2010**, *51*, 763-773.

(210) Kidoaki, S.; Matsuda, T. Microelastic gradient gelatinous gels to induce cellular mechanotaxis. *J Biotechnol* **2008**, *133*, 225-230.

(211) Tanaka, M.; Sackmann, E. Polymer-supported membranes as models of the cell surface. *Nature* **2005**, *437*, 656-663.

(212) Kourouklis, A. P.; Lerum, R. V.; Bermudez, H. Cell adhesion mechanisms on laterally mobile polymer films. *Biomaterials* **2014**, *35*, 4827-4834.

(213) Tristram-Nagle, S.; Nagle, J. F. Lipid bilayers: thermodynamics, structure, fluctuations, and interactions. *Chem Phys Lipids* **2004**, *127*, 3-14.

(214) Kang, E.; Park, J. W.; McClellan, S. J.; Kim, J. M.; Holland, D. P.; Lee, G. U.; Franses, E. I.; Park, K.; Thompson, D. H. Specific adsorption of histidine-tagged proteins on silica surfaces modified with Ni2+/NTA-derivatized poly(ethylene glycol). *Langmuir : the ACS journal of surfaces and colloids* **2007**, *23*, 6281-6288.

(215) Penic, S.; Iglic, A.; Bivas, I.; Fosnaric, M. Bending elasticity of vesicle membranes studied by Monte Carlo simulations of vesicle thermal shape fluctuations. *Soft Matter* **2015**, *11*, 5004-5009.

(216) Bivas, I. Shape fluctuations of nearly spherical lipid vesicles and emulsion droplets. *Phys Rev E Stat Nonlin Soft Matter Phys* **2010**, *81*, 061911.

(217) Bivas, I.; Meleard, P. Bending elasticity and bending fluctuations of lipid bilayer containing an additive. *Phys Rev E Stat Nonlin Soft Matter Phys* **2003**, *67*, 012901.

(218) Pangule, R. C.; Banerjee, I.; Sharma, A. Adhesion induced mesoscale instability patterns in thin PDMS-metal bilayers. *J Chem Phys* **2008**, *128*, 234708.

(219) Siegel, A. P.; Murcia, M. J.; Johnson, M.; Reif, M.; Jordan, R.; Ruhe, J.; Naumann, C. A. Compartmentalizing a lipid bilayer by tuning lateral stress in a physisorbed polymer-tethered membrane. *Soft Matter* **2010**, *6*, 2723-2732.

(220) Siegel, A. P.; Hussain, N. F.; Johnson, M.; Naumann, C. A. Metric between buckling structures and elastic properties in physisorbed polymer-tethered lipid monolayers. *Soft Matter* **2012**, *8*, 5873-5880.

(221) Deverall, M. A.; Gindl, E.; Sinner, E. K.; Besir, H.; Ruehe, J.; Saxton, M. J.; Naumann, C. A. Membrane lateral mobility obstructed by polymer-tethered lipids studied at the single molecule level. *Biophysical journal* **2005**, *88*, 1875-1886.

(222) Almeida, P. F.; Vaz, W. L.; Thompson, T. E. Lateral diffusion in the liquid phases of dimyristoylphosphatidylcholine/cholesterol lipid bilayers: a free volume analysis. *Biochemistry* **1992**, *31*, 6739-6747.

(223) Ratto, T. V.; Longo, M. L. Obstructed diffusion in phase-separated supported lipid bilayers: a combined atomic force microscopy and fluorescence recovery after photobleaching approach. *Biophys J* **2002**, *83*, 3380-3392.

(224) Chung, M.; Boxer, S. G. Stability of DNA-tethered lipid membranes with mobile tethers. *Langmuir* **2011**, *27*, 5492-5497.

(225) Han, X.; Pradeep, S. N.; Critchley, K.; Sheikh, K.; Bushby, R. J.; Evans, S. D. Supported bilayer lipid membrane arrays on photopatterned self-assembled monolayers. *Chemistry* **2007**, *13*, 7957-7964.

(226) Benkoski, J. J.; Hook, F. Lateral mobility of tethered vesicle-DNA assemblies. *J Phys Chem B* **2005**, *109*, 9773-9779.

(227) Arora, P. D.; Wang, Y.; Bresnick, A.; Dawson, J.; Janmey, P. A.; McCulloch, C. A. Collagen remodeling by phagocytosis is determined by collagen substrate topology and calcium-dependent interactions of gelsolin with nonmuscle myosin IIA in cell adhesions. *Mol Biol Cell* **2013**, *24*, 734-747.

(228) Jiang, H.; Qu, W.; Li, Y.; Zhong, W.; Zhang, W. Platelet-derived growth factors-BB and fibroblast growth factors-base induced proliferation of Schwann cells in a 3D environment. *Neurochem Res* **2013**, *38*, 346-355.

(229) Gu, Z.; Tang, Y. Enzyme-assisted photolithography for spatial functionalization of hydrogels. *Lab Chip* **2010**, *10*, 1946-1951.

(230) Mendez, M. G.; Restle, D.; Janmey, P. A. Vimentin enhances cell elastic behavior and protects against compressive stress. *Biophys J* **2014**, *107*, 314-323.

(231) Yahiro, K.; Satoh, M.; Nakano, M.; Hisatsune, J.; Isomoto, H.; Sap, J.; Suzuki, H.; Nomura, F.; Noda, M.; Moss, J.; Hirayama, T. Low-density lipoprotein receptor-related protein-1 (LRP1) mediates autophagy and apoptosis caused by Helicobacter pylori VacA. *J Biol Chem* **2012**, *287*, 31104-31115.

(232) Phelps, E. A.; Enemchukwu, N. O.; Fiore, V. F.; Sy, J. C.; Murthy, N.; Sulchek, T. A.; Barker, T. H.; Garcia, A. J. Maleimide cross-linked bioactive PEG hydrogel exhibits improved reaction kinetics and cross-linking for cell encapsulation and in situ delivery. *Adv Mater* **2012**, *24*, 64-70, 62.

(233) Minner, D. E.; Rauch, P.; Kas, J.; Naumann, C. A. Polymer-tethered lipid multi-bilayers: a biomembrane-mimicking cell substrate to probe cellular mechano-sensing. *Soft Matter* **2014**, *10*, 1189-1198.

(234) Chao, P. H.; Sheng, S. C.; Chang, W. R. Micro-composite substrates for the study of cell-matrix mechanical interactions. *J Mech Behav Biomed Mater* **2014**, *38*, 232-241.

(235) Deverall, M. A.; Garg, S.; Ludtke, K.; Jordan, R.; Ruhe, J.; Naumann, C. A. Transbilayer coupling of obstructed lipid diffusion in polymer-tethered phospholipid bilayers. *Soft Matter* **2008**, *4*, 1899-1908.

(236) Warriner, H. E.; Idziak, S. H.; Slack, N. L.; Davidson, P.; Safinya, C. R. Lamellar biogels: fluid-membrane-based hydrogels containing polymer lipids. *Science* **1996**, *271*, 969-973.

(237) Zhang, L.; Granick, S. Slaved diffusion in phospholipid bilayers. *Proc Natl Acad Sci U S A* **2005**, *102*, 9118-9121.

(238) Chopra, A.; Tabdanov, E.; Patel, H.; Janmey, P. A.; Kresh, J. Y. Cardiac myocyte remodeling mediated by N-cadherin-dependent mechanosensing. *American Journal of Physiology - Heart and Circulatory Physiology* **2011**, *300*, H1252-H1266.

(239) Discher, D. E.; Janmey, P.; Wang, Y.-l. Tissue Cells Feel and Respond to the Stiffness of Their Substrate. *Science* **2005**, *310*, 1139-1143.

(240) Chopra, A.; Tabdanov, E.; Patel, H.; Janmey, P. A.; Kresh, J. Y. Cardiac myocyte remodeling mediated by N-cadherin-dependent mechanosensing. *Am J Physiol Heart Circ Physiol* **2011**, *300*, H1252-1266.

(241) Genova, J.; Ulrih, N. P.; Kralj-Iglic, V.; Iglic, A.; Bivas, I. Bending elasticity modulus of giant vesicles composed of aeropyrum pernix k1 archaeal lipid. *Life (Basel)* **2015**, *5*, 1101-1110.

(242) Genova, J.; Vitkova, V.; Bivas, I. Registration and analysis of the shape fluctuations of nearly spherical lipid vesicles. *Phys Rev E Stat Nonlin Soft Matter Phys* **2013**, *88*, 022707.

(243) Lin, Y.-H.; Minner, D.; Herring, V.; Naumann, C. Physisorbed Polymer-Tethered Lipid Bilayer with Lipopolymer Gradient. *Materials* **2012**, *5*, 2243.

(244) Groves, J. T.; Ulman, N.; Boxer, S. G. Micropatterning fluid lipid bilayers on solid supports. *Science* **1997**, *275*, 651-653.

(245) Jonkheijm, P.; Weinrich, D.; Kohn, M.; Engelkamp, H.; Christianen, P. C.; Kuhlmann, J.; Maan, J. C.; Nusse, D.; Schroeder, H.; Wacker, R.; Breinbauer, R.; Niemeyer, C. M.; Waldmann, H. Photochemical surface patterning by the thiol-ene reaction. *Angew Chem Int Ed Engl* **2008**, *47*, 4421-4424.

(246) Wagner, M. L.; Tamm, L. K. Tethered polymer-supported planar lipid bilayers for reconstitution of integral membrane proteins: silane-polyethyleneglycol-lipid as a cushion and covalent linker. *Biophysical journal* **2000**, *79*, 1400-1414.

(247) Cao, L.; Guilak, F.; Setton, L. A. Three-dimensional finite element modeling of pericellular matrix and cell mechanics in the nucleus pulposus of the intervertebral disk based on in situ morphology. *Biomech Model Mechanobiol* **2011**, *10*, 1-10.

(248) Chen, W.; Shao, Y.; Li, X.; Zhao, G.; Fu, J. Nanotopographical Surfaces for Stem Cell Fate Control: Engineering Mechanobiology from the Bottom. *Nano Today* **2014**, *9*, 759-784.

(249) Gaggioli, C.; Sahai, E. Melanoma invasion - current knowledge and future directions. *Pigment Cell Res* **2007**, *20*, 161-172.

VITA

VITA

Education

Ph.D. **Biochemistry**. Department of Chemistry and Chemical Biology, Purdue School of Science. IUPUI, Indianapolis, IN. 2009-2015, GPA 3.6/4

M.S. **Applied Chemistry**. School of Science, National Tsing-Hus University, HsinChu, Taiwan 2003-2005, GPA 4/4

B.S. **Chemistry.** School of Science, National Tsing-Hua University, HsinChu Taiwan 1999-2003, GPA 3.67/4

Selected Honors and Awards

Fellowship (Sponsor: NSF) Aug 2009-Jun 2010

Travel Award of School of Science in IUPUI July 2010

Professional Experiences

Title: Graduate research assistant & Teaching assistant, IUPUI *Aug.2011-May 2014*

Supervisor: Christoph Naumann

Title: Teaching Assistant, National Taiwan University *Aug 2011-May 2014*

Supervisor: Associate Chair & Professor Man-kit Leung, Chair & Prof. Pi-Tai Chou

Title: Research assistance, Institute of Chemistry, Academia Sinica *Aug 2005-Jan 2007*

Major response: Conduct an independent research; coordinates between academic and industry institutes; assistance to daily lab management.

Supervisor: Professor Sunney I. Chan, Professor Steve S.-F. Yu

Skill and Techniques

Specific Instruments:

- Fluorescent correlation microscopy; Confocal Microscopy; Fluorescent Microscopy
- Electrochemical analysis methods (square wave analysis, electrochemical potential analysis, potential- current analysis, resistance analysis)
- UV-Vis, Fluorescent spectrometry; HPLC-MS; UPLC-MS; ESI-MS; FPLC. Infar-red Spectrumscopy.

Chemistry:

- Protein Labeling, simple organic reactions, surface chemical decoration
- Design of Drug delivery vehicles.

Biology:

- Cell culture (Mice cell line: MEF Fibroblast, C2C12 Myoblast and PC 12)
- Bacteria culture (Yeast, *E. Coli*, and *Methylococcus capsulatus* (Bath) (pMMO).)
- Immunostaining for F-Actin, FAK and Beta-catenin.
- Transient and stable transfection on mammal cells such as MEF Fibroblast.

Data image process and software: Origin Lab; Image J; Photoshop; ChemDraw

Affiliations/Memberships

- Biophysical Society
- American Chemistry Society

List of Publications

1. Lautscham, L. A.; Lin, C. Y.; Auernheimer, V.; Naumann, C. A.; Goldmann, W. H.; Fabry, B. Biomembrane-mimicking lipid bilayer system as a mechanically tunable cell substrate. *Biomaterials* **2014**, *35*, 3198-3207
2. Lin, Y.-H.; Minner, D.; Herring, V.; Naumann, C. Physisorbed Polymer-Tethered Lipid Bilayer with Lipopolymer Gradient. *Materials* **2012**, *5*, 2243.
3. Lawrence, K.; Dolai, S.;Lin, Y.-H.; Dass, A.; Sardar, R. Enhancing the physicochemical and photophysical properties of small (<2.0 nm) CdSe nanoclusters for intracellular imaging applications. RSC Advances **2014**, *4,* 30742